Rice University

Random Access Cooperative Systems

by

Christopher R. Hunter

A Thesis Submitted
in Partial Fulfillment of the
Requirements for the Degree

Master of Science

Approved, Thesis Committee:

Dr. Ashutosh Sabharwal, *Chair*
Assistant Professor of Electrical and Computer Engineering

Dr. Behnaam Aazhang
J.S. Abercrombie Professor of Electrical and Computer Engineering

---

Dr. Joseph R. Cavallaro
Professor of Electrical and Computer Engineering

Houston, Texas

April 2008

Abstract

Random Access Cooperative Systems

by

Christopher R. Hunter

User-cooperation has been studied extensively in the literature. This mechanism achieves many of the same gains that can be had by using multi-antenna (MIMO) communications in applications where the size of a node is limited. Existing analysis assumes that the system is scheduled; both the relay knows to listen when a packet is being sent. We present analysis of a class of random-access cooperative systems and show that the same performance as the scheduled systems can be achieved as long as certain requirements are met in the packet detection scheme of the relay. In particular, we find that a static decision threshold on energy detection results in a cooperative network that performs asymptotically no better than a simple point-to-point network with no relay at all. However, a decision threshold that dynamically shifts with average SNR allows the system to achieve full spatial diversity.

Contents

Abstract **ii**

1 Introduction **1**
1.1 Historical Context 1
1.2 Problem Description 4
1.3 Organization of Thesis 5
1.4 Summary of Results 7

2 Network Model **8**
2.1 Orthogonal Amplify-and-Forward 10
2.1.1 Results 15
2.2 Non-Orthogonal Amplify-and-Forward 26
2.2.1 Results 30
2.3 Summary 45

3 Energy Detection **46**
3.1 System Model and Nomenclature 48
3.1.1 H_0 - Idle Source Hypothesis 49
3.1.2 H_1 - Busy Source Hypothesis 49
3.1.3 Probability of Packet Detection Errors 50
3.1.4 Exponential Order Nomenclature 52
3.2 Static Threshold Relay Detection 52
3.2.1 Effect on OAF States 54
3.2.2 Effect on NAF States 57
3.3 Dynamic Threshold Relay Detection 59
3.3.1 Effect on OAF States 62

3.3.2 Effect on NAF States 66
3.4 Summary 70

4 Orthogonal Amplify-and-Forward Analysis 71
4.1 Conditional Performance 72
4.1.1 Best Case 72
4.1.2 Neutral Case 78
4.1.3 Worst Case 81
4.2 Total Performance 84
4.2.1 Static Relay Detection 84
4.2.2 Dynamic Relay Detection 86
4.3 Summary 90

5 Non-Orthogonal Amplify-and-Forward Analysis 91
5.1 Conditional Performance 91
5.1.1 Best Case 91
5.1.2 Neutral Case 94
5.1.3 Worst Case 1 97
5.1.4 Worst Case 2 100
5.2 Total Performance 102
5.2.1 Static Relay Detection 102
5.2.2 Dynamic Relay Detection 103
5.3 Summary 107

6 Conclusions 108
6.1 Extensions and Future Work 110

A Mutual Information Calculations for OAF 111
A.1 Best Case 111
A.2 Neutral Case 113
A.3 Worst Case 115

B Mutual Information Calculations for NAF 117
B.1 Best Case 117
B.2 Neutral Case 119
B.3 Worst Case 1 121
B.4 Worst Case 2 123

C Asymptotic CDF Approximations 125

List of Figures

1.1 Orthogonal Amplify-and-Forward cooperation. 3
1.2 Non-Orthogonal Amplify-and-Forward cooperation. 4
1.3 Outline of thesis 6

2.1 Packet detection events 9
2.2 Example sequence of events and relay behavior for OAF 10
2.3 Channel states for OAF protocol 11
2.4 Visualization of Markov chain for OAF protocol 14
2.5 Probability of state B_1 16
2.6 Probability of state B_2 17
2.7 Probability of state B_3 18
2.8 Probability of state B_4 19
2.9 Probability of state B_5 20
2.10 Probability of state I_1 21
2.11 Probability of state I_2 22
2.12 Probability of state I_3 23
2.13 Probability of state I_4 24
2.14 Probability of state I_5 25
2.15 Example sequence of packet detection events and relay behavior for NAF 26
2.16 Channel states for NAF protocol 27
2.17 Visualization of Markov chain for NAF protocol 29
2.18 Probability of state B_1 31
2.19 Probability of state B_2 32
2.20 Probability of state B_3 33
2.21 Probability of state B_4 34

2.22 Probability of state B_5 35
2.23 Probability of state B_6 36
2.24 Probability of state B_7 37
2.25 Probability of state I_1 38
2.26 Probability of state I_2 39
2.27 Probability of state I_3 40
2.28 Probability of state I_4 41
2.29 Probability of state I_5 42
2.30 Probability of state I_6 43
2.31 Probability of state I_7 44

3.1 Packet detection events 47
3.2 Static threshold 53
3.3 Likelihood of busy states for different static thresholds 55
3.4 Likelihood of idle states for different static thresholds 55
3.5 Likelihood of busy states for different static thresholds 57
3.6 Likelihood of idle states for different static thresholds 57
3.7 Path Loss scenario 59
3.8 Dynamic threshold 60
3.9 Likelihood of busy states for different dynamic thresholds 62
3.10 Likelihood of idle states for different dynamic thresholds 63
3.11 Likelihood of busy states for different dynamic thresholds 66
3.12 Likelihood of idle states for different dynamic thresholds 67

4.1 Best case state: B_1 72
4.2 Best case outage probability Monte Carlo simulation ($R = \frac{1}{2}$ and $\lambda_{s,d} = \lambda_{s,r} = \lambda_{r,d} = 1$) 77
4.3 Neutral case states 78
4.4 Neutral case outage probability Monte Carlo simulation ($R = \frac{1}{2}$ and $\lambda_{s,d} = 1$) 80
4.5 Worst case states 81
4.6 Worst case outage probability bounds 83
4.7 Outage Probability with $\Lambda = 20$ 86
4.8 Outage Probability with $\Lambda = 20 + \log(1 + \mathrm{SNR})$ 88
4.9 Outage Probability with $\Lambda = 20 + \mathrm{SNR}$ 90

5.1 Best case state: B_1 92

5.2 Best case outage probability Monte Carlo simulation ($R = \frac{1}{2}$ and $\lambda_{s,d} = \lambda_{s,r} = \lambda_{r,d} = 1$) 94
5.3 Neutral case states 94
5.4 Neutral case outage probability Monte Carlo simulation 96
5.5 First worst case states 97
5.6 Worst case outage probability bounds 99
5.7 Second Worst case states 100
5.8 Outage Probability with $\Lambda = 20$ 103
5.9 Outage Probability with $\Lambda = 20 + \log(1 + \mathrm{SNR})$ 105
5.10 Outage Probability with $\Lambda = 20 + \mathrm{SNR}$ 106

6.1 Outage probability of NAF with different static energy thresholds . . 109

List of Tables

2.1 Labeled Markov chain probability transition matrix for OAF 12
2.2 Labeled Markov chain probability transition matrix for NAF 28

3.1 Summary of state likelihoods for OAF 70
3.2 Summary of state likelihoods for NAF 70

Chapter 1

Introduction

Multi-antenna communications (MIMO) is a class of techniques that have shown dramatic performance gains in terms of both the reliability and throughput of wireless communication links [1]. In order to produce statistically independent communication channels, however, these techniques require antenna arrays with enough physical separation between elements. While this spatial limitation is of minor concern for devices like notebook computers or cellular base stations, it can be infeasible in applications such as mobile phones or sensor networks where the devices must be small or be of limited architectural complexity.

User cooperation employs multiple single-antenna nodes that work together in such a way that the system appears to be a single multi-antenna transmitter from the perspective of the destination node. Intuitively, this MIMO-like interpretation motivates why cooperative networks can exhibit many of the same performance gains as multi-antenna systems.

1.1 Historical Context

The first foray into user cooperation was the study of the relay channel. This channel was first studied by van der Meulen [2, 3], and later by Cover and El Gamal [4]. In

the context of discrete memoryless and Gaussian degraded channels, this information theoretic analysis concluded that cooperation can improve the capacity of a wireless network. An achievable rate region was presented by Sendonaris *et al.* for the relay channel [5–7]. This analysis focused on an ergodic fading scenario with applications to CDMA technologies.

More recently, basic and foundational protocols for cooperation have been presented and analyzed in the context of delay-constrained quasi-static fading channels by Laneman *et al.* [8]. In addition to relying on half-duplex radios, this work separated itself from prior work by considering outage probability as a performance metric. This work was later extended to apply to larger networks of N cooperative relays [9]. The simple protocols in Laneman's original works have served as the basis for many powerful extensions to target new applications such as high-spectral efficiency scenarios [10–13]. Additionally, work has been performed in the development of practical coding schemes to achieve the performance benefits shown by the information theoretic analysis in the literature [14–17]. As we discuss in Section 1.2, a critical assumption in these works is that a cooperative relay must know *when* a source transmits with perfect accuracy. In other words, these protocols and their analyses apply to the area of scheduled access systems.

Other work in the field has been performed on random access systems. Specifically, a proposed cooperative random access protocol extended from the Network-assisted Diversity Multiple Access (NDMA) protocol uses cooperative retransmissions to allow a base station to decode the collided packets that occur in random access networks [18, 19]. The use of cooperation in this protocol is not intentended, however, to improve the physical-layer reliability of a transmission. Instead, cooperation serves to improve network-layer throughput by eliminating collisions. Our problem, described in Section 1.2, is different in that we analyze the negative effects of random access on the physical-layer reliability of a transmission. In that sense, while they have

attempted to answer the problem of how physical-layer cooperation can aid random-access networks, the work in this thesis attempts to answer the question of how badly random-access networks can corrupt the physical-layer performance gains shown in the prior literature.

Additionally, there has been work on solving issues of symbol-level asynchronism in cooperative networks [20]. However, these works do not analyze the effects of uncertainty surrounding a source's transmission or lack thereof in a random access system. This packet-level uncertainty is the focus of this work. In particular, we analyze a class of amplify-and-forward protocols originally proposed by Laneman under the conditions of a random access system.

In Laneman's work [8], cooperative transmission is coded over two time slots. In the first slot, the source broadcasts a message to both an altruistic relay and the destination. In the second slot, the relay transmits what it heard while the source is silent. Alternatively, the protocol can be extended to allow the source to continue transmitting during the second slot. We adopt the terminology in [11] and describe the former case as "Orthogonal Amplify-and-Forward" (OAF) and the latter case as "Non-Orthogonal Amplify-and-Forward" (NAF). For our problem, the distinction between these cases is important. As such, each case is analyzed separately in Chapters 4 and 5 respectively.

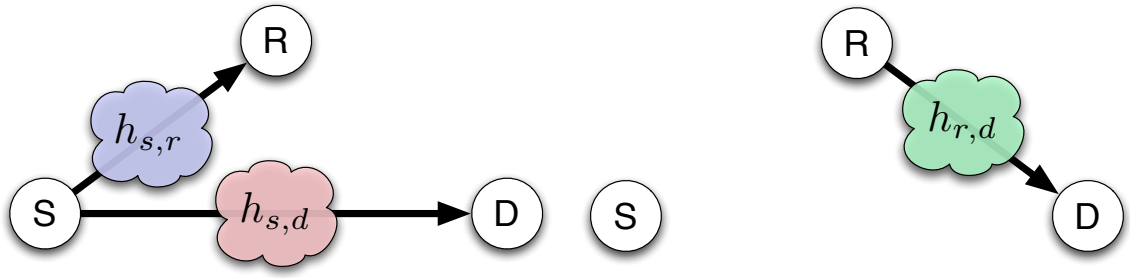

(a) Slot 1 (b) Slot 2

Figure 1.1: Orthogonal Amplify-and-Forward cooperation.

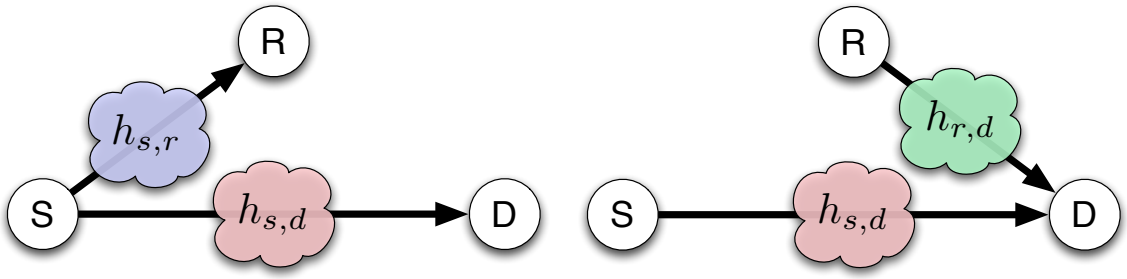

(a) Slot 1 (b) Slot 2

Figure 1.2: Non-Orthogonal Amplify-and-Forward cooperation.

As shown in Figures 1.1 and 1.2, the principle gain in such protocols is that the message has more than one path to the destination in the event of poor channel conditions. Through Gaussian random coding arguments, Laneman shows that such systems achieve full spatial diversity (i.e. the probability of outage decays asymptotically as SNR^{-2} with two transmitting nodes). Implicit in this analysis is that the source, relay, and destination all know *a priori* that the source has something to send. This is equivalent to a scheduled access system where medium access occurs deterministically via a centralized scheduler. This thesis relaxes this assumption to consider an additional randomness of the source itself.

1.2 Problem Description

We focus on describing the performance of random access cooperative systems where the source's transmission *time*, as well as content, is unknown. By studying the problem under these relaxed assumptions, we can answer the fundamental question of whether or not full cooperative diversity can be achieved in random access systems. The source randomness requires an additional level of detection at nodes to determine whether or not a message is present that needs to be processed. Throughout the analysis in this thesis, we still assume perfect scheduling between source and destination.

In other words, only the relay is susceptible to errors in this extra level of packet detection. This assumption is fitting not only as a lower bound on the performance of the more general case where all nodes are unsynchronized, but also applies to a potential deployment scenario of interest. Existing cellular data networks are centralized with scheduling between mobile units and base stations. As demand for mobile data expands, system capacity must be increased to support it. One idea to increase this capacity is to deploy altruistic relays to cooperate with mobile devices. Ideally, these relays would be inexpensive, "dumb" nodes that could be scattered throughout the cellular network. There are potentially significant cost savings to network operators if these relays are decentralized devices that act on their own. In other words, source and destinations remain synchronous while, from the perspective of the relay, the system appears as a random access cooperative link. This thesis analyzes the theoretical performance of this scenario.

1.3 Organization of Thesis

This thesis has two major parts. Chapters 2 and 3 describe the various error events that can occur and the likelihood of their occurrence with an unsynchronized relay. This analysis is generic and can be used to analyze any relaying protocol that uses fixed slot durations (e.g. decode-and-forward). We then apply this general analysis and study one class of protocols, amplify-and-forward, in depth. Amplify-and-forward protocols are perhaps the simplest to implement, requiring only memory and a multiplier at the relay. Chapters 4 and 5 analyze the system performance conditioned on the aforementioned error events. This analysis coupled with the error event likelihoods culminates in analysis of overall system performance.

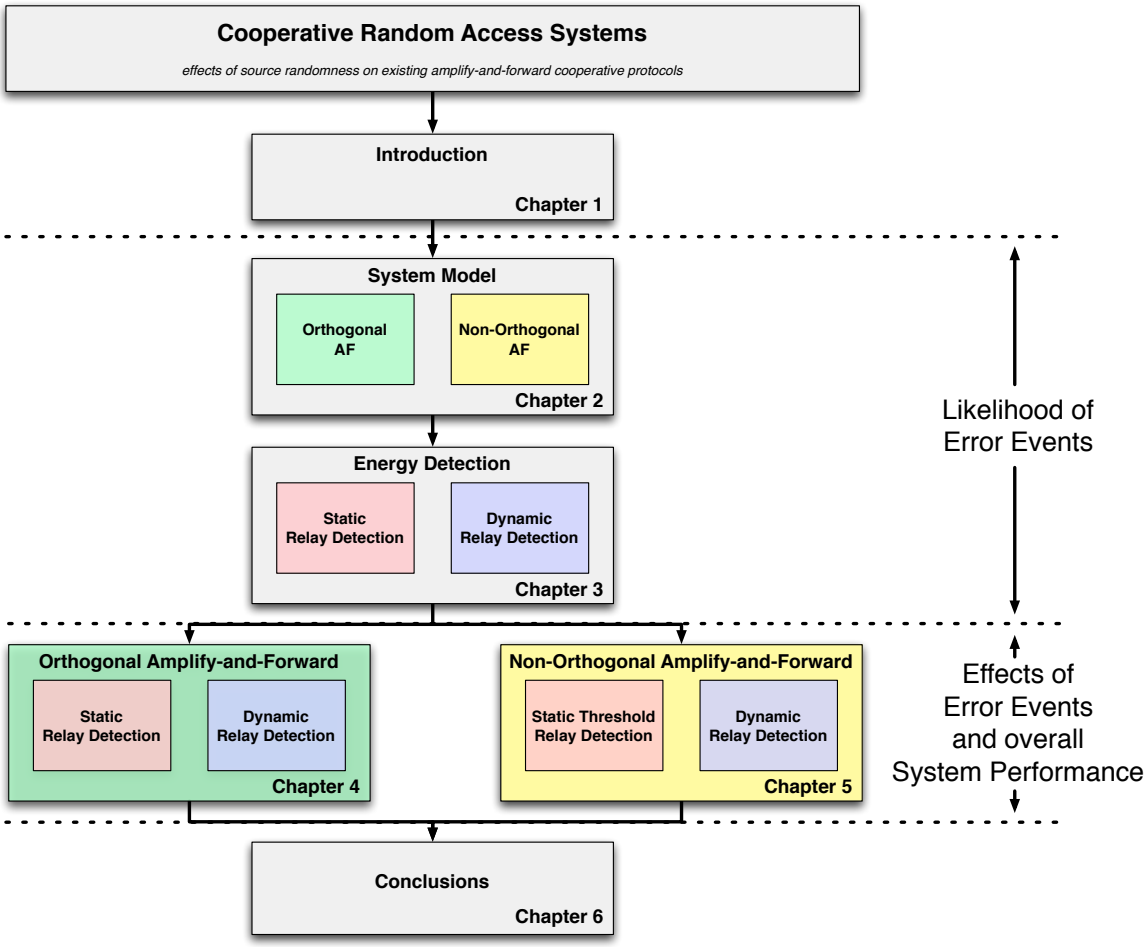

Figure 1.3: Outline of thesis

As shown in Figure 1.3, we consider two forms of cooperative relaying: Orthogonal Amplify-and-Forward (OAF) and Non-Orthogonal Amplify-and-Forward (NAF). Additionally, we consider two types of packet detection schemes: static thresholds for energy detection at the relay and dynamic thresholds for energy detection at the relay. We analyze all combinations of these cooperative relaying and packet detection schemes.

1.4 Summary of Results

We analyze the outage performance of the two random access cooperative protocols under the two classes of energy detection strategies.

	Orthogonal	**Non-Orthogonal**
Static Relay	Section 4.2.1	Section 5.2.1
Dynamic Relay	Section 4.2.2	Section 5.2.2

The four results associated with each of these combinations can be found in the sections specified by the above table. We find that, for both the OAF and NAF protocols, a static decision threshold on energy detection results in a cooperative network that performs asymptotically no better than a simple point-to-point network with no relay at all. However, a decision threshold that dynamically shifts with average SNR allows systems with either protocol to achieve full spatial diversity.

Chapter 2

Network Model

Under the source-destination synchronization assumption, the source transmits at known times from the perspective of the destination. As such, the destination never fails to observe a transmitted message nor does it mistake a noise event with the presence of a message. The relay's task, however, is not merely to amplify-and-forward what it receives, but also to decide whether or not something was sent in the first place. To describe the possible error events in this scenario, we introduce a slotted random-access network model.

In this model, the source is assumed to contend for the medium on known slot boundaries for a duration of L symbols in two slots. The relay's behavior is the following:

- If a packet is detected in the previous slot, amplify-and-forward the waveform in the current slot
- If not, purge the received waveform and continue sensing the medium

As shown in Figure 2.1 we define four possible packet detection events at the relay. Successfully detecting the presence of a packet (P$\mapsto$P) corresponds to event $\mathcal{S}_1$. Similarly, successfully ignoring a slot when no transmit occurs (0$\mapsto$0) corresponds

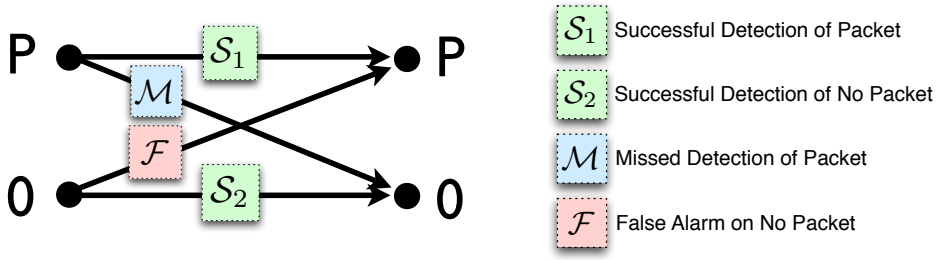

Figure 2.1: Packet detection events

to event $\mathcal{S}_2$. However, in the event that a transmitted codeword is missed (P$\mapsto$0) we say that event $\mathcal{M}$ occurs. Finally, falsely identifying noise as a transmission (0$\mapsto$P) is deemed event $\mathcal{F}$. We use the notation $P_{\mathcal{M}}$ and $P_{\mathcal{F}}$, respectively, to describe the probability of these error events. Likewise, we use the notation $P_{\mathcal{S}_1} = \bar{P_{\mathcal{M}}}$ and $P_{\mathcal{S}_2} = \bar{P_{\mathcal{F}}}$ to describe the probability of the successful events. For the purposes of this chapter, the particular detection scheme employed by the relay is inconsequential. We investigate the effects of these errors for arbitrary $(P_{\mathcal{M}}, P_{\mathcal{F}})$ pairs. In Chapter 3, we analyze energy detection as a particular packet detection scheme that can be employed by the relay to assign $P_{\mathcal{M}}$ and $P_{\mathcal{F}}$ as a functions of average SNR as well as a particular fading channel gains.

The rest of this section describes the different possible states of the cooperative network and and the likelihood of each occurring. Orthogonal Amplify-and-Forward and Nonorthogonal Amplify-and-Forward models yields very different possible network states. As such, each is analyzed separately.

2.1 Orthogonal Amplify-and-Forward

As stated earlier, the Orthogonal Amplify-and-Forward (OAF) protocol employs strict temporal orthogonality between the source and relay. We assume that the source contends for the medium in frames, which we define to be a two-slot unit. The first slot, it transmits with some average power (denoted by P), and it is silent in the second slot (denoted by 0). If the source has nothing to send, we assume that it remains silent over two slots.[1] We assume a quasi-static fading model whose instantaneous channel conditions are constant for the duration of a single frame (i.e. two slots). This assumption aligns source channel usage with independent channel draws (i.e. the channel does not change between the first and second slot of a frame). The purpose of this assumption is to ensure that any diversity improvements in the system are spatial and not temporal.

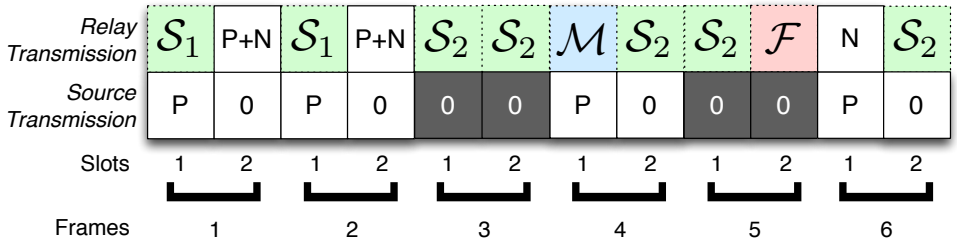

Figure 2.2: Example sequence of events and relay behavior for OAF

In Figure 2.2, we show potential sequences of events in this system. The figure shows the transmits and lack thereof of the source and relay. Per the behavioral description earlier, events $\mathcal{S}_1$ and $\mathcal{F}$ trigger action at the relay. For either of these events, the relay transmits an amplified stored waveform in the following slot. Depending on what waveform was *actually* transmitted, we, the omniscient observers, externally apply labels to the relay's waveform. In the event that $\mathcal{S}_1$ occurs at the beginning of a transmission slot, the transmitted waveform from the relay is denoted

[1] This assumption yields a special case of a transmitter that, in general, can be silent for any integer number of slots. We do not, however, exploit this analytical convenience at the relay. As such, we assume the relay is only slot-synchronized and has no notion of frames.

as $P + N$, representing the fact that the slot contains both source data and noise.[1] In the event that $\mathcal{F}$ occurs, the waveform transmitted by the relay is amplified noise and is represented by N. The sequence in Figure 2.2 shows four "busy" frames (one, two, four, and six) and two "idle" frames (three and five). Of the busy frames, we can see that relay behaves perfectly in frames one and two by successfully detecting the presence of a source transmission in the first slot and forwarding the received waveform in the second slot. However, in the fourth frame, the relay never transmits because it missed the detection of the source's transmission in the first slot. In the sixth frame, the relay actively hurts the source's ability to communicate by transmitting noise during the first slot of the frame because it falsely believed the source transmitted in the second slot of the previous frame.

For any given channel draw (i.e. a given frame), any one of ten channel states is possible.

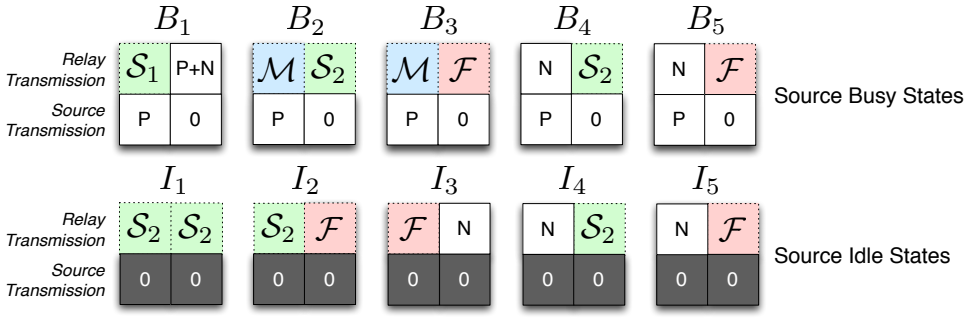

Figure 2.3: Channel states for OAF protocol

Figure 2.3 shows the ten channel states that can occur. States B_1 to B_5 represent the source "busy" states, where the source is actively transmitting. Similarly, states I_1 to I_5 represent the source "idle" states. We further categorize the busy states to describe their importance from the perspective of the destination node trying to decode the packet.

[1]Note, the label $P + N$ is not intended to imply that the power of the relay's transmission is simply the power of the source's transmission added to the power of receiver noise. The label is simply to indicate the pieces of information present in that particular slot. The relay's transmission power is significantly more subtle and is described in Chapters 4 and 5

- **Best Case:** B_1 represents the case where the relay behaves perfectly. The relay actively helps the source communicate by forwarding its received waveform in the second slot of the frame.

- **Neutral Cases:** B_2 and B_3 represent cases where the relay neither helps nor hurts the source. In both slots of the frame, the relay senses the medium, and thus, never transmits due to a half-duplex constraint.

- **Worst Cases:** B_4 and B_5 represent cases where the relay actively hurts the source's ability to communicate by transmitting noise during the first slot of the frame.

Each of these states have some likelihood of occurring. Given the present state, the future states are independent of the past states. Thus, the stationary probability of the states can be computed by considering the probabilities of the *transitions* between these states and treating the system as a Markov chain. We collect these state transition probabilities into a table representing the Markov chain probability transition matrix.

	B_1	B_2	B_3	B_4	B_5	I_1	I_2	I_3	I_4	I_5
B_1	$qP_{\mathcal{M}}$	$qP_{\mathcal{M}}\bar{P_{\mathcal{F}}}$	$qP_{\mathcal{M}}P_{\mathcal{F}}$	0	0	$\bar{q}\bar{P_{\mathcal{F}}}\bar{P_{\mathcal{F}}}$	$\bar{q}\bar{P_{\mathcal{F}}}P_{\mathcal{F}}$	$\bar{q}P_{\mathcal{F}}$	0	0
B_2	$qP_{\mathcal{M}}$	$qP_{\mathcal{M}}\bar{P_{\mathcal{F}}}$	$qP_{\mathcal{M}}P_{\mathcal{F}}$	0	0	$\bar{q}\bar{P_{\mathcal{F}}}\bar{P_{\mathcal{F}}}$	$\bar{q}\bar{P_{\mathcal{F}}}P_{\mathcal{F}}$	$\bar{q}P_{\mathcal{F}}$	0	0
B_3	0	0	0	$q\bar{P_{\mathcal{F}}}$	$qP_{\mathcal{F}}$	0	0	0	$\bar{q}\bar{P_{\mathcal{F}}}$	$\bar{q}P_{\mathcal{F}}$
B_4	$qP_{\mathcal{M}}$	$qP_{\mathcal{M}}\bar{P_{\mathcal{F}}}$	$qP_{\mathcal{M}}P_{\mathcal{F}}$	0	0	$\bar{q}\bar{P_{\mathcal{F}}}\bar{P_{\mathcal{F}}}$	$\bar{q}\bar{P_{\mathcal{F}}}P_{\mathcal{F}}$	$\bar{q}P_{\mathcal{F}}$	0	0
B_5	0	0	0	$q\bar{P_{\mathcal{F}}}$	$qP_{\mathcal{F}}$	0	0	0	$\bar{q}\bar{P_{\mathcal{F}}}$	$\bar{q}P_{\mathcal{F}}$
I_1	$qP_{\mathcal{M}}$	$qP_{\mathcal{M}}\bar{P_{\mathcal{F}}}$	$qP_{\mathcal{M}}P_{\mathcal{F}}$	0	0	$\bar{q}\bar{P_{\mathcal{F}}}\bar{P_{\mathcal{F}}}$	$\bar{q}\bar{P_{\mathcal{F}}}P_{\mathcal{F}}$	$\bar{q}P_{\mathcal{F}}$	0	0
I_2	0	0	0	$q\bar{P_{\mathcal{F}}}$	$qP_{\mathcal{F}}$	0	0	0	$\bar{q}\bar{P_{\mathcal{F}}}$	$\bar{q}P_{\mathcal{F}}$
I_3	$qP_{\mathcal{M}}$	$qP_{\mathcal{M}}\bar{P_{\mathcal{F}}}$	$qP_{\mathcal{M}}P_{\mathcal{F}}$	0	0	$\bar{q}\bar{P_{\mathcal{F}}}\bar{P_{\mathcal{F}}}$	$\bar{q}\bar{P_{\mathcal{F}}}P_{\mathcal{F}}$	$\bar{q}P_{\mathcal{F}}$	0	0
I_4	$qP_{\mathcal{M}}$	$qP_{\mathcal{M}}\bar{P_{\mathcal{F}}}$	$qP_{\mathcal{M}}P_{\mathcal{F}}$	0	0	$\bar{q}\bar{P_{\mathcal{F}}}\bar{P_{\mathcal{F}}}$	$\bar{q}\bar{P_{\mathcal{F}}}P_{\mathcal{F}}$	$\bar{q}P_{\mathcal{F}}$	0	0
I_5	0	0	0	$q\bar{P_{\mathcal{F}}}$	$qP_{\mathcal{F}}$	0	0	0	$\bar{q}\bar{P_{\mathcal{F}}}$	$\bar{q}P_{\mathcal{F}}$

Table 2.1: Labeled Markov chain probability transition matrix for OAF

Table 2.1 shows the likelihood of transitioning from any state to any other state. The only new parameter in this table is q, which we use to represent the source transmission probability. The rows represents the starting states and the columns represent the ending states. For brevity, we will not exhaustively describe each of these transitions, but instead describe a few representative examples. Determining the probabilities of the other transitions follows similar reasoning.

State B_1 can transition to itself if the source transmits again (q) and that transmission is not missed ($\bar{P_{\mathcal{M}}}$). Because these probabilities are independent, the probability of this transition occurring is their product.

As another example, B_1 can transition to I_2 if the source is idle in the next frame ($\bar{q}$), the first slot of noise does not result in a false alarm ($\bar{P_{\mathcal{F}}}$), and the second slot does result in a false alarm ($P_{\mathcal{F}}$). When conditioned on a particular channel gain, these probabilities arise from random noise. Hence, the probability of this transition occurring is their product.

Finally, consider the transition from state B_3 to B_1. This transition is impossible due to the $\mathcal{F}$ event in the second slot of B_3, which dictates that the relay will transmit noise in the first slot of the next state. Thus, the probability of the transition is zero.

As long as $q \in (0,1)$, $P_{\mathcal{M}} \in (0,1)$, and $P_{\mathcal{F}} \in (0,1)$, we can say that each state in the Markov chain is *accessible* in that there is a non-zero probability of entering any state at some point in the future while originating from any other state. Thus, the Markov chain is *irreducible* under these conditions, which allows us to perform steady-state analysis of the stationary probabilities.

We can visualize the system as states with certain possible transitions between them as in Figure 2.4.

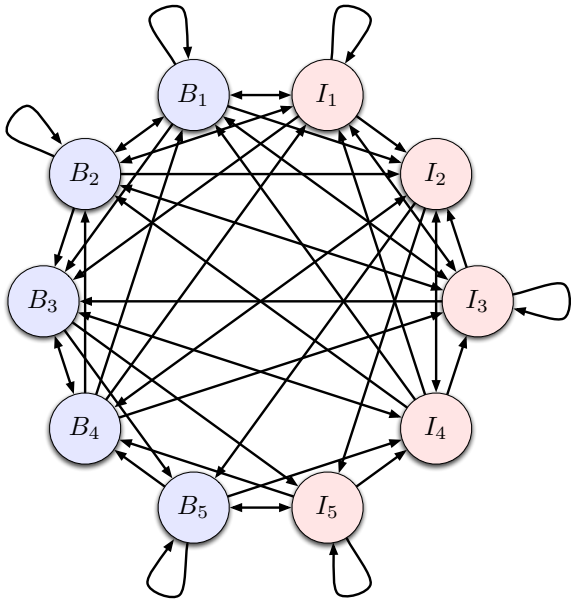

Figure 2.4: Visualization of Markov chain for OAF protocol

Finally, we can solve for the stationary probabilities of each of these states by solving the following system of equations:

$$\begin{bmatrix} B_1 & B_2 & B_3 & B_4 & B_5 & I_1 & I_2 & I_3 & I_4 & I_5 \end{bmatrix} \begin{bmatrix} & & & & & & & & & & \\ & & & & & & & & & & \\ & & & & & & & & & & \\ & & & & & & & & & & \\ & & & & & & & & & & \\ & & & & & & & & & & \\ & & & & & & & & & & \\ & & & & & & & & & & \\ & & & & & & & & & & \\ & & & & & & & & & & \end{bmatrix} \begin{bmatrix} 1 \\ 1 \\ 1 \\ 1 \\ 1 \\ 1 \\ 1 \\ 1 \\ 1 \\ 1 \end{bmatrix} = \begin{bmatrix} B_1 & B_2 & B_3 & B_4 & B_5 & I_1 & I_2 & I_3 & I_4 & I_5 & 1 \end{bmatrix}$$

Transition Probability Matrix

This problem amounts to solving a system of 11 equations for 10 unknowns, giving us a unique stationary distribution of the states in the network. While this sort of problem is straightforward to solve, the size of the matrix leads us to use a symbolic solver (such as Mathematica).

2.1.1 Results

The following expressions relate the stationary probability of each of the states to the probability of transmission, the probability of missed detections, and the probability of false alarms:

$$
\begin{aligned}
P_{B_1} &= \frac{(P_{\mathcal{F}}-1)(P_{\mathcal{M}}-1)q}{qP_{\mathcal{F}}^2-P_{\mathcal{F}}^2+P_{\mathcal{M}}qP_{\mathcal{F}}-qP_{\mathcal{F}}+1} \\
P_{B_2} &= \frac{(P_{\mathcal{F}}-1)^2P_{\mathcal{M}}q}{qP_{\mathcal{F}}^2-P_{\mathcal{F}}^2+P_{\mathcal{M}}qP_{\mathcal{F}}-qP_{\mathcal{F}}+1} \\
P_{B_3} &= -\frac{(P_{\mathcal{F}}-1)P_{\mathcal{F}}P_{\mathcal{M}}q}{qP_{\mathcal{F}}^2-P_{\mathcal{F}}^2+P_{\mathcal{M}}qP_{\mathcal{F}}-qP_{\mathcal{F}}+1} \\
P_{B_4} &= -\frac{(P_{\mathcal{F}}-1)P_{\mathcal{F}}q(qP_{\mathcal{F}}-P_{\mathcal{F}}+P_{\mathcal{M}}q-q+1)}{qP_{\mathcal{F}}^2-P_{\mathcal{F}}^2+P_{\mathcal{M}}qP_{\mathcal{F}}-qP_{\mathcal{F}}+1} \\
P_{B_5} &= \frac{P_{\mathcal{F}}^2q(qP_{\mathcal{F}}-P_{\mathcal{F}}+P_{\mathcal{M}}q-q+1)}{qP_{\mathcal{F}}^2-P_{\mathcal{F}}^2+P_{\mathcal{M}}qP_{\mathcal{F}}-qP_{\mathcal{F}}+1} \\
P_{I_1} &= \frac{(P_{\mathcal{F}}-1)^3(q-1)}{qP_{\mathcal{F}}^2-P_{\mathcal{F}}^2+P_{\mathcal{M}}qP_{\mathcal{F}}-qP_{\mathcal{F}}+1} \\
P_{I_2} &= \frac{(P_{\mathcal{F}}-1)^2P_{\mathcal{F}}(q-1)}{qP_{\mathcal{F}}^2-P_{\mathcal{F}}^2+P_{\mathcal{M}}qP_{\mathcal{F}}-qP_{\mathcal{F}}+1} \\
P_{I_3} &= \frac{(P_{\mathcal{F}}-1)P_{\mathcal{F}}(q-1)}{qP_{\mathcal{F}}^2-P_{\mathcal{F}}^2+P_{\mathcal{M}}qP_{\mathcal{F}}-qP_{\mathcal{F}}+1} \\
P_{I_4} &= \frac{(P_{\mathcal{F}}-1)P_{\mathcal{F}}(q-1)(qP_{\mathcal{F}}-P_{\mathcal{F}}+P_{\mathcal{M}}q-q+1)}{qP_{\mathcal{F}}^2-P_{\mathcal{F}}^2+P_{\mathcal{M}}qP_{\mathcal{F}}-qP_{\mathcal{F}}+1} \\
P_{I_5} &= -\frac{P_{\mathcal{F}}^2(q-1)(qP_{\mathcal{F}}-P_{\mathcal{F}}+P_{\mathcal{M}}q-q+1)}{qP_{\mathcal{F}}^2-P_{\mathcal{F}}^2+P_{\mathcal{M}}qP_{\mathcal{F}}-qP_{\mathcal{F}}+1},
\end{aligned}
$$

for $q \in (0,1)$, $P_{\mathcal{M}} \in (0,1)$, and $P_{\mathcal{F}} \in (0,1)$.

In the next sections, we will discuss each of these probabilities in context of the greater problem.

2.1.1.1 State B_1

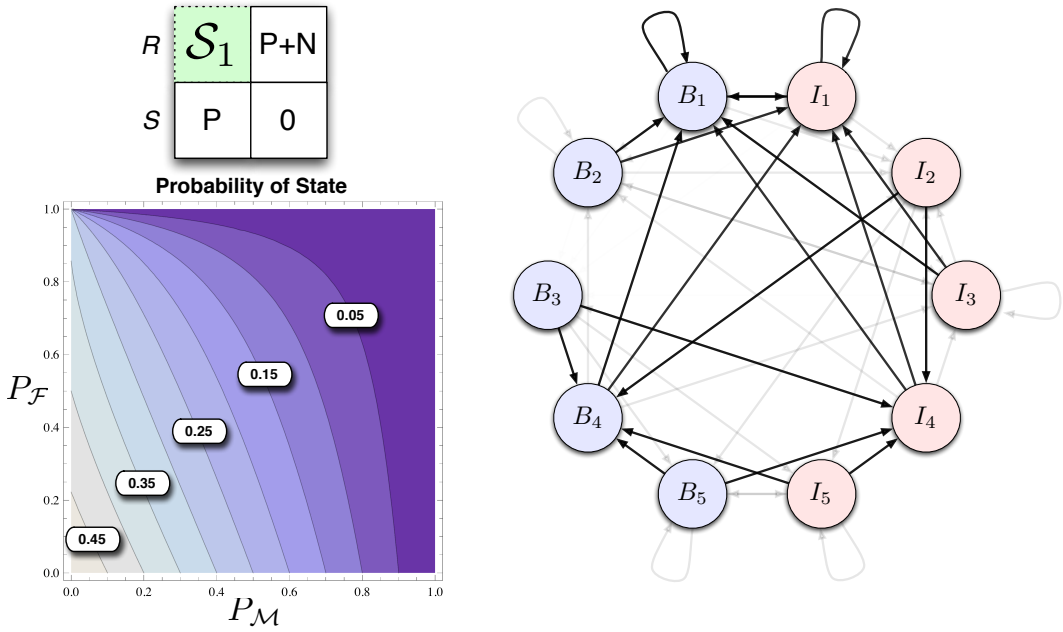

Figure 2.5: Probability of state B_1

The state B_1 represents the best case for the system where the relay successfully cooperates with the source. Figure 2.5 contains a contour plot that shows the probability of this state occurring as a function of the probability of missed detections at the relay ($P_{\mathcal{M}}$) and the probability of false alarms at the relay ($P_{\mathcal{F}}$). For this plot, as well as those in all later sections, the probability of transmission q is assumed to be $\frac{1}{2}$ without loss of generality. Intuitively, the best case state should occur most often when $P_{\mathcal{M}}$ and $P_{\mathcal{F}}$ are small. This is verified by the contour plot above that shows that the likelihood of the state approaches $\frac{1}{2}$ in the white region.

A modified state diagram is also shown in Figure 2.5, where each transition's opacity is scaled by the likelihood of it occurring given a $P_{\mathcal{M}}$ and $P_{\mathcal{F}}$ drawn from the most likely (white) region of the contour plot. Starting from any state and only following the most likely (darkest) paths, the system ends up in either B_1 or I_1. Hence, B_1 occurs whenever the source is busy, which occurs with probability $q = \frac{1}{2}$.

2.1.1.2 State B_2

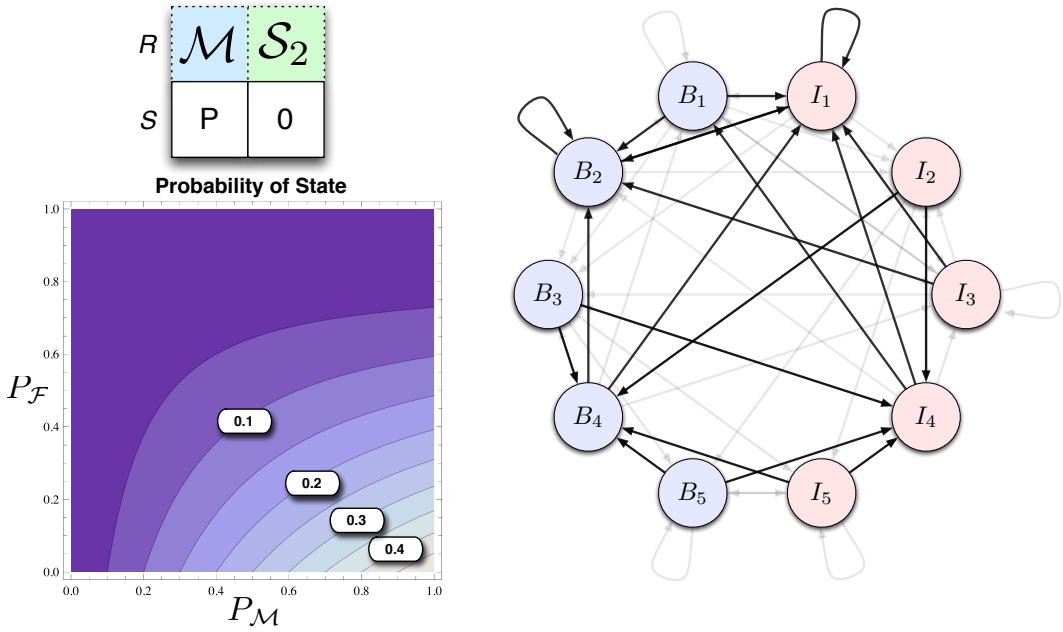

Figure 2.6: Probability of state B_2

The state B_2 represents a neutral case where the relay neither helps nor hurts the communication link. The relay misses the packet in the first slot of the frame. One would expect this event to be increasingly likely as $P_{\mathcal{M}}$ grows large, and the contour plot in Figure 2.6 confirms this. This state is also defined by a successful detection of nothing in the second slot. This event is equivalent to the statement that the second slot cannot be have a false alarm detection at the relay. Hence, the likelihood of this state increases as $P_{\mathcal{F}}$ decreases. With increasing $P_{\mathcal{M}}$ and decreasing $P_{\mathcal{F}}$, the probability of this state occurring approaches $\frac{1}{2}$ in the white region. That would mean that this state occurs whenever the source transmits.

In the opacity-modified state diagram in Figure 2.6, the steady state behavior of the system is to be in either state B_2 or I_1 when $P_{\mathcal{M}}$ and $P_{\mathcal{F}}$ are drawn from the white region of the contour plot.

2.1.1.3 State B_3

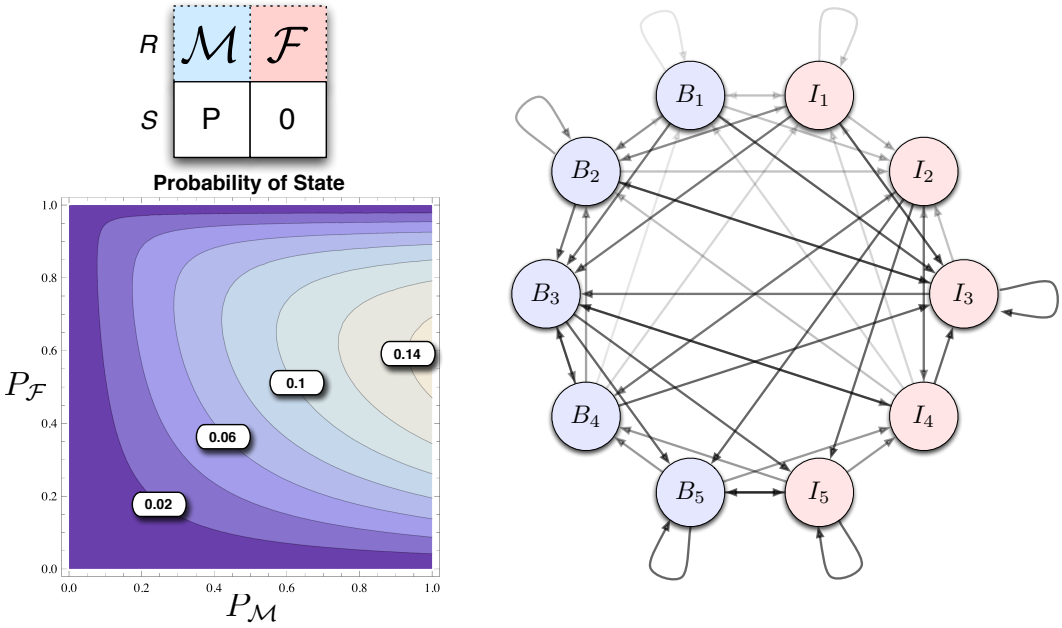

Figure 2.7: Probability of state B_3

The state B_3 represents another neutral case where the relay neither helps nor hurts the communication link. The likelihood of this state grows with $P_{\mathcal{M}}$ because the first slot is defined by a missed detection event at the relay. The likelihood of this state increases with $P_{\mathcal{F}}$ because the second slot is defined by a false alarmat the relay. However, notice that every state in the OAF protocol is characterized by the absence of a source transmission in the second slot. If $P_{\mathcal{F}}$ is too large, states that begin with the transmission of noise, and not with $P_{\mathcal{M}}$ as is needed in this state, become more likely. Hence, the maximum probability of this state occurring corresponds to a $P_{\mathcal{F}}$ that is neither too small nor too large.

Even when $P_{\mathcal{M}}$ and $P_{\mathcal{F}}$ are drawn from the white region of the contour plot, the state's likelihood is less than 0.16. As seen in state diagram of Figure 2.7, many of the state transitions are quite likely when the likelihood of the state is maximized, accounting for the state's relative rarity.

2.1.1.4 State B_4

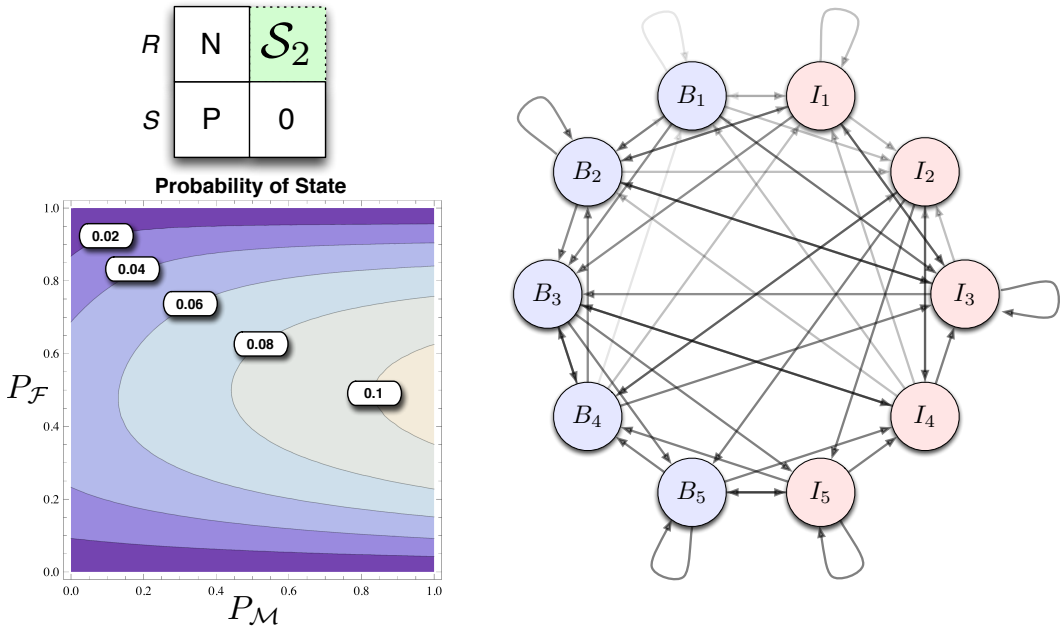

Figure 2.8: Probability of state B_4

The state B_4 represents a worst case where the relay actively deteriorates the source's transmission by transmitting noise during the same slot. This state requires that the second slot of the previous frame contain a false alarm at the relay. Assuming the previous frame is a busy frame, this can only happen when the relay misses the packet from the source. Hence, the probability of this state occurring is an increasing function of $P_{\mathcal{M}}$. This state also needs large $P_{\mathcal{F}}$ in order to account for the noise event at the relay in the first slot. However, this state needs small $P_{\mathcal{F}}$ in order to ensure an $\mathcal{S}_2$ event in the second slot. The likelihood of this state is maximized when $P_{\mathcal{F}}$ is neither too large nor too small.

Because of the tradeoff regarding $P_{\mathcal{F}}$, the overall probability of this state occurring is small. This rarity is captured by the modified state diagram in Figure 2.8 by showing that many of the state transitions are quite likely, thus reducing the stationary likelihood of any one particular state.

2.1.1.5 State B_5

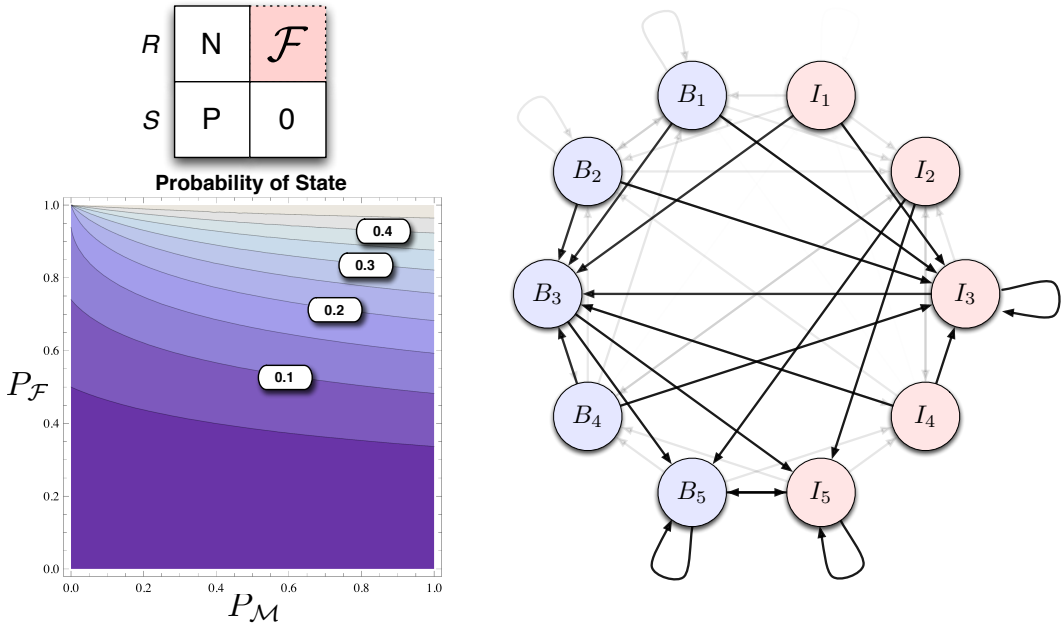

Figure 2.9: Probability of state B_5

The state B_5 represents another worst case where the relay actively deteriorates the source's transmission by transmitting noise during the same slot. False alarms not only account for the relay noise transmission event in the first slot, but also account for the false alarm event in the second slot. Thus, the likelihood of this state occurring is a strictly increasing function of $P_{\mathcal{F}}$. Like in the previously described state, missed detections make this event more likely because they increase the likelihood of a false positive in the second slot, which in turn guarantees a noise transmission during the first slot of the current frame. Thus, the likelihood is also a strictly increasing function of $P_{\mathcal{M}}$.

As shown in the state diagram of Figure 2.9, the steady state behavior of this system with $P_{\mathcal{M}}$ and $P_{\mathcal{F}}$ drawn from the white region of the contour plot is that the network spends all of its time in B_5 when the source is transmitting and I_5 when it is idle. This intuitively explains why the likelihood of the state approaches $q = \frac{1}{2}$.

2.1.1.6 State I_1

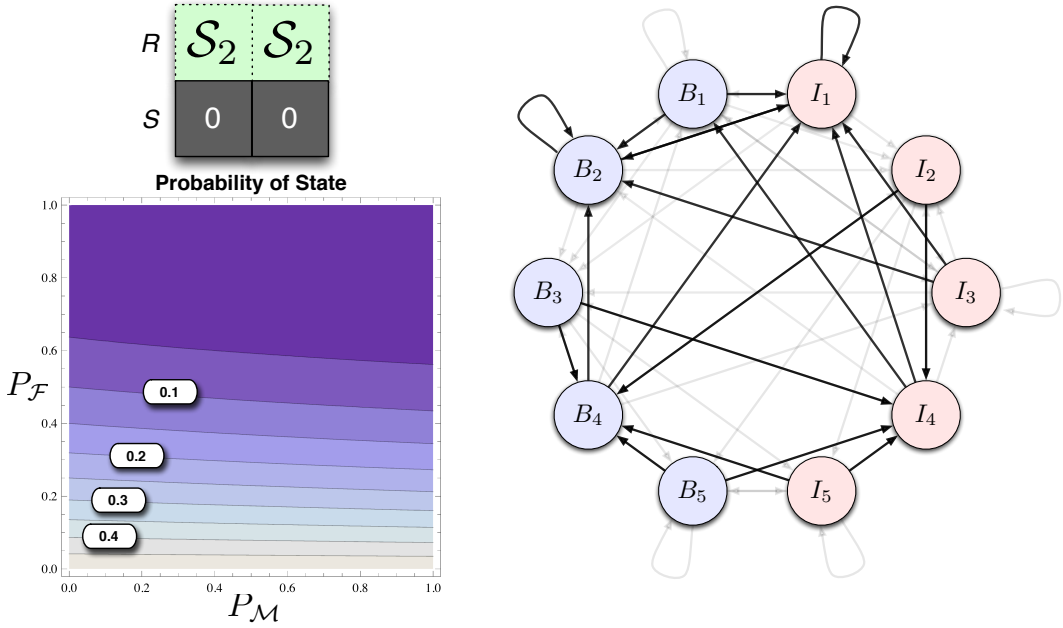

Figure 2.10: Probability of state I_1

The state I_1 represents the case where the relay successfully detects nothing in both slots. As such, a small $P_{\mathcal{F}}$ increases the likelihood of this state. $P_{\mathcal{M}}$ only relates to this likelihood in the sense that missed detections allow for false positives in the second slot of the previous frame. Because this event would make state I_1 impossible, the likelihood of this state is increased slightly with small $P_{\mathcal{M}}$.

When $P_{\mathcal{M}}$ and $P_{\mathcal{F}}$ are drawn from the white region of the contour plot, Figure 2.10 shows how the steady state behavior of the system is state I_1 when the source is idle.

2.1.1.7 State I_2

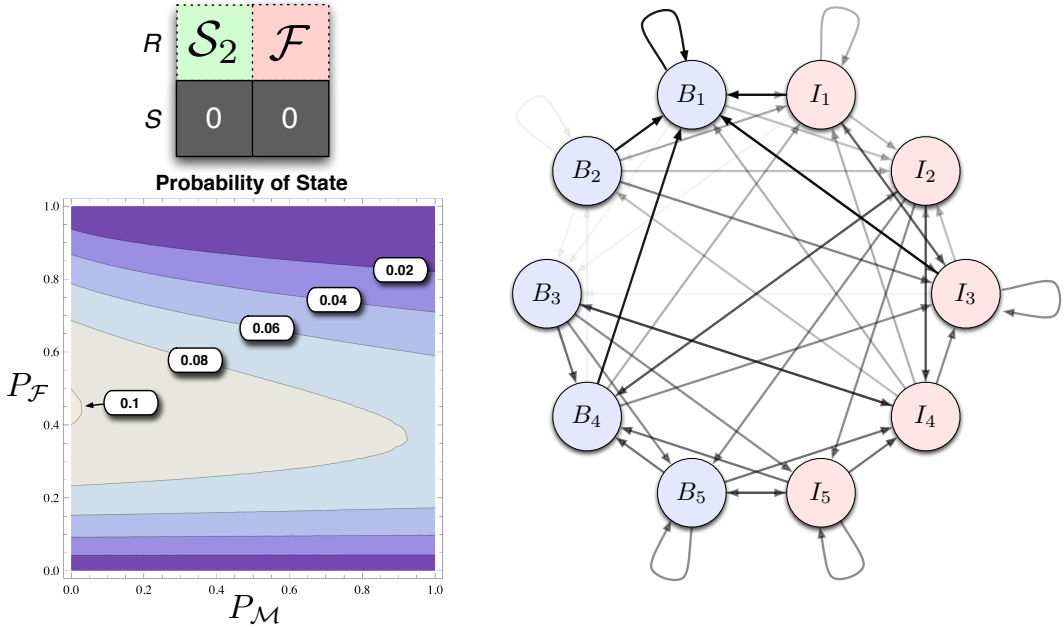

Figure 2.11: Probability of state I_2

Like state I_1, state I_2 still sees no transmissions from the relay in either slot. Also like the previous state, missed detections can only make this state less likely to occur since they increase the likelihood of false positives in the second slot of the previous frame. Hence, the probability of this state occurring increases with decreasing $P_{\mathcal{M}}$. Unlike the previous state, however, a false alarm occurs during the second slot. A large $P_{\mathcal{F}}$ makes the first slot less likely and the second slot more likely. A small $P_{\mathcal{F}}$ makes the first slot more likely and the second slot less likely. Hence, this state occurs the most when $P_{\mathcal{F}}$ is neither too large nor too small. Because of this tradeoff, the overall probability of this state is lower than many of the others in the system. This low probability is captured by Figure 2.11 in that many different state transitions are likely in the system. Thus, the likelihood of one particular state is small.

2.1.1.8 State I_3

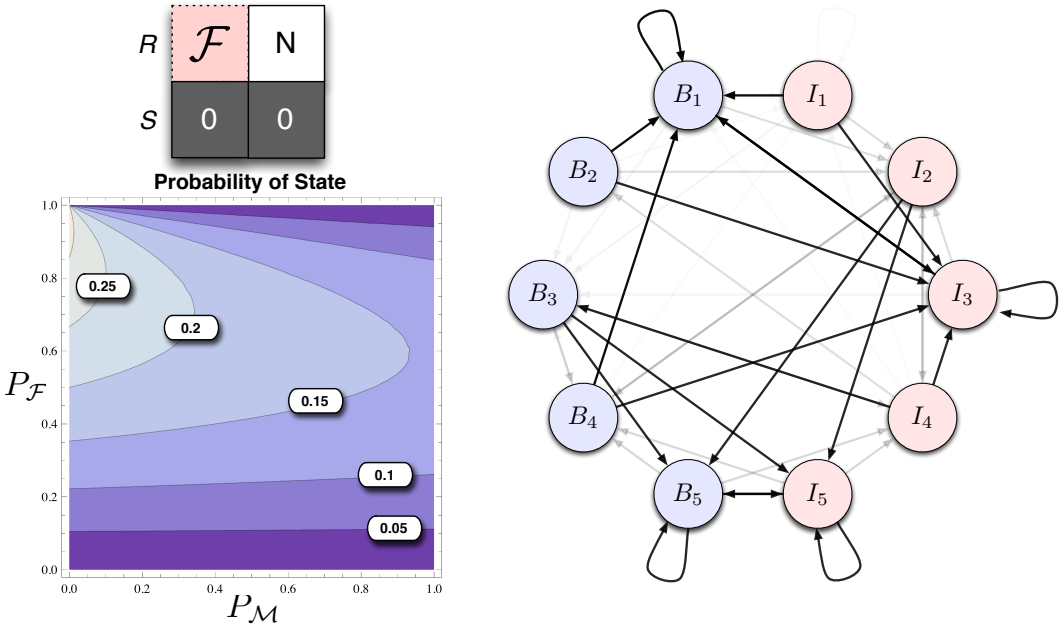

Figure 2.12: Probability of state I_3

I_3 has a sensing period during its first slot. The likelihood of having this sensing period occur increases if the likelihood of having a false alarm in the second slot of the previous frame is small. This probability, in turn, is decreased if missed detections are unlikely events because the relay is busy during the second slot of previous busy frames. Hence, this state occurs most often for small values of $P_{\mathcal{M}}$. $P_{\mathcal{F}}$ both helps and hurts the probability of this state occurring. It helps in that the first slot of this state is, in fact, an $\mathcal{F}$ event. However, the likelihood of event having a sensing event in the first slot is reduced if the second slot of the previous frame had a large $\mathcal{F}$. Additionally, with a small $P_{\mathcal{M}}$, it is very unlikely for any busy state to have an opportunity to have a false alarm in its second slot because the relay would be busy forwarding its received waveform. Busy states are more likely to enter I_3 even if $P_{\mathcal{F}}$ is large. In other words, for small $P_{\mathcal{M}}$, state I_3 is more likely to occur with a large $P_{\mathcal{F}}$ than it is for a larger $P_{\mathcal{M}}$. This effect is shown in the state diagram above.

2.1.1.9 State I_4

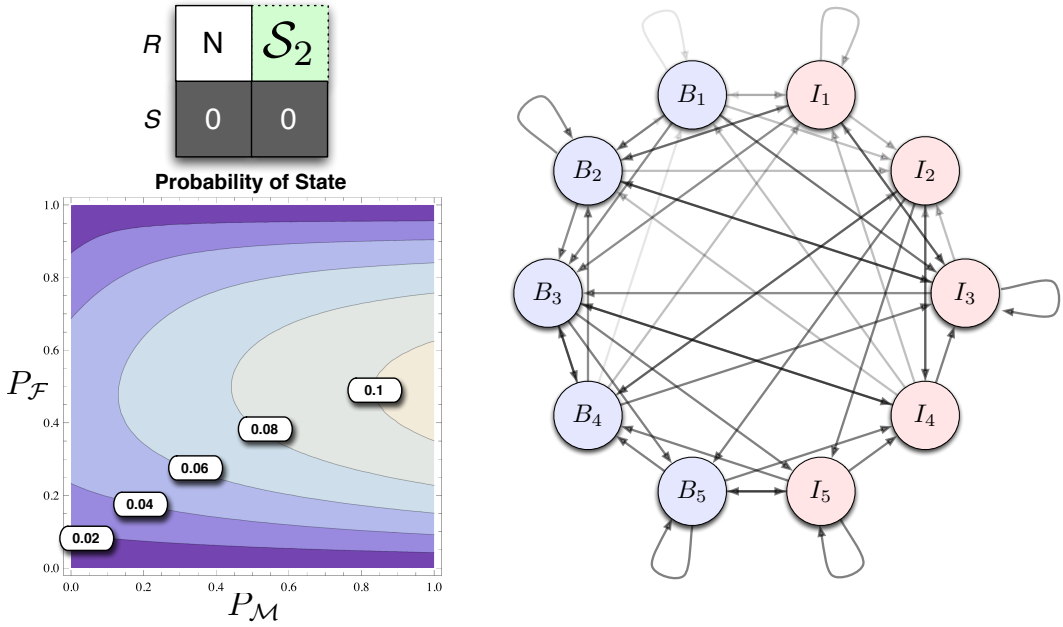

Figure 2.13: Probability of state I_4

In terms of the relay's behavior, state I_4 is very similar to state B_4. In the first slot, the relay transmits noise because of false alarm event in the second slot of the previous frame. In the second slot, the relay successfully detects that nothing was transmitted. Missed detections increase the likelihood of entering this state since they allow for the possibility of a false alarm event in the second slot of a busy state. As such, the likelihood of this state occurring increases with $P_{\mathcal{M}}$. Like in state B_4, some false alarms are required to enter this state, but some successful detections of no signal are required as well. Thus, we again see the tradeoff with regard to $P_{\mathcal{F}}$. The probability of this state occurring is maximized when $P_{\mathcal{F}}$ is neither too small nor too large. The state diagram above shows that even when the likelihood of this state is at its maximum, many other states can be reached. This confirms the fact that the overall likelihood of this state is relatively small compared to those previously mentioned.

2.1.1.10 State I_5

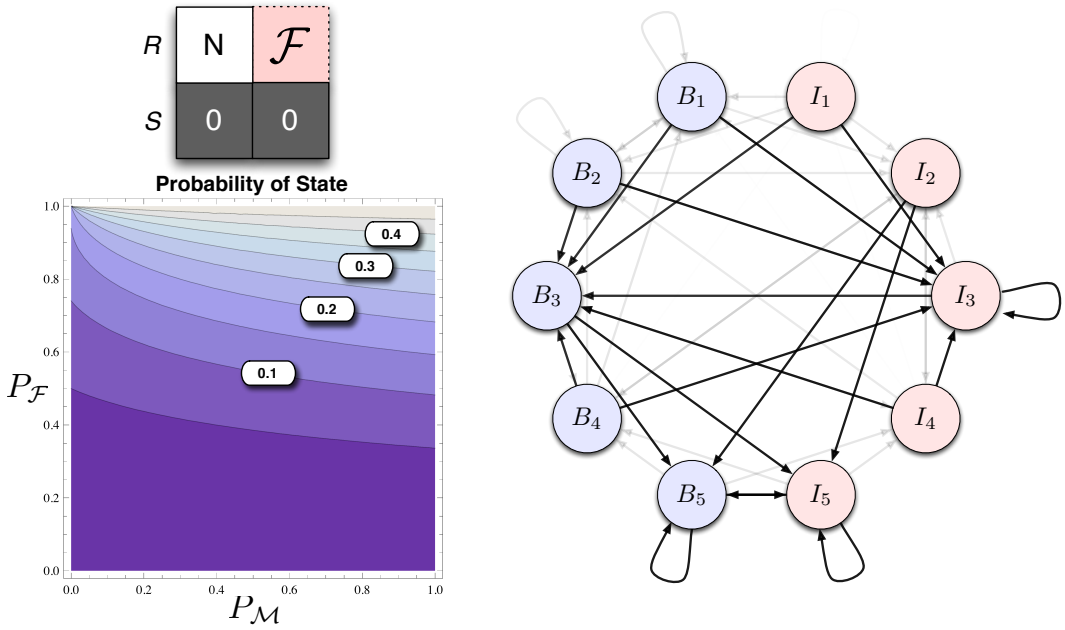

Figure 2.14: Probability of state I_5

State I_5, like state B_5, occurs more often when $P_{\mathcal{F}}$ is large. The first slot, which sees noise transmitted from the relay, implies that a false alarm has occurred in the second slot of the previous frame. Likewise, a false alarm is explicitly necessary in the second slot of this frame. The state likelihood is relatively independent of the likelihood of missed detections, provided it is not too small. A large $P_{\mathcal{M}}$ increases the likelihood of this state occurring because it allows for busy states to transition into this state. The state diagram in Figure 2.14 shows that, with high probability, the eventual state of the system is I_5 whenever the source is idle, which accounts for the probability $\bar{q} = \frac{1}{2}$ of the system being in this state.

2.2 Non-Orthogonal Amplify-and-Forward

We now describe the Non-Orthogonal Amplify-and-Forward (NAF) protocol. The assumptions underlying the model are exactly the same as the OAF protocol presented earlier: the source still contends on two-slot boundaries and the channel is assumed to be static over this duration. However, unlike the OAF protocol, the source continues to transmit at the same power level during its second slot. We assume the relay has the exact same behavior as before. In fact, the relay does not even need to know whether the system it is helping is an OAF or an NAF system. The rest of this section is dedicated to describing the various possible states that can occur in this cooperative network.

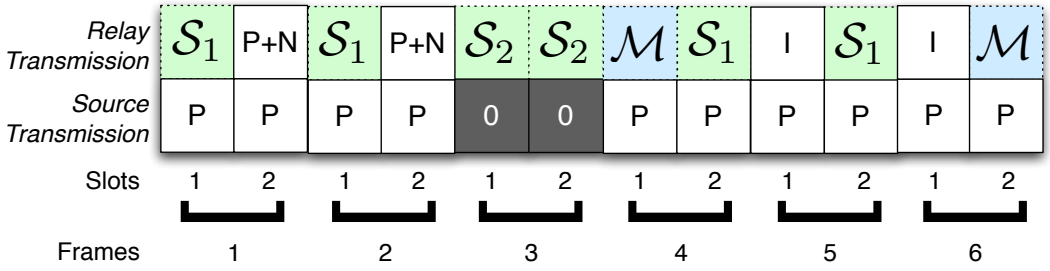

Figure 2.15: Example sequence of packet detection events and relay behavior for NAF

In Figure 2.15, we show an example sequence that can potentially occur under this protocol. A key difference between the NAF protocol and OAF protocol can be seen in the fourth frame of the above figure. In this frame, the relay misses the packet detection during the first slot, but successfully detects the presence of a source transmission in the second slot, mistaking it for the beginning of the codeword. This causes interference (denoted by I) to appear in the first slot of the next frame. In the OAF protocol, this event can never happen simply because the source never transmits during the second slot of a frame. This opens up a new class of errors that can occur in the NAF protocol, thus increasing the total number of possible states.

As shown in Figure 2.16, there are a total of 14 different states for this protocol.

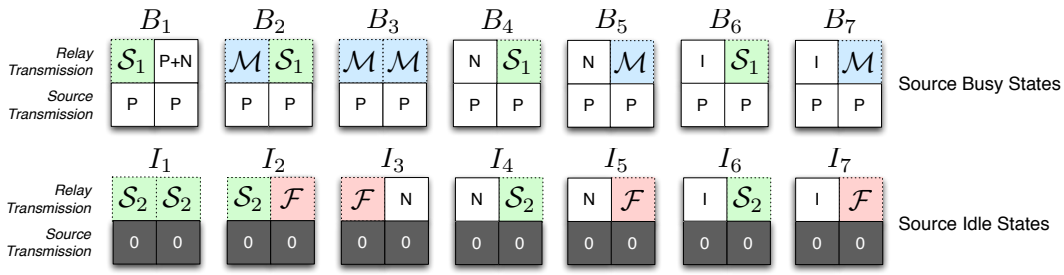

Figure 2.16: Channel states for NAF protocol

States B_1 to B_7 represent the source busy states while states I_1 to I_7 represent source idle states. Many of these states are very similar to those under the OAF protocol. For example, state B_1 under NAF is identical to B_1 under OAF in the sense of the relay's behavior. The only difference is that the source continues to transmit during the second slot. We can, again, classify the busy states based on their effect on the system from the perspective of the destination.

- **Best Case:** B_1 represents the case where the relay behaves perfectly. The relay actively helps the source communicate by forwarding its received waveform in the second slot of the frame.

- **Neutral Cases:** B_2 and B_3 represent cases where the relay neither helps nor hurts the source. In both slots of the frame, the relay senses the medium, and thus, never transmits.

- **Worst Cases:** B_4 and B_5 represent cases where the relay actively hurts the source's ability to communicate by transmitting noise during the first slot of the frame. Additionally, B_6 and B_7 represent cases where the relay actively hurts the link, but the origin of the failure is interference-driven as opposed to noise-driven.

In exactly the same way as the analysis of the OAF system before, we can build a transition probability matrix for these 14 states in order to calculate their stationary probabilities.

	B_1	B_2	B_3	B_4	B_5	B_6	B_7	I_1	I_2	I_3	I_4	I_5	I_6	I_7
B_1	$qP_{\mathcal{M}}$	$qP_{\mathcal{M}}P_{\mathcal{M}}$	$qP_{\mathcal{M}}P_{\mathcal{M}}$	0	0	0	0	$\bar{q}P_{\mathcal{F}}P_{\mathcal{F}}$	$\bar{q}P_{\mathcal{F}}P_{\mathcal{F}}$	$\bar{q}P_{\mathcal{F}}$	0	0	0	0
B_2	0	0	0	0	0	$qP_{\mathcal{M}}$	$qP_{\mathcal{M}}$	0	0	0	0	0	$\bar{q}P_{\mathcal{F}}$	$\bar{q}P_{\mathcal{F}}$
B_3	$qP_{\mathcal{M}}$	$qP_{\mathcal{M}}P_{\mathcal{M}}$	$qP_{\mathcal{M}}P_{\mathcal{M}}$	0	0	0	0	$\bar{q}P_{\mathcal{F}}P_{\mathcal{F}}$	$\bar{q}P_{\mathcal{F}}P_{\mathcal{F}}$	$\bar{q}P_{\mathcal{F}}$	0	0	0	0
B_4	0	0	0	0	0	$qP_{\mathcal{M}}$	$qP_{\mathcal{M}}$	0	0	0	0	0	$\bar{q}P_{\mathcal{F}}$	$\bar{q}P_{\mathcal{F}}$
B_5	$qP_{\mathcal{M}}$	$qP_{\mathcal{M}}P_{\mathcal{M}}$	$qP_{\mathcal{M}}P_{\mathcal{M}}$	0	0	0	0	$\bar{q}P_{\mathcal{F}}P_{\mathcal{F}}$	$\bar{q}P_{\mathcal{F}}P_{\mathcal{F}}$	$\bar{q}P_{\mathcal{F}}$	0	0	0	0
B_6	0	0	0	0	0	$qP_{\mathcal{M}}$	$qP_{\mathcal{M}}$	0	0	0	0	0	$\bar{q}P_{\mathcal{F}}$	$\bar{q}P_{\mathcal{F}}$
B_7	$qP_{\mathcal{M}}$	$qP_{\mathcal{M}}P_{\mathcal{M}}$	$qP_{\mathcal{M}}P_{\mathcal{M}}$	0	0	0	0	$\bar{q}P_{\mathcal{F}}P_{\mathcal{F}}$	$\bar{q}P_{\mathcal{F}}P_{\mathcal{F}}$	$\bar{q}P_{\mathcal{F}}$	0	0	0	0
I_1	$qP_{\mathcal{M}}$	$qP_{\mathcal{M}}P_{\mathcal{M}}$	$qP_{\mathcal{M}}P_{\mathcal{M}}$	0	0	0	0	$\bar{q}P_{\mathcal{F}}P_{\mathcal{F}}$	$\bar{q}P_{\mathcal{F}}P_{\mathcal{F}}$	$\bar{q}P_{\mathcal{F}}$	0	0	0	0
I_2	0	0	0	$qP_{\mathcal{M}}$	$qP_{\mathcal{M}}$	0	0	0	0	0	$\bar{q}P_{\mathcal{F}}$	$\bar{q}P_{\mathcal{F}}$	0	0
I_3	$qP_{\mathcal{M}}$	$qP_{\mathcal{M}}P_{\mathcal{M}}$	$qP_{\mathcal{M}}P_{\mathcal{M}}$	0	0	0	0	$\bar{q}P_{\mathcal{F}}P_{\mathcal{F}}$	$\bar{q}P_{\mathcal{F}}P_{\mathcal{F}}$	$\bar{q}P_{\mathcal{F}}$	0	0	0	0
I_4	$qP_{\mathcal{M}}$	$qP_{\mathcal{M}}P_{\mathcal{M}}$	$qP_{\mathcal{M}}P_{\mathcal{M}}$	0	0	0	0	$\bar{q}P_{\mathcal{F}}P_{\mathcal{F}}$	$\bar{q}P_{\mathcal{F}}P_{\mathcal{F}}$	$\bar{q}P_{\mathcal{F}}$	0	0	0	0
I_5	0	0	0	$qP_{\mathcal{M}}$	$qP_{\mathcal{M}}$	0	0	0	0	0	$\bar{q}P_{\mathcal{F}}$	$\bar{q}P_{\mathcal{F}}$	0	0
I_6	$qP_{\mathcal{M}}$	$qP_{\mathcal{M}}P_{\mathcal{M}}$	$qP_{\mathcal{M}}P_{\mathcal{M}}$	0	0	0	0	$\bar{q}P_{\mathcal{F}}P_{\mathcal{F}}$	$\bar{q}P_{\mathcal{F}}P_{\mathcal{F}}$	$\bar{q}P_{\mathcal{F}}$	0	0	0	0
I_7	0	0	0	$qP_{\mathcal{M}}$	$qP_{\mathcal{M}}$	0	0	0	0	0	$\bar{q}P_{\mathcal{F}}$	$\bar{q}P_{\mathcal{F}}$	0	0

Table 2.2: Labeled Markov chain probability transition matrix for NAF

The transition probabilities presented in Table 2.2 are constructed in a similar fashion to those in Table 2.1 . Like before, we will describe the construction process of several of these transitions while noting that the others follow through the same techniques.

In a case that is identical to the same case in the OAF protocol, state B_1 can transition to itself if the source transmits again (q) and the transmission is not missed ($P_{\mathcal{M}}$). These probabilities are independent, so the probability of this transition occurring is their product.

For state B_1 to transition to state B_3, the source must transmit again (q), the first slot's transmission must be missed by the relay ($P_{\mathcal{M}}$), and then the second slot's transmission must also be missed a second time to account of the second transmission from the source ($P_{\mathcal{M}}$). Given some particular channel realization, these likelihoods are independent due to noise. Hence, the likelihood of this transition occurring is their product.

Finally, for state B_1 to transition to state I_1, the source must be silent during

the next frame ($\bar{q}$), the relay must successfully detect no transmission ($\bar{P_{\mathcal{F}}}$), and the relay must successfully detect no transmission in the second slot as well ($\bar{P_{\mathcal{F}}}$). Again, given a particular channel realization, these likelihoods are independent and thus the likelihood of this transition occurring is their product.

As long as $q \in (0,1)$, $P_{\mathcal{M}} \in (0,1)$, and $P_{\mathcal{F}} \in (0,1)$ we can perform steady-state analysis of the stationary probabilities. We can visualize the system as states with certain possible transitions between them as in Figure 2.17.

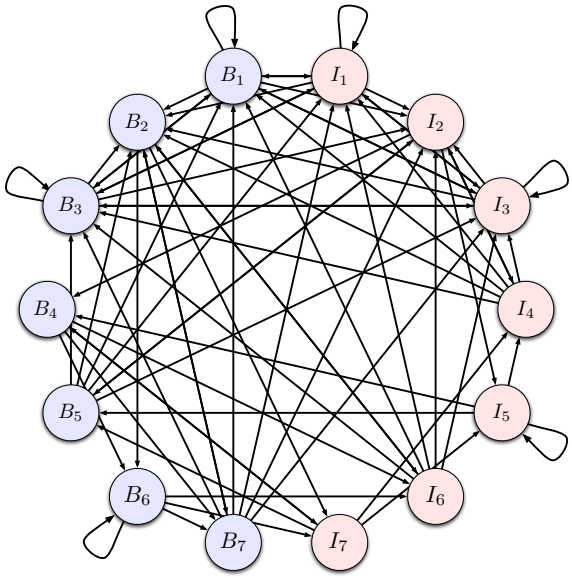

Figure 2.17: Visualization of Markov chain for NAF protocol

Finally, we can solve for the stationary probabilities of each of these states by solving the following system of equations:

$$\begin{bmatrix} B_1 & B_2 & B_3 & B_4 & B_5 & B_6 & B_7 & I_1 & I_2 & I_3 & I_4 & I_5 & I_6 & I_7 \end{bmatrix} \begin{bmatrix} \text{Transition Probability Matrix} \end{bmatrix} \begin{bmatrix} 1 \\ 1 \\ 1 \\ 1 \\ 1 \\ 1 \\ 1 \\ 1 \\ 1 \\ 1 \\ 1 \\ 1 \\ 1 \\ 1 \end{bmatrix} = \begin{bmatrix} B_1 & B_2 & B_3 & B_4 & B_5 & B_6 & B_7 & I_1 & I_2 & I_3 & I_4 & I_5 & I_6 & I_7 & 1 \end{bmatrix}$$

Solving this system of 15 equations is straightforward, but involved. Like before, we turn to symbolic solvers like Mathematica.

2.2.1 Results

The following expressions are of the stationary probability of each of the states:

$$
\begin{aligned}
P_{B_1} &= -\frac{(P_{\mathcal{M}}-1)q(qP_{\mathcal{F}}-P_{\mathcal{F}}+Pq-q+1)}{qP_{\mathcal{F}}^2-P_{\mathcal{F}}^2-P_{\mathcal{M}}^2q+2P_{\mathcal{M}}q-q+1}\\
P_{B_2} &= -\frac{(P_{\mathcal{M}}-1)P_{\mathcal{M}}q(qP_{\mathcal{F}}-P_{\mathcal{F}}+P_{\mathcal{M}}q-q+1)}{qP_{\mathcal{F}}^2-P_{\mathcal{F}}^2-P_{\mathcal{M}}^2q+2P_{\mathcal{M}}q-q+1}\\
P_{B_3} &= \frac{P_{\mathcal{M}}^2q(qP_{\mathcal{F}}-P_{\mathcal{F}}+P_{\mathcal{M}}q-q+1)}{qP_{\mathcal{F}}^2-P_{\mathcal{F}}^2-P_{\mathcal{M}}^2q+2P_{\mathcal{M}}q-q+1}\\
P_{B_4} &= -\frac{P_{\mathcal{F}}(P_{\mathcal{M}}-1)(q-1)q\left(qP_{\mathcal{M}}^2+P_{\mathcal{F}}qP_{\mathcal{M}}-2qP_{\mathcal{M}}+P_{\mathcal{F}}-P_{\mathcal{F}}q+q-1\right)}{qP_{\mathcal{F}}^2-P_{\mathcal{F}}^2-P_{\mathcal{M}}^2q+2P_{\mathcal{M}}q-q+1}\\
P_{B_5} &= \frac{P_{\mathcal{F}}P_{\mathcal{M}}(q-1)q\left(qP_{\mathcal{M}}^2+P_{\mathcal{F}}qP_{\mathcal{M}}-2qP_{\mathcal{M}}+P_{\mathcal{F}}-P_{\mathcal{F}}q+q-1\right)}{qP_{\mathcal{F}}^2-P_{\mathcal{F}}^2-P_{\mathcal{M}}^2q+2P_{\mathcal{M}}q-q+1}\\
P_{B_6} &= \frac{(P_{\mathcal{M}}-1)^2q^2\left(qP_{\mathcal{F}}^2-P_{\mathcal{F}}^2-P_{\mathcal{M}}P_{\mathcal{F}}+P_{\mathcal{M}}qP_{\mathcal{F}}-qP_{\mathcal{F}}+P_{\mathcal{F}}+P_{\mathcal{M}}\right)}{qP_{\mathcal{F}}^2-P_{\mathcal{F}}^2-P_{\mathcal{M}}^2q+2P_{\mathcal{M}}q-q+1}\\
P_{B_7} &= -\frac{(P_{\mathcal{M}}-1)P_{\mathcal{M}}q^2\left(qP_{\mathcal{F}}^2-P_{\mathcal{F}}^2-P_{\mathcal{M}}P_{\mathcal{F}}+P_{\mathcal{M}}qP_{\mathcal{F}}-qP_{\mathcal{F}}+P_{\mathcal{F}}+P_{\mathcal{M}}\right)}{qP_{\mathcal{F}}^2-P_{\mathcal{F}}^2-P_{\mathcal{M}}^2q+2P_{\mathcal{M}}q-q+1}\\
P_{I_1} &= -\frac{(P_{\mathcal{F}}-1)^2(q-1)(qP_{\mathcal{F}}-P_{\mathcal{F}}+P_{\mathcal{M}}q-q+1)}{qP_{\mathcal{F}}^2-P_{\mathcal{F}}^2-P_{\mathcal{M}}^2q+2P_{\mathcal{M}}q-q+1}\\
P_{I_2} &= \frac{(P_{\mathcal{F}}-1)P_{\mathcal{F}}(q-1)(qP_{\mathcal{F}}-P_{\mathcal{F}}+P_{\mathcal{M}}q-q+1)}{qP_{\mathcal{F}}^2-P_{\mathcal{F}}^2-P_{\mathcal{M}}^2q+2P_{\mathcal{M}}q-q+1}\\
P_{I_3} &= -\frac{P_{\mathcal{F}}(q-1)(qP_{\mathcal{F}}-P_{\mathcal{F}}+P_{\mathcal{M}}q-q+1)}{qP_{\mathcal{F}}^2-P_{\mathcal{F}}^2-P_{\mathcal{M}}^2q+2P_{\mathcal{M}}q-q+1}\\
P_{I_4} &= \frac{(P_{\mathcal{F}}-1)P_{\mathcal{F}}(q-1)^2\left(qP_{\mathcal{M}}^2+P_{\mathcal{F}}qP_{\mathcal{M}}-2qP_{\mathcal{M}}+P_{\mathcal{F}}-P_{\mathcal{F}}q+q-1\right)}{qP_{\mathcal{F}}^2-P_{\mathcal{F}}^2-P_{\mathcal{M}}^2q+2P_{\mathcal{M}}q-q+1}\\
P_{I_5} &= -\frac{P_{\mathcal{F}}^2(q-1)^2\left(qP_{\mathcal{M}}^2+P_{\mathcal{F}}qP_{\mathcal{M}}-2qP_{\mathcal{M}}+P_{\mathcal{F}}-P_{\mathcal{F}}q+q-1\right)}{qP_{\mathcal{F}}^2-P_{\mathcal{F}}^2-P_{\mathcal{M}}^2q+2P_{\mathcal{M}}q-q+1}\\
P_{I_6} &= -\frac{(P_{\mathcal{F}}-1)(P_{\mathcal{M}}-1)(q-1)q\left(qP_{\mathcal{F}}^2-P_{\mathcal{F}}^2-P_{\mathcal{M}}P_{\mathcal{F}}+P_{\mathcal{M}}qP_{\mathcal{F}}-qP_{\mathcal{F}}+P_{\mathcal{F}}+P_{\mathcal{M}}\right)}{qP_{\mathcal{F}}^2-P_{\mathcal{F}}^2-P_{\mathcal{M}}^2q+2P_{\mathcal{M}}q-q+1}\\
P_{I_7} &= \frac{P_{\mathcal{F}}(P_{\mathcal{M}}-1)(q-1)q\left(qP_{\mathcal{F}}^2-P_{\mathcal{F}}^2-P_{\mathcal{M}}P_{\mathcal{F}}+P_{\mathcal{M}}qP_{\mathcal{F}}-qP_{\mathcal{F}}+P_{\mathcal{F}}+P_{\mathcal{M}}\right)}{qP_{\mathcal{F}}^2-P_{\mathcal{F}}^2-P_{\mathcal{M}}^2q+2P_{\mathcal{M}}q-q+1},
\end{aligned}
$$

for $q \in (0,1)$, $P_{\mathcal{M}} \in (0,1)$, and $P_{\mathcal{F}} \in (0,1)$.

In the next sections, we will discuss each of these probabilities in the context of the greater problem.

2.2.1.1 State B_1

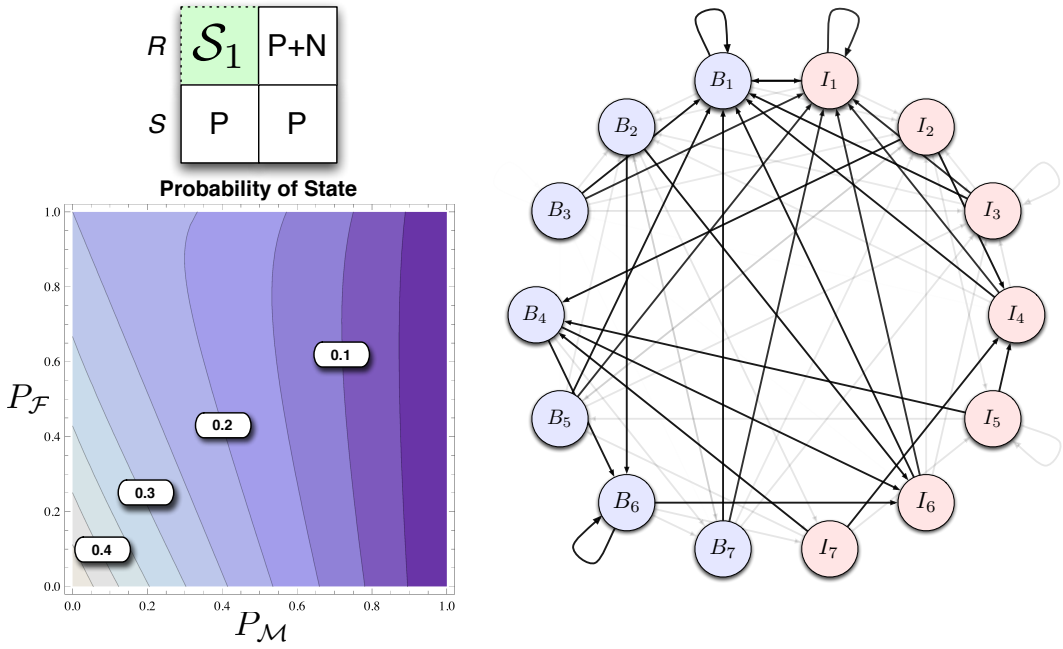

Figure 2.18: Probability of state B_1

The state B_1 represents the best case for the system where the relay successfully cooperates with the source. Therefore, we would like it to occur as often as possible. As shown in the contour plot of Figure 2.18, the highest probability happens when both $P_{\mathcal{M}}$ and $P_{\mathcal{F}}$ are low. As these error probabilities decrease, the likelihood of this state approaches $q = \frac{1}{2}$. This would mean that whenever the source decides to transmit, the network has a very high probability of being in the B_1 state.

The state diagram is also shown in Figure 2.18, where the opacity of each transition corresponds to the likelihood of it occurring for $P_{\mathcal{M}}$ and $P_{\mathcal{F}}$ drawn from the white region of the contour plot. From any given starting state, the system ends up in either state B_1 or I_1 with high probability. This implies that whenever the source has something to send, the relay helps it.

2.2.1.2 State B_2

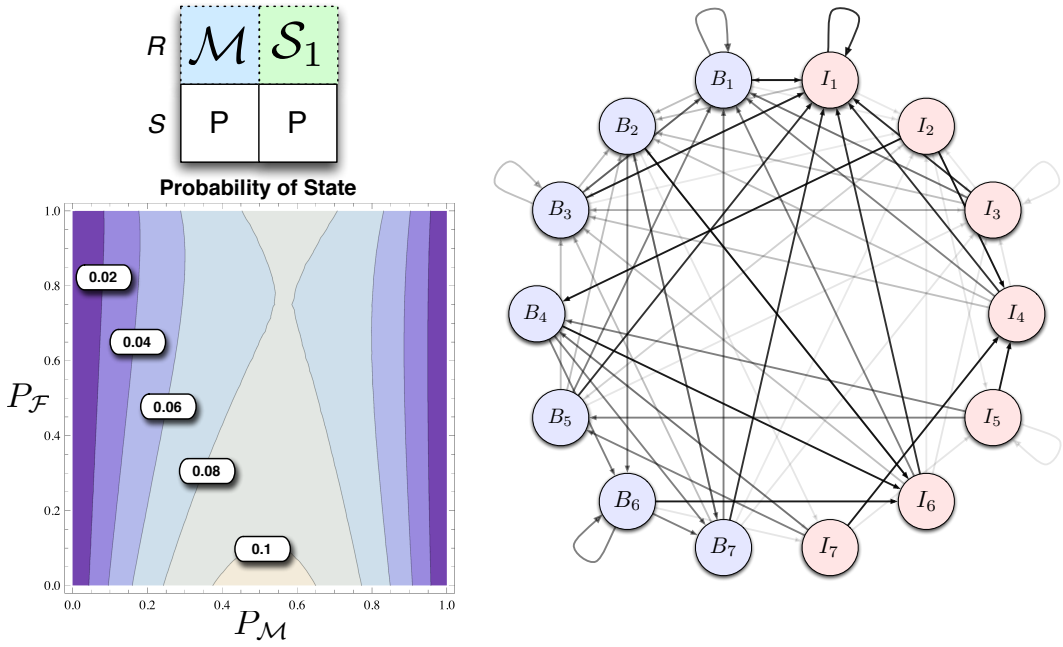

Figure 2.19: Probability of state B_2

The state B_2 represents a neutral case where the relay neither helps nor hurts the communication link. In particular, this state represents the case where the relay misses the transmission in the first slot, but successfully detects the transmission in the second slot despite the fact this is not the intended behavior of the relay. The likelihood of this state occurring is maximized when both missed detections and successful detections are as likely as possible. Hence, as the contour plot in Figure 2.19 shows, this state is most likely to occur when $P_{\mathcal{M}}$ is mid-valued. False alarm events reduce the likelihood of this event because a false alarm in the second slot of the previous frame would necessitate the relay transmitting in the first slot of this frame. Hence, the likelihood of this state occurring is maximized as $P_{\mathcal{F}}$ is decreases.

The state diagram shows that even when $P_{\mathcal{M}}$ and $P_{\mathcal{F}}$ are drawn from the white region of the contour plot, the sheer quantity of likely transitions makes the state still rather rare.

2.2.1.3 State B_3

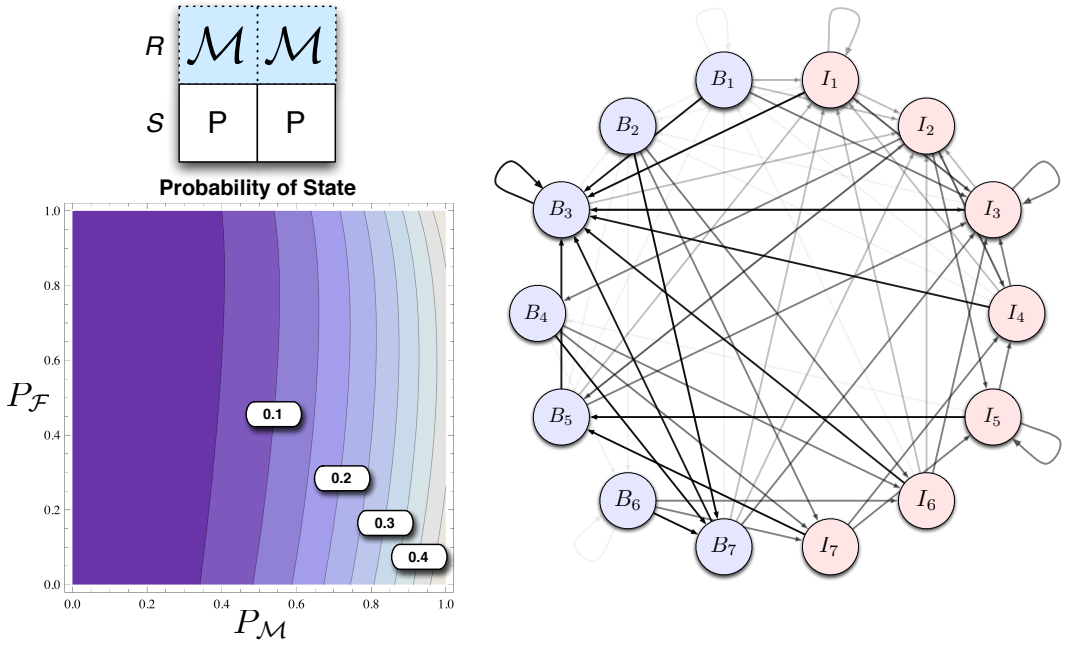

Figure 2.20: Probability of state B_3

The state B_3 represents another neutral case where the relay neither helps nor hurts the communication link. In this case, the relay fails to detect the presence of the source's transmission in both slots. For this state to occur, missed detections must be likely. Hence, we can see in Figure 2.20 that the likelihood of this state increases monotonically with $P_{\mathcal{M}}$. False alarms in the second slot of the previous frame would cause the relay to transmit in the first slot of the current frame, thereby making this state impossible. However, if $P_{\mathcal{F}}$ approaches one, the relay cannot have a false alarm in the second slot of the previous frame because it would have been busy transmitting noise that it had received from the false alarm in the first slot of the previous frame. The likelihood of this state occurring increases as $P_{\mathcal{F}}$ approaches one of its extrema.

The state diagram above shows that B_3 and I_3 form a communicating class of the Markov chain when $P_{\mathcal{M}}$ and $P_{\mathcal{F}}$ are drawn from the white region of the contour plot.

2.2.1.4 State B_4

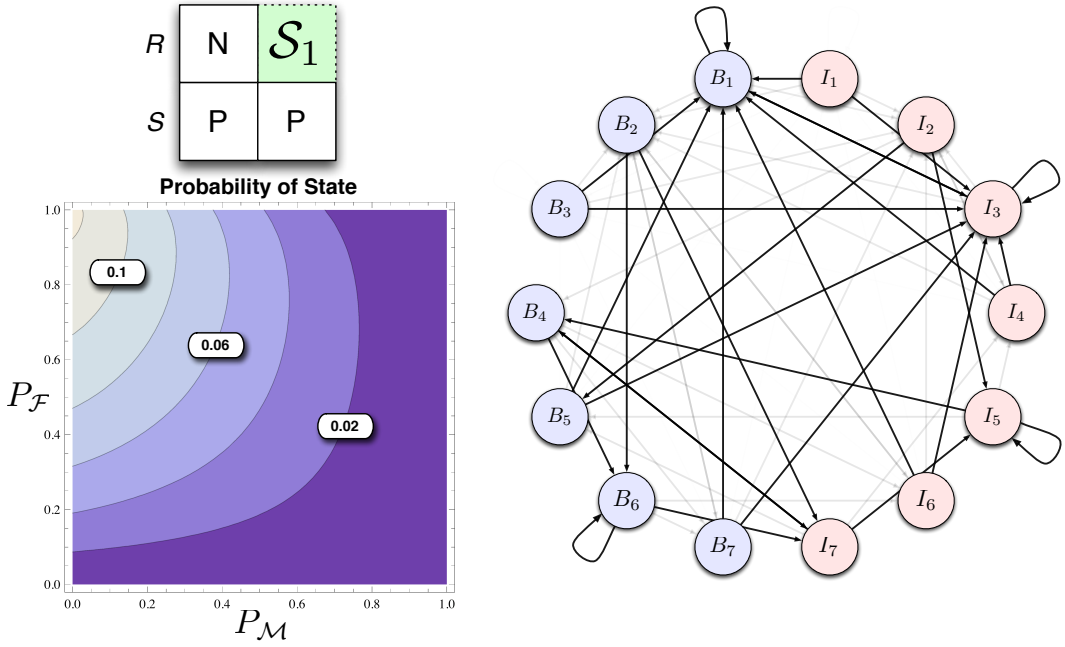

Figure 2.21: Probability of state B_4

This state is slightly different than the corresponding B_4 state of the OAF protocol. Under that protocol, the state could be entered from either a busy or idle state because both classes of states are characterized by the lack of a source transmission in the second slot. Under the NAF protocol, the only way to enter this state is via an idle state because, by definition, a false detection can not occur in the second slot of a busy state since the source is still transmitting. The likelihood of this state increases with decreasing $P_{\mathcal{M}}$ because the second slot is characterized by the successful detection of the source's transmission. The likelihood of this state increases with increasing $P_{\mathcal{F}}$ because there must be a false alarm in the second slot of the previous frame in order for this state to occur.

The state diagram above shows that B_4 is just one of many likely states when $P_{\mathcal{M}}$ and $P_{\mathcal{F}}$ approach zero and one, respectively. Because of this, the overall likelihood of this state is somewhat small.

2.2.1.5 State B_5

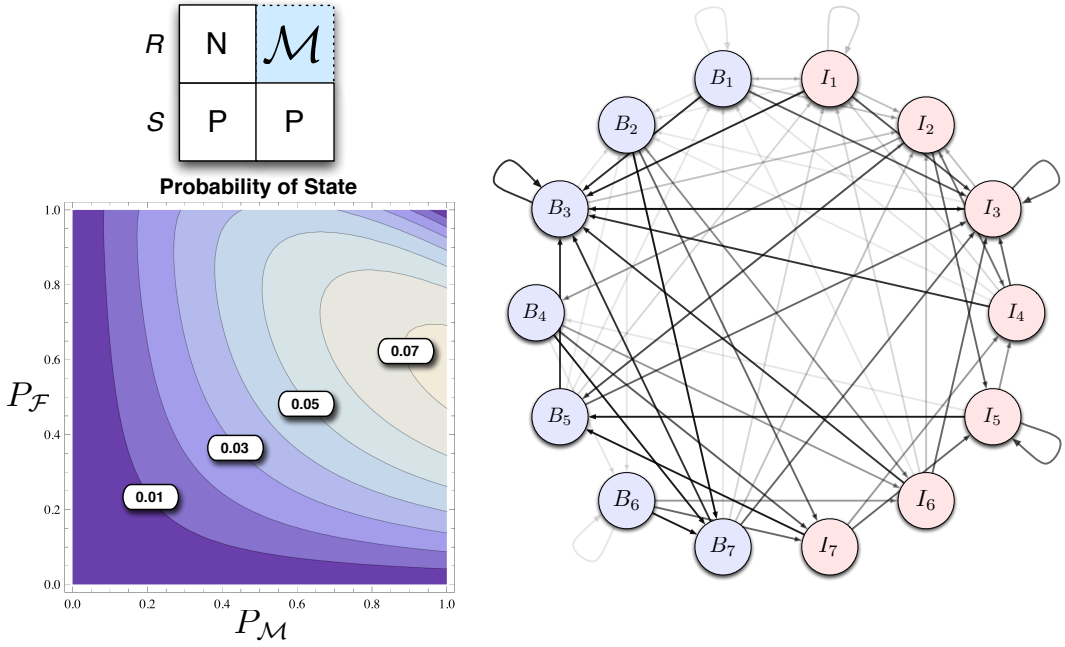

Figure 2.22: Probability of state B_5

The state B_4 represents another worst case where the relay actively deteriorates the source's transmission by transmitting noise during the same slot. In the second slot of this frame, the relay misses the source's transmission. As shown in the contour plot of Figure 2.22, the likelihood of this state increases with increasing $P_{\mathcal{M}}$. While a false alarm is necessary in the second slot of the previous frame, a false alarm in the first slot of the previous frame would make this state impossible because the relay would be busy transmitting when it would need to be sensing. Hence, we observe a tradeoff that tells us that the likelihood of this state occurring is maximized with $P_{\mathcal{F}}$ is neither too big nor too small.

The state diagram above shows this state is merely one of many valid destination states, thus accounting for its relative rarity.

2.2.1.6 State B_6

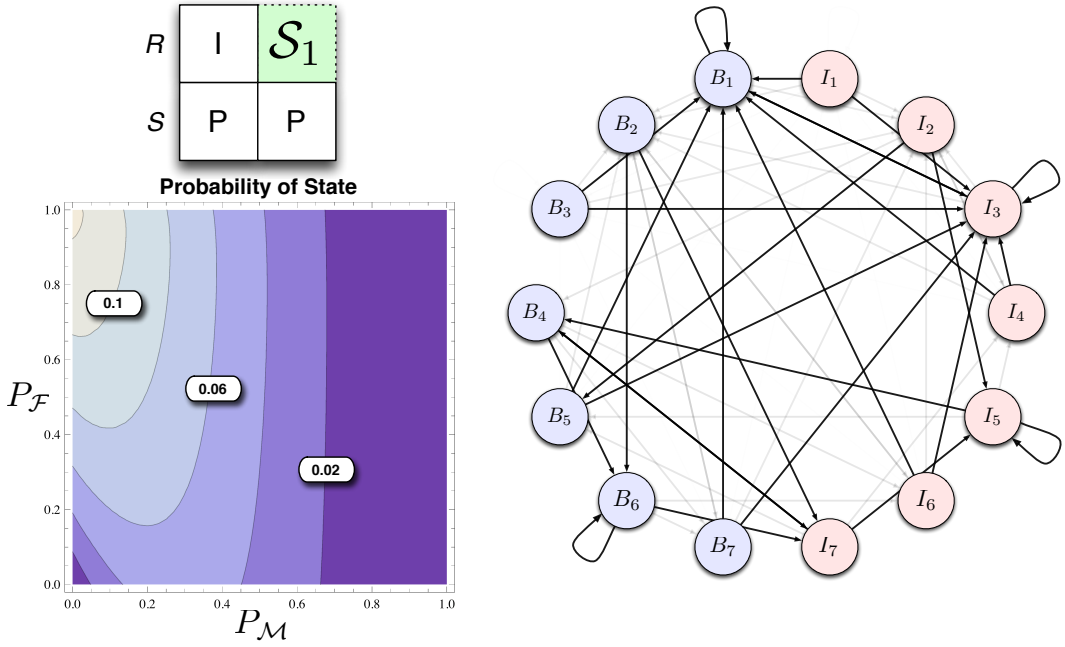

Figure 2.23: Probability of state B_6

State B_6 is similar in spirit to state B_4. They both fundamentally represent cases where the relay actively hurts the transmission between source and destination. However, the states differ in their origin. While B_4 originates from the false alarm on noise in the second slot of the previous frame, B_6 originates from the successful, but late, detection of a source's transmission in the previous frame. Hence, we label the relay's transmission as interference as opposed to noise. Because of the successful detection in the second slot of this frame, the probability of missed detections needs to be small for this state to occur. Given a small $P_{\mathcal{M}}$, the previous busy frame must have a successful detection in the second slot, which in turn requires that the relay must be busy transmitting during the first slot. Hence, the likelihood of this state increases with increasing false alarm probability.

2.2.1.7 State B_7

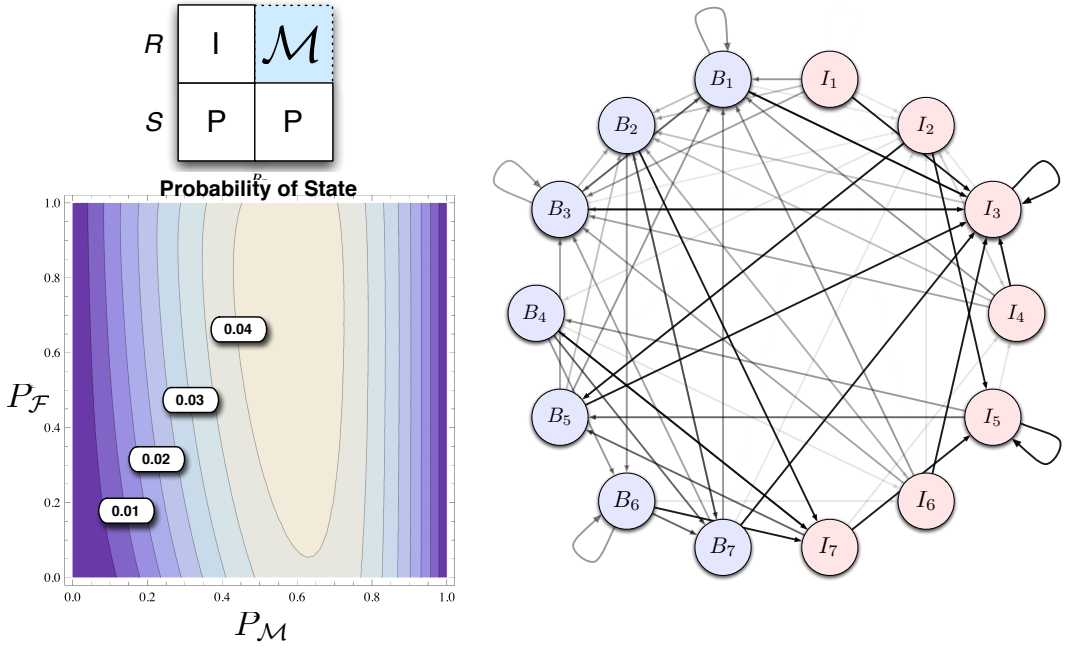

Figure 2.24: Probability of state B_7

State B_7 is to B_5 in the same way that B_6 is to B_4. The relay interferes with the source's transmission due to a detection event in the second slot of the previous frame and misses the packet in the second slot. As shown in the contour plot of Figure 2.24, the likelihood of this state is maximized when both $P_{\mathcal{M}}$ and $P_{\mathcal{F}}$ are not at their extrema. The state is defined by the presence of a missed detection in the second slot, hence $P_{\mathcal{M}}$ needs be bounded away from zero. However, a $P_{\mathcal{M}}$ that is too large makes the relay's interference unlikely since it likely would have missed the packet in the second slot of the last frame anyway. The state's likelihood is much less sensitive to $P_{\mathcal{F}}$. In the extreme case of a very small $P_{\mathcal{F}}$, this state is still possible, but the class of busy states that begin with noise transmissions from the relay are unlikely as origins since noise transmissions arise from false alarms. Also, in the extreme case of a large $P_{\mathcal{F}}$, those states are also impossible as origins since any idle state would be too busy during the second slot to even have a false alarm.

2.2.1.8 State I_1

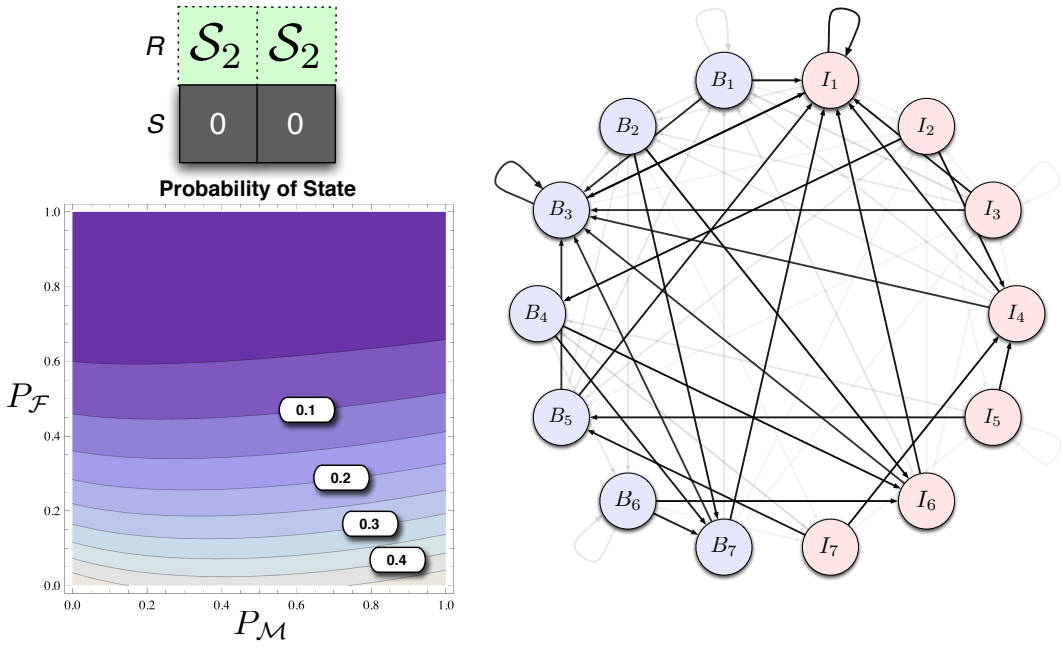

Figure 2.25: Probability of state I_1

The state I_1 represents the case where the relay recognizes that no signal is present in both slots. As shown in the contour plot of Figure 2.25, the likelihood of this state is increased with small $P_{\mathcal{F}}$. If missed detections are near-impossible, it guarantees that there cannot be interference in the first slot of the current frame simply because any previous busy state would have the relay forwarding its received waveform during the second slot instead of sensing the medium. Likewise, if missed detections are guaranteed, there cannot be interference in the first slot of the current frame because the relay would be unable to detect the presence of the packet in the second slot of the previous busy frame. Hence, as long as $P_{\mathcal{M}}$ is near one of its extremes, the likelihood of this state is high.

The state diagram shown above displays the likely transitions for when $P_{\mathcal{M}}$ and $P_{\mathcal{F}}$ are near one and zero respectively. Starting at any state, the system ends up in the communicating class of I_1 or B_3.

2.2.1.9 State I_2

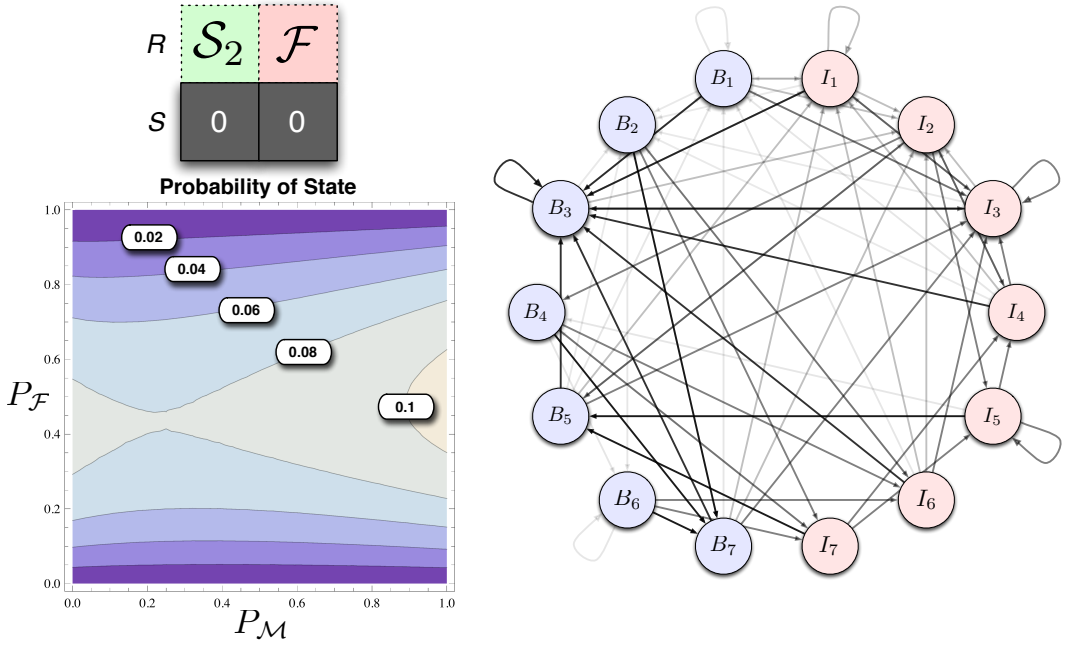

Figure 2.26: Probability of state I_2

State I_2 represents the idle case where the relay mistakes a noise event for a source transmission during the second slot, but not the first. A large $P_{\mathcal{F}}$ would make the false alarm in the second slot likely, but it would make the successful detection in the first slot unlikely. The inverse of this statement is also true. If $P_{\mathcal{M}}$ is large, interference during the first slot of the current frame is unlikely due to the same reasons argued for state I_1. However, unlike the previous state, a very small $P_{\mathcal{M}}$ is not as beneficial to this state because the fact that false alarms can occur in this setting does not eliminate the possibility that a detection event can occur in the second slot of the previous busy frame (i.e. the previous busy frame could start off with a relay noise transmission).

The above state diagram shows that, while the likelihood of this state is increased for these values of $P_{\mathcal{M}}$ and $P_{\mathcal{F}}$, the event is still rather rare due to the sheer number of valid state transitions that can occur.

2.2.1.10 State I_3

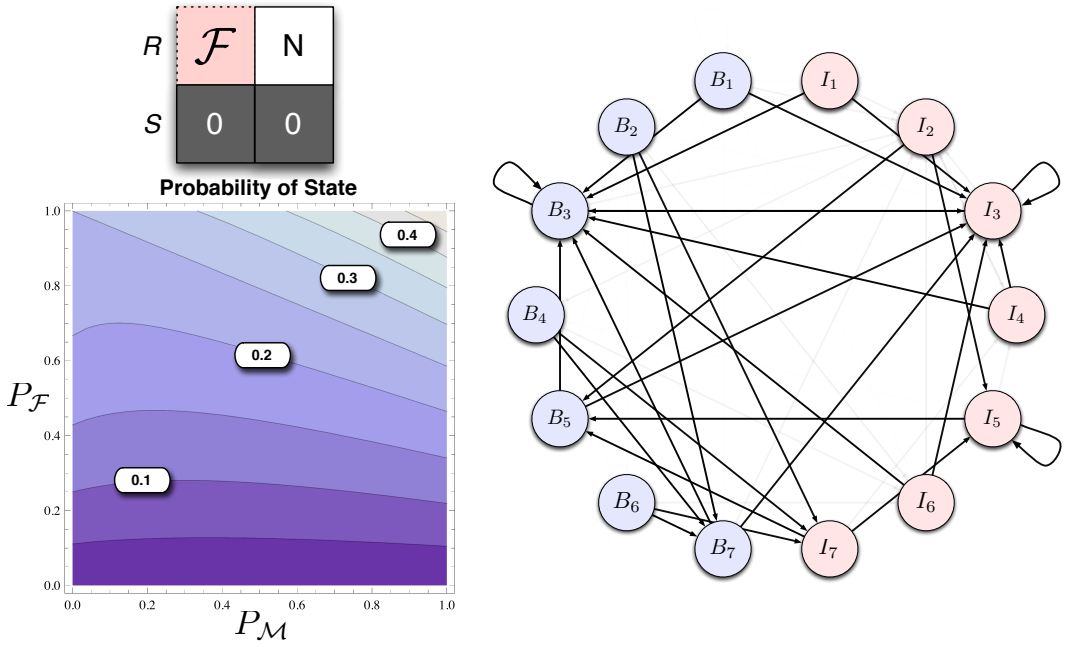

Figure 2.27: Probability of state I_3

State I_3 is an interesting state where an error occurs in packet detection at the relay, but the effects of that error do not propagate outside of this particular frame. Because the destination is assumed to be synchronized to the source, it simply does not care that this error has occurred. Intuitively, the likelihood of the state increases monotonically with $P_{\mathcal{F}}$ because a false alarm is present in the first slot of the frame. Similarly, the likelihood of the state is maximized for large $P_{\mathcal{M}}$. If the previous frame is busy, no successful detection can occur during the second slot because this event would cause interference during the first slot of the current frame.

The state diagram above shows that the system ends up in state I_3 whenever the source is idle.

2.2.1.11 State I_4

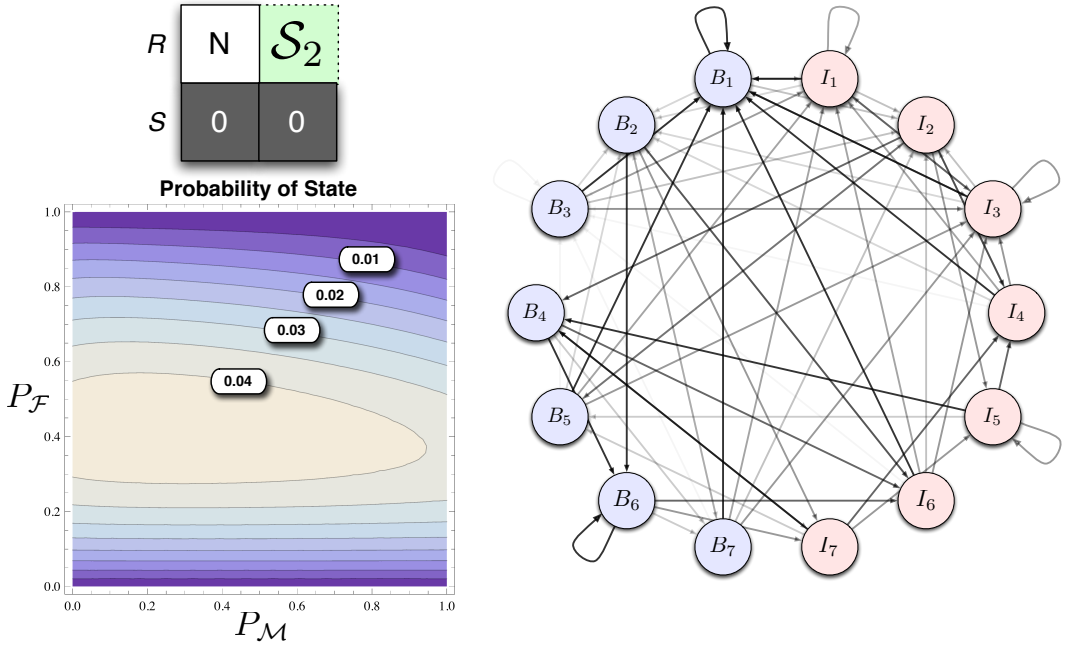

Figure 2.28: Probability of state I_4

State I_4 represents case where the relay where the relay starts off by transmitting noise from a false alarm in the previous frame. However, a false positive cannot occur in the second slot of the current frame. Because of this, the probability of this state occurring is maximized whenever $P_{\mathcal{F}}$ is neither too large nor too big. As shown in the contour plot of Figure 2.28, the likelihood of this state is largely insensitive to the probability of missed detections.

In the state diagram above, it can be seen that this state is actually quite rare. Even when $P_{\mathcal{F}}$ and $P_{\mathcal{M}}$ are drawn from the white region of the contour plot, basically every other state in the system is an equally valid destination after a transition.

2.2.1.12 State I_5

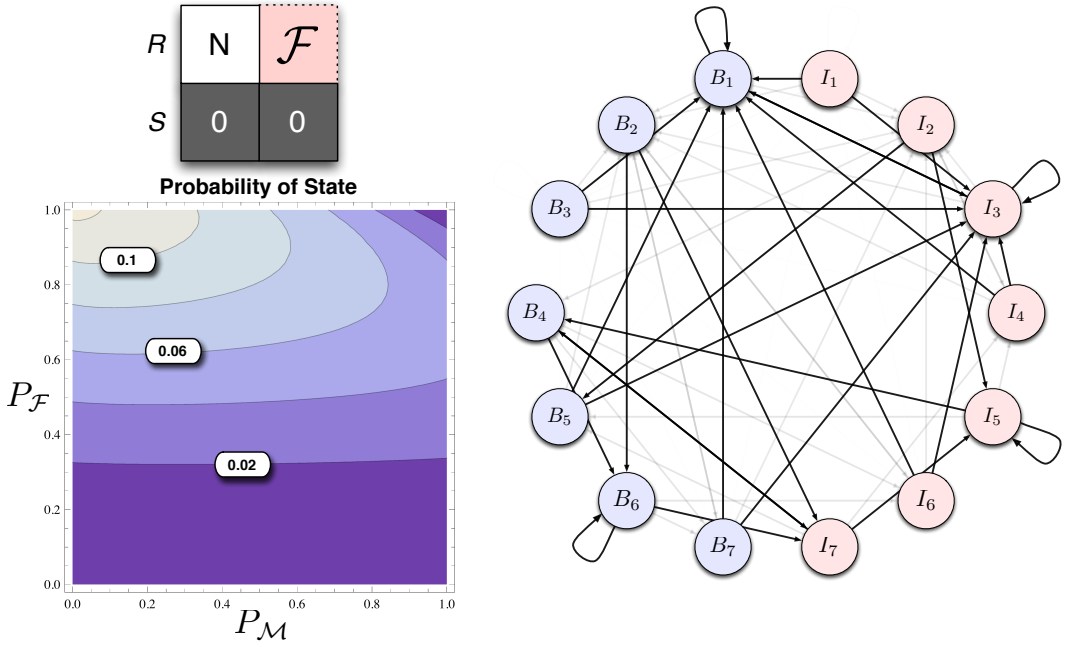

Figure 2.29: Probability of state I_5

State I_5 represents the case where the relay transmits noise during the first slot due to a previous false alarm and also has a false alarm that occurs during the second slot. These two events are well-matched in the sense that both slots positively relate to false alarms, so the overall likelihood of this event is relatively large. As shown in the contour plot of Figure 2.29, the likelihood of this state increases with $P_{\mathcal{F}}$ when $P_{\mathcal{M}}$ is small.

When $P_{\mathcal{F}}$ and $P_{\mathcal{M}}$ are drawn from the white region of the contour plot, the above state diagram shows that the only entry point into state I_5 is via states I_2, I_7, or itself. When $P_{\mathcal{M}}$ is large, the likelihood of entering state I_7 is very small (as discussed in Section 2.2.1.14). In other words, a primary entry point into this state is disabled when $P_{\mathcal{M}}$ is large, thus accounting for the decreased likelihood of state I_5 when that is the case.

2.2.1.13 State I_6

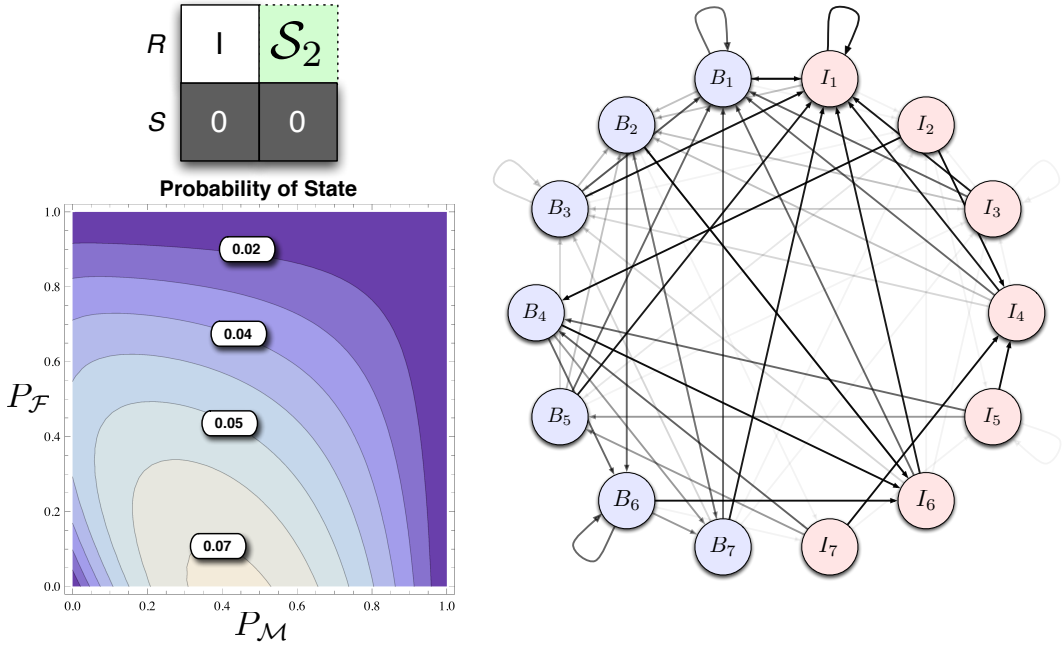

Figure 2.30: Probability of state I_6

If the relay is put into a position where it successfully detected the packet in the previous frame, but did so during the second slot instead of the first, this causes interference during the first slot of this frame. Because the second slot of this state is defined by a successful detection of silence, the likelihood of this state is maximized when $P_{\mathcal{F}}$ is small. When $P_{\mathcal{M}}$ is too large, this state is unlikely because the successful, but late, detection of the previous frame's packet is impossible. When $P_{\mathcal{M}}$ is too small, this state is unlikely because the previous frame's packet would only be detected during the first slot and not the second. Hence, we see the likelihood of this state is maximized when $P_{\mathcal{M}}$ is neither too large nor too small. This relationship to $P_{\mathcal{F}}$ and $P_{\mathcal{M}}$ is shown in the contour plot of Figure 2.30. Because of this tradeoff, the overall likelihood of this state is rather small compared to others. This is evidenced by the state diagram above, showing that many of the transitions are quite likely when $P_{\mathcal{F}}$ and $P_{\mathcal{M}}$ are chosen such that the likelihood of this state is maximized.

2.2.1.14 State I_7

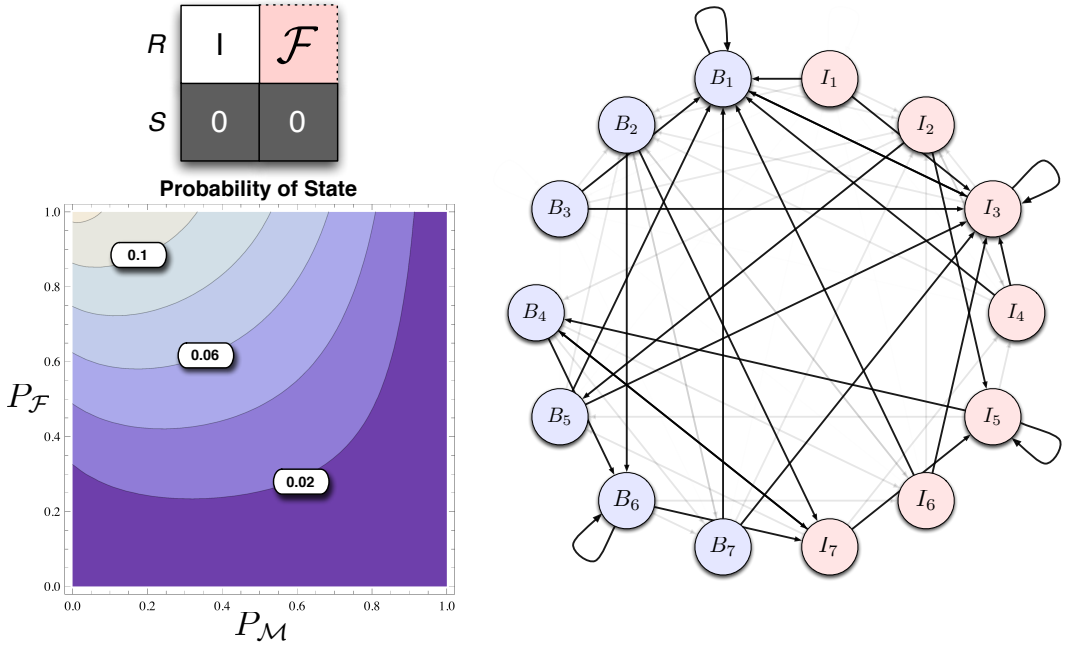

Figure 2.31: Probability of state I_7

The state I_7 begins with interference from the relay due to a successful, but late, detection of the previous frame's packet. The second slot contains a false detection at the relay as opposed to a successful detection of silence. This implies that the likelihood of this state increases with $P_{\mathcal{F}}$, and this effect is shown in the contour plot of Figure 2.31. When $P_{\mathcal{F}}$ is large, this state does not need missed detections to cause the late detections of the packet of the previous frame. After all, the detection can be late simply because of a noise transmission event during the first slot of the previous frame (e.g. state B_4). Because of this, the likelihood of this state is increased by making missed detection events very unlikely at the relay. The contour plot of Figure 2.31 shows the the likelihood of this state is maximized when $P_{\mathcal{F}}$ and $P_{\mathcal{M}}$ are large and small, respectively.

2.3 Summary

In the previous sections, we have defined all the possible network states for both the OAF and NAF protocols in this random-access environment. Additionally, the steady-state likelihoods of these states have been derived to relate the probability of a state occurring to three parameters: q (the source transmission probability), $P_{\mathcal{M}}$ (the missed packet detection probability of the relay), and $P_{\mathcal{F}}$ (the false alarm packet detection probability of the relay). These latter two error probabilities have simply been parameters in this system; the analysis thus far has been agnostic to how these parameters relate to average SNR or instantaneous channel realizations. Since we would like to be able to discuss the likelihood of these states occurring as functions of *these* parameters, we move on to studying energy detection as the particular detection mechanism.

Chapter 3

Energy Detection

In this chapter, we investigate a particular packet detection scheme that can be employed at the relay terminal.

One of the main advantages of amplify-and-forward cooperation over decode-and-forward cooperation (also presented in [8]) is the potential for reduced complexity of a relay's architecture. For amplify-and-forward, the relay is not required to decode, and hence is not required to even know what coding strategy is employed. In our analysis of random access amplify-and-forward networks, we would like to maintain as much simplicity at the relay as possible in order to stay aligned with the motivations of amplify-and-forward cooperation in the first place. As such, we consider a packet detection scheme that is agnostic to the particular coding scheme that is employed: energy detection.

In the role of packet detection, energy detection is intuitively very satisfying. If a relay detects a large amount of energy, it can decide that the source is transmitting. If a small amount of energy is detected, it might decide that the energy is only due to noise. From an implementation standpoint, this detection scheme is also attractive in that it is virtually free. All radios provide some sort of received signal strength indicator (RSSI). This entire detection scheme amounts to comparing this value to

a threshold. It should be noted that the purpose of this chapter is not to determine an optimal energy thresholding scheme. Instead, we will propose a variety schemes and show that one of them is capable of producing the desired performance without making any claims as to the uniqueness of that solution.

In this chapter, we analyze the performance of an energy detection strategy and combine the results with those from Chapter 2 to discuss the likelihood of the various states in our system as functions of average SNR.

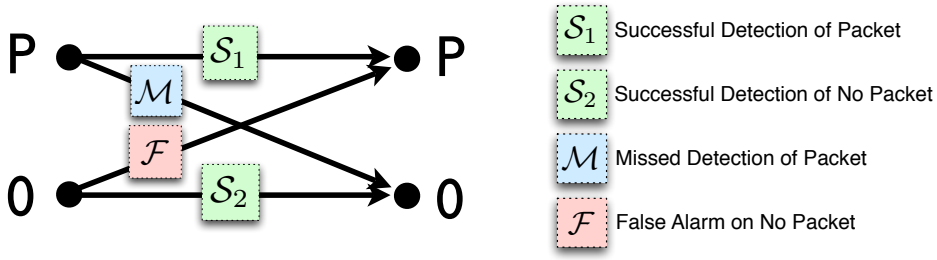

Figure 3.1: Packet detection events

In particular, we would like to analyze this energy detector in order to assign the probabilities of the packet detection events depicted again in Figure 3.1 to functions of average SNR as well as to instantaneous channel channel realizations.

Energy detection is a well-studied problem dating back to Urkowitz who studied the problem of detection of unknown, but deterministic, signals in AWGN channels [21]. In recent years, Digham has extended this work to a variety of different quasi-static fading channels [22] [23]. In this chapter, we relax the deterministic assumption in these prior works to consider energy detection of random signals. This relaxation aligns this analysis to the random-coding arguments presented in Chapters 4 and 5.

3.1 System Model and Nomenclature

Throughout this and later chapters, we adopt the following system model and nomenclature. In particular, we model the signal received by the relay as

$$y_r[n] = h_{s,r} M x_s[n] + z_r[n], \tag{3.1}$$

where $n \in \left[0, 1, 2, \ldots, \frac{L}{2}\right]$ (i.e. half of a frame), x_s is assumed to be a zero-mean, circularly symmetric Gaussian random vector of variance SNR, z_r is assumed to be a zero-mean, circularly symmetric Gaussian random vector of unit variance, and $h_{s,r}$ is the instantaneous quasi-static channel realization assumed to be constant for the duration of L. For the purposes of this chapter, the $h_{s,r}$ is assumed to be unknown to the relay. Thus, energy detection is a non-coherent detection problem.

$$M = \begin{cases} 0 & \text{source is idle} \\ 1 & \text{source is busy} \end{cases} \tag{3.2}$$

represents the source's state. With this nomenclature in place, we can construct the statistic that will be used by the energy detector to make a hard decision on the presence of a packet or lack thereof. This decision is the energy of the vector, or equivalently, the sum of squared amplitudes of the vector elements. Formally,

$$S = \sum_{n=1}^{\frac{L}{2}} |\sqrt{2} \cdot y_r[n]|^2 \tag{3.3}$$

where the $\sqrt{2}$ is simply a scaling factor that eases the notation later in the analysis. From this point, we consider the distribution on S for one of two hypotheses: nothing is sent or something is sent. We represent the hypothesis by H_M, where M is the source activity defined in Equation (3.2).

3.1.1 H_0 - Idle Source Hypothesis

Given that source is idle, we can rewrite Equation (3.1) as

$$y_r[n] = z_r[n].$$

Because we have constructed our decision statistic in Equation (3.3) with the $\sqrt{2}$ scale factor, the distribution on S under this hypothesis is simply a central Chi-square distribution with L degrees of freedom.[1] We will adopt the following notation to capture these parameters:

$$S|H_0 \sim \chi^2_L(s). \tag{3.4}$$

Because we have fixed the noise variance in this system, the distribution on S under this hypothesis does not depend on SNR or instantaneous channel realization.

3.1.2 H_1 - Busy Source Hypothesis

Given that the source is busy, we can rewrite Equation (3.1) as

$$y_r[n] = h_{s,r}x_s[n] + z_r[n].$$

Under this hypothesis, the decision statistic of Equation (3.3) is not simply a central Chi-square distribution because the variance of y_r is not normalized. Effectively, this additional variance is a scale factor on the s-axis that spreads the distribution outwards as a function of SNR and the instantaneous channel power. We notate this

[1] It should be noted that the length of the summation is only $\frac{L}{2}$, but the degrees of freedom are a full L. These extra degrees of freedom arise from the fact that the underlying Gaussian random variable is complex.

distribution as

$$S|H_1 \sim \frac{\chi^2_L\left(\frac{s}{1+|h_{s,r}|^2\text{SNR}}\right)}{1+|h_{s,r}|^2\text{SNR}}. \tag{3.5}$$

Intuitively, in the case of SNR = 0 or $|h_{s,r}|^2 = 0$, this expression reduces to the same distribution as presented in Equation (3.4). By normalizing the noise vector in this model, we have constructed the problem such that only hypothesis H_1 depends on SNR and instantaneous channel realization.

3.1.3 Probability of Packet Detection Errors

Combining Equations (3.4) and (3.4) yields

$$S \sim \begin{cases} \chi^2_L(x) & H_0 \\ \frac{\chi^2_L\left(\frac{s}{1+|h_{s,r}|^2\text{SNR}}\right)}{1+|h_{s,r}|^2\text{SNR}} & H_1 \end{cases}, \tag{3.6}$$

which represents the distribution of S for either hypothesis. With these distributions, we are finally ready to assign functions relating the probabilities of the transitions shown in Figure 3.1 to SNR and $|h_{s,r}|^2$.

3.1.3.1 Probability of False Alarm

The false alarm event represents the case where a particular noise vector has "too much" energy. More formally,

$$P_{\mathcal{F}} = Pr\{S > \Lambda | H_0\}, \tag{3.7}$$

where Λ is the decision threshold in the system. This expression is equivalent to the complement of the cumulative density function (CDF) of the distribution evaluated at Λ. Because this CDF is known for central Chi-square distributions, we can write

the probability of a false alarm event as

$$P_{\mathcal{F}} = 1 - \frac{\gamma\left(\frac{L}{2}, \frac{\Lambda}{2}\right)}{\Gamma\left(\frac{L}{2}\right)} = 1 - \mathcal{P}\left(\frac{L}{2}, \frac{\Lambda}{2}\right), \tag{3.8}$$

where γ is the lower incomplete Gamma function, Γ is the Gamma function, and $\mathcal{P}$ is the regularized Gamma function. This expression relates the probability of false alarms to the decision threshold Λ and the codeword length L.

3.1.3.2 Probability of Missed Detection

The missed detection event represents the case where a particular channel realization suppresses the source's energy below the required threshold. Formally,

$$P_{\mathcal{M}} = Pr\{S < \Lambda | H_1\}, \tag{3.9}$$

where Λ is the decision threshold in the system. This expression is the CDF of the distribution evaluated at a Λ that is scaled according to the received SNR at the relay. We write this missed detection probability as

$$P_{\mathcal{M}} = \frac{\gamma\left(\frac{L}{2}, \frac{\Lambda}{2(1+|h_{s,r}|^2\text{SNR})}\right)}{\Gamma\left(\frac{L}{2}\right)} = \mathcal{P}\left(\frac{L}{2}, \frac{\Lambda}{2\left(1+|h_{s,r}|^2\text{SNR}\right)}\right), \tag{3.10}$$

where γ is the lower incomplete Gamma function, Γ is the Gamma function, and $\mathcal{P}$ is the regularized Gamma function. This expression relates the probability of missed detections to the decision threshold Λ, the codeword length L, the average SNR, and the instantaneous channel realization $h_{s,r}$.

The remaining sections in this chapter will discuss the likelihood of the states presented in Chapter 2 as functions of average SNR for energy detection with different decision thresholding strategies at the relay.

3.1.4 Exponential Order Nomenclature

Throughout this thesis, we use a convenient shorthand to represent the exponential orders of functions of SNR. We define this shorthand in order to more concisely describe the trends of functions at large SNR values. By exponential order, we formally mean that a function $f\,(\mathrm{SNR})$ that satisfies

$$\lim_{\mathrm{SNR}\to\infty} \frac{\log f\,(\mathrm{SNR})}{\log \mathrm{SNR}} = b \tag{3.11}$$

has an exponential order of b. We denote this relationship with the shorthand

$$f\,(\mathrm{SNR}) \doteq \mathrm{SNR}^b, \tag{3.12}$$

where $\doteq$ represents "equal in exponential order." For example, $K\mathrm{SNR}^{-\alpha} \doteq \mathrm{SNR}^{-\alpha}$ for any K,α. The shorthand notations $\dot{\leq}$ and $\dot{\geq}$ are similarly defined. The use of these symbols is identical to that in Azarian's work [11].

3.2 Static Threshold Relay Detection

The first decision thresholding strategy we consider is that of static thresholds. In this case, the relay compares its received energy to a constant that is fixed for all values of average SNR.

This strategy places the threshold some fixed amount above the noise floor in the system. The effect of this can be seen in Figure 3.2. In both the small and large SNR plots, the threshold Λ is fixed to the same value. Because the probability density function (pdf) of $S|H_0$ does not depend on average SNR, the probability of false alarms is a fixed number that also does not depend on average SNR. However, with a large SNR, the probability of a missed detection is much smaller. As the pdf of $S|H_1$ spreads outwards with increasing SNR, much less area under the distribution is

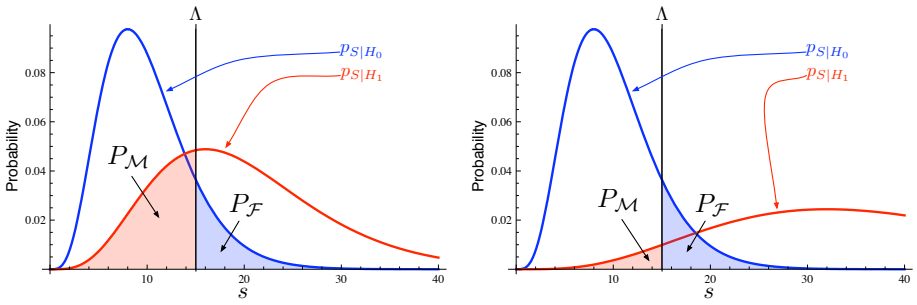

(a) Small SNR (b) Large SNR

Figure 3.2: Static threshold

in the fixed region between zero and Λ.

Formally, let

$$\Lambda = K, \tag{3.13}$$

where K is an arbitrary constant. Substituting this constant into Equations (3.8) and (3.10) yields

$$P_{\mathcal{F}} = 1 - P\left(\frac{L}{2}, \frac{K}{2}\right) \tag{3.14}$$

$$P_{\mathcal{M}} = P\left(\frac{L}{2}, \frac{K}{2\left(1 + H \cdot \mathrm{SNR}\right)}\right), \tag{3.15}$$

where $H = |h_{s,r}|^2$ is the instantaneous channel power. This substitution is merely to ease notation. These expression can be substituted for the $P_{\mathcal{F}}$ and $P_{\mathcal{M}}$ terms that appear in the equations in Sections 2.1.1 and 2.2.1. These substitutions, which we will not explicitly carry out for the sake of brevity, relate the probability of each state to three parameters: q (the source transmission probability), the average SNR, and H (the instantaneous channel power). More formally, we write this substitution as

$$P_{B_i}(q, \mathrm{SNR}, H) = P_{B_i}(P_{\mathcal{F}}, P_{\mathcal{M}}) \tag{3.16}$$

$$P_{I_i}(q, \mathrm{SNR}, H) = P_{I_i}(P_{\mathcal{F}}, P_{\mathcal{M}}), \tag{3.17}$$

where $i \in [1, 2, 3, 4, 5]$ for the OAF protocol and $i \in [1, 2, 3, 4, 5, 6, 7]$ for the NAF protocol. These expressions relate to an instantaneous channel draw and are not immediately suitable to discussing overall trends with SNR. We consider a Rayleigh fading channel model where H is distributed as an exponential random variable with rate parameter $\lambda = 1$.[1] Thus, we can average over the channel power distribution to derive expressions relating the probability of each state to a function of only average SNR and source transmission probability:

$$P_{B_i}(q, \mathrm{SNR}) = \int_0^\infty P_{B_i}(q, \mathrm{SNR}, H)\, e^{-H}\, dH \tag{3.18}$$

$$P_{I_i}(q, \mathrm{SNR}) = \int_0^\infty P_{I_i}(q, \mathrm{SNR}, H)\, e^{-H}\, dH. \tag{3.19}$$

Due to the complexity of the integrands in these expressions, these integrals are analytically intractable. However, adaptive numerical quadrature can still lend significant insights on the behavior of these states for both the OAF and NAF protocols.

3.2.1 Effect on OAF States

In this section, we discuss the effect of a static energy detection threshold on the state probabilities of the OAF protocol. In particular, we are most interested in their high-SNR behavior.

Figure 3.3(a) shows the busy state likelihoods for a small threshold of $\Lambda = 10$,

[1] This distribution comes from $|h_{s,r}|^2$ where $h_{s,r} \sim \mathcal{C}(0, 1)$, a zero-mean unit-variance circularly symmetric Gaussian random variable.

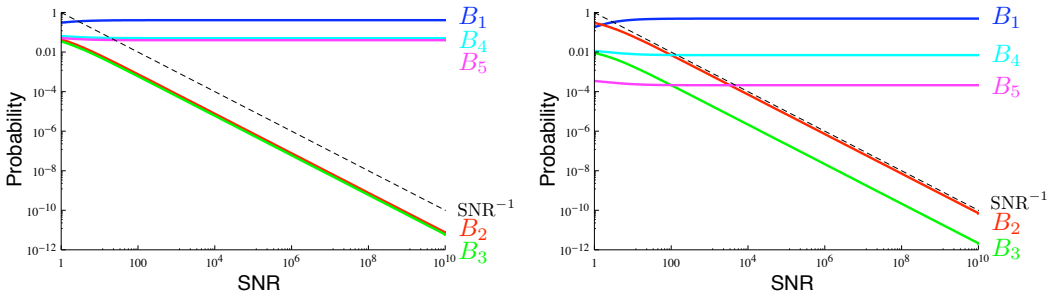

(a) $\Lambda = 10$, $q = \frac{1}{2}$, $L = 10$ (b) $\Lambda = 20$, $q = \frac{1}{2}$, $L = 10$

Figure 3.3: Likelihood of busy states for different static thresholds

while Figure 3.3(b) shows the busy state likelihoods for a larger threshold of $\Lambda = 20$. In both cases, the asymptotic behavior is the same. States B_1, B_4, B_5 do not decay in likelihood with increasing SNR. Recalling Figure 2.3, this is a good thing for B_1; it represents the best case where the relay actively helps the source's transmission. We certainly would not want its likelihood to decay with increasing SNR. However, for states B_4 and B_5, this is unfortunate; the relay actively interferes with the source's transmission due to a false alarm in the previous frame which makes them the worst cases in the system. States B_2 and B_3 decay with the same slope as SNR^{-1}.

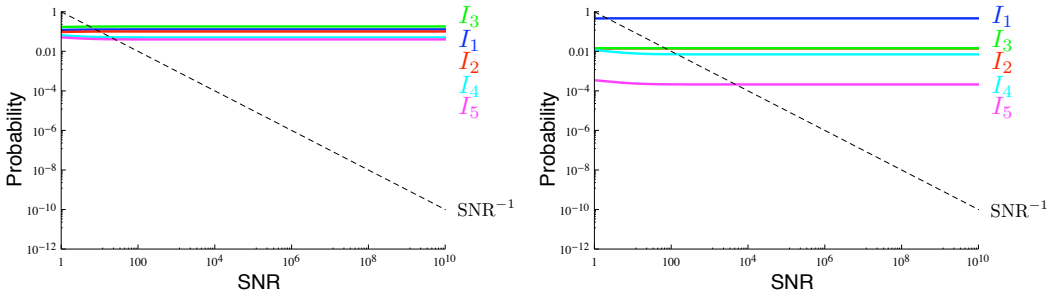

(a) $\Lambda = 10$, $q = \frac{1}{2}$, $L = 10$ (b) $\Lambda = 20$, $q = \frac{1}{2}$, $L = 10$

Figure 3.4: Likelihood of idle states for different static thresholds

Every idle state in the system does not decay in likelihood with SNR.

In summary, the probability of the OAF states for a static energy detection threshold are:

$$P_{B_1|\Lambda=K} \doteq \mathrm{SNR}^{0} \tag{3.20}$$

$$P_{B_2|\Lambda=K} \doteq \mathrm{SNR}^{-1} \tag{3.21}$$

$$P_{B_3|\Lambda=K} \doteq \mathrm{SNR}^{-1} \tag{3.22}$$

$$P_{B_4|\Lambda=K} \doteq \mathrm{SNR}^{0} \tag{3.23}$$

$$P_{B_5|\Lambda=K} \doteq \mathrm{SNR}^{0} \tag{3.24}$$

$$P_{I_1|\Lambda=K} \doteq \mathrm{SNR}^{0} \tag{3.25}$$

$$P_{I_2|\Lambda=K} \doteq \mathrm{SNR}^{0} \tag{3.26}$$

$$P_{I_3|\Lambda=K} \doteq \mathrm{SNR}^{0} \tag{3.27}$$

$$P_{I_4|\Lambda=K} \doteq \mathrm{SNR}^{0} \tag{3.28}$$

$$P_{I_5|\Lambda=K} \doteq \mathrm{SNR}^{0}, \tag{3.29}$$

where $\doteq$ is the shorthand notation defined in Section 3.1.4. The salient point here is that some error states do not decay with SNR.

3.2.2 Effect on NAF States

In this section, we analyze the effects of static threshold energy detection on the likelihood of states under the NAF protocol.

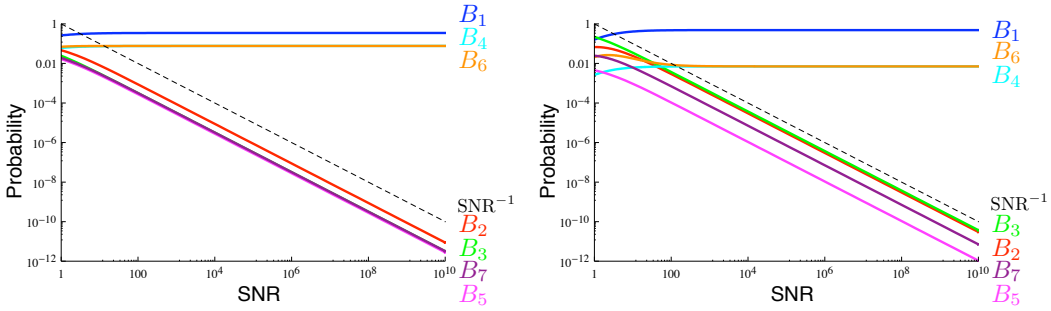

(a) $\Lambda = 10$, $q = \frac{1}{2}$, $L = 10$ (b) $\Lambda = 20$, $q = \frac{1}{2}$, $L = 10$

Figure 3.5: Likelihood of busy states for different static thresholds

We can immediately observe that, regardless of the particular static threshold value, states B_1, B_4, and B_6 do not decay in likelihood with SNR. Like under the OAF protocol, these states represent the best case and two of the worst cases respectively.

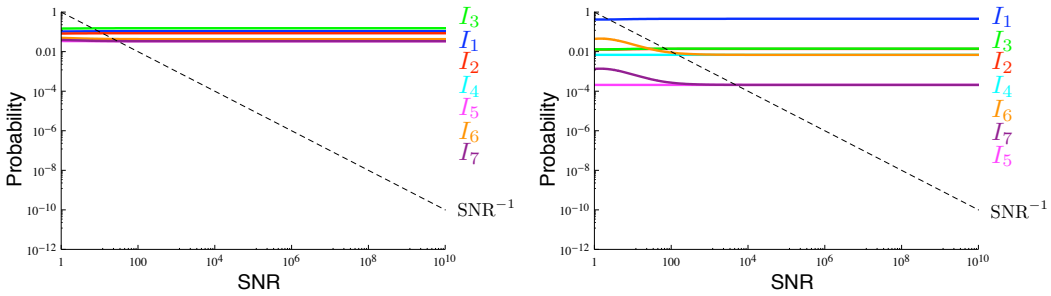

(a) $\Lambda = 10$, $q = \frac{1}{2}$, $L = 10$ (b) $\Lambda = 20$, $q = \frac{1}{2}$, $L = 10$

Figure 3.6: Likelihood of idle states for different static thresholds

Also similar to the OAF protocol, the likelihood of the idle states do not decay with SNR.

In summary, the probability of the NAF states for a static energy detection threshold are:

$$P_{B_1|\Lambda=K} \doteq \mathrm{SNR}^{0} \tag{3.30}$$

$$P_{B_2|\Lambda=K} \doteq \mathrm{SNR}^{-1} \tag{3.31}$$

$$P_{B_3|\Lambda=K} \doteq \mathrm{SNR}^{-1} \tag{3.32}$$

$$P_{B_4|\Lambda=K} \doteq \mathrm{SNR}^{0} \tag{3.33}$$

$$P_{B_5|\Lambda=K} \doteq \mathrm{SNR}^{-1} \tag{3.34}$$

$$P_{B_6|\Lambda=K} \doteq \mathrm{SNR}^{0} \tag{3.35}$$

$$P_{B_7|\Lambda=K} \doteq \mathrm{SNR}^{-1} \tag{3.36}$$

$$P_{I_1|\Lambda=K} \doteq \mathrm{SNR}^{0} \tag{3.37}$$

$$P_{I_2|\Lambda=K} \doteq \mathrm{SNR}^{0} \tag{3.38}$$

$$P_{I_3|\Lambda=K} \doteq \mathrm{SNR}^{0} \tag{3.39}$$

$$P_{I_4|\Lambda=K} \doteq \mathrm{SNR}^{0} \tag{3.40}$$

$$P_{I_5|\Lambda=K} \doteq \mathrm{SNR}^{0} \tag{3.41}$$

$$P_{I_6|\Lambda=K} \doteq \mathrm{SNR}^{0} \tag{3.42}$$

$$P_{I_7|\Lambda=K} \doteq \mathrm{SNR}^{0}. \tag{3.43}$$

The salient point here is that some error states do not decay with SNR.

3.3 Dynamic Threshold Relay Detection

We now consider a different class of energy thresholding strategies at the relay. In this class, we assume the relay has access to the average SNR parameter in the system so it can adaptively shift its energy threshold with that parameter. In the three-node scenario we are studying, this is reasonable to assume. However, in more complicated topologies, this assumption is more problematic. While we will not explicitly study any such topologies in this work, it is worthwhile to briefly describe the additional complexities that will be faced in this extension. For example, consider a multiple source system where path loss (i.e. large-scale fading) is considered.

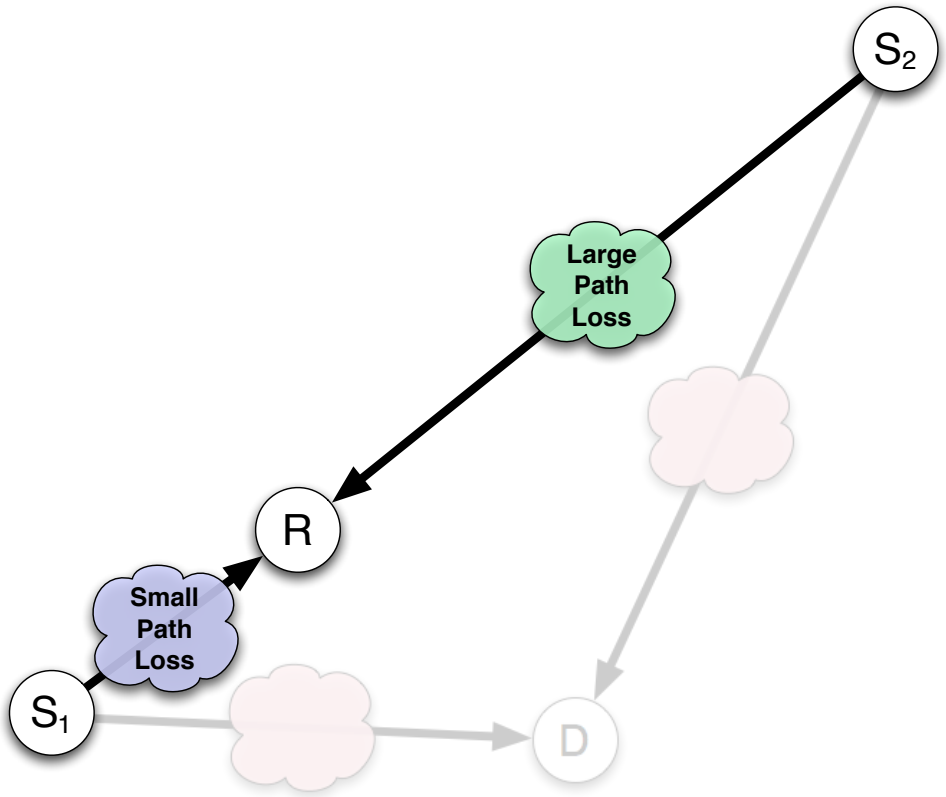

Figure 3.7: Path Loss scenario

In this scenario, one source is significantly closer to the relay than the other source. The effective received average SNR is larger for one source than the other. Because this is a random access system, the relay does not know which source, if any, will be

transmitting in the immediate future. As such, it cannot know the average SNR *a priori* without an additional handshaking protocol to tell the relay which source it will be helping, and thus the average SNR it can expect. In the work presented in this thesis, we do not consider what such a protocol would be, but rather acknowledge that any gains associated with a dynamic energy detection threshold should be weighed against the increased overhead of the system.

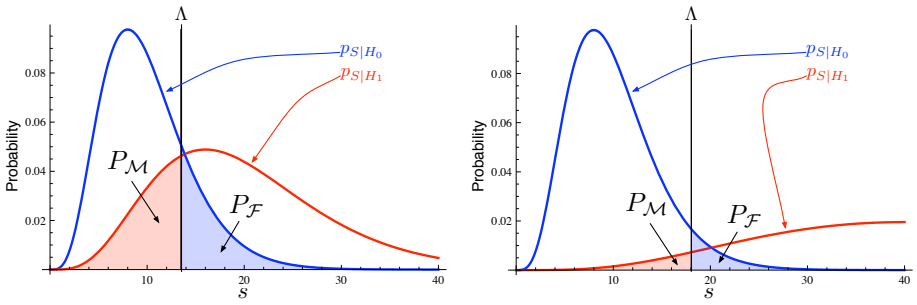

(a) Small SNR (b) Large SNR

Figure 3.8: Dynamic threshold

The effect of a dynamic energy detection threshold can be seen in Figure 3.3. In the large SNR plot, the threshold Λ is shifted further right. This effectively scales both $P_{\mathcal{M}}$ and $P_{\mathcal{F}}$ as functions of SNR. Specifically, we consider two specific forms of dynamic energy detection thresholds. The first form is that of

$$\Lambda = K_1 + K_2 \cdot \log\left(1 + \text{SNR}\right), \tag{3.44}$$

where K_1 and K_2 are arbitrary constants, and log is the natural logarithm.[1] We will describe this strategy with logarithmic dependence on SNR as a "slow" dynamic threshold.

The next strategy we consider is that of

$$\Lambda = K_1 + K_2 \cdot \text{SNR}, \tag{3.45}$$

[1]Unless otherwise stated, all logarithms in this thesis are base-e

where K_1 and K_2 are arbitrary constants. Analogously, this strategy will be known as a "fast" dynamic threshold due the lack of the logarithm.

In precisely the same way as the static threshold analysis, these decision thresholds can be substituted into Equations (3.8) and (3.10) to yield expressions that relate the probabilities of packet detection errors to average SNR as well as instantaneous channel realizations. Those expressions, in turn, can be substituted into the state probability expressions of Sections 2.1.1 and 2.2.1 and then numerically integrated over channel realizations.

3.3.1 Effect on OAF States

In this section, we discuss the effect of the different dynamic energy threshold strategies on the state probabilities of the OAF protocol.

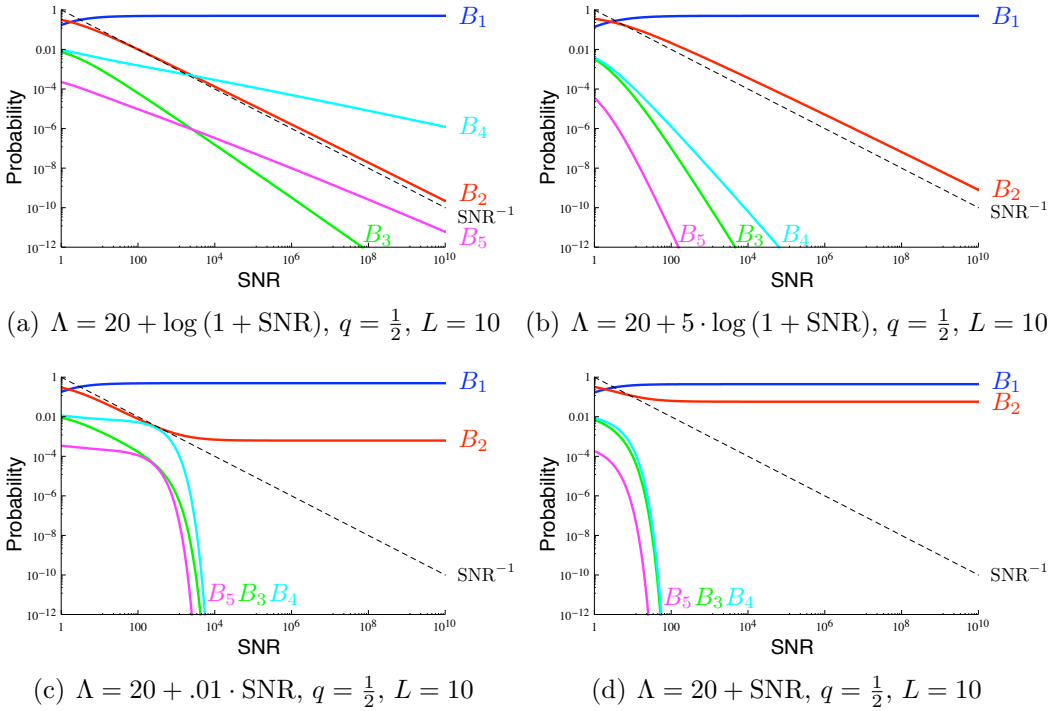

(a) $\Lambda = 20 + \log(1 + \text{SNR})$, $q = \frac{1}{2}$, $L = 10$ (b) $\Lambda = 20 + 5 \cdot \log(1 + \text{SNR})$, $q = \frac{1}{2}$, $L = 10$

(c) $\Lambda = 20 + .01 \cdot \text{SNR}$, $q = \frac{1}{2}$, $L = 10$ (d) $\Lambda = 20 + \text{SNR}$, $q = \frac{1}{2}$, $L = 10$

Figure 3.9: Likelihood of busy states for different dynamic thresholds

As can be seen in Figure 3.3.1, these different strategies each produce radically different behaviors in the dependence of the state likelihoods on average SNR. Figures 3.9(a) and 3.9(b) show two examples of the "slow" dynamic threshold strategy presented in Equation (3.44). In Figure 3.9(a), we see that, while B_4 and B_5 at least decay somewhat with average SNR, they still decay slower than an exponential order of one. By increasing the K_2 parameter of Equation (3.44), we see that these states can decay arbitrarily fast in Figure 3.9(b). In fact, the only parameter-independent exponential orders in the system are associated with B_1, which does not decay, and B_2, which decays with an exponential order of one.

In Figures 3.9(c) and 3.9(d), the "fast" dynamic threshold is employed at the

relay. The effect can be seen in states B_3, B_4, and B_5. These are all suboptimal states where the relay is not helping the system, and they all decay exponentially fast with SNR. However, state B_2 does not decay at all. In effect, the fast dynamic threshold is simply too fast. It makes some error states disappear very quickly but only at the cost of making another error state remain even at high SNR values.

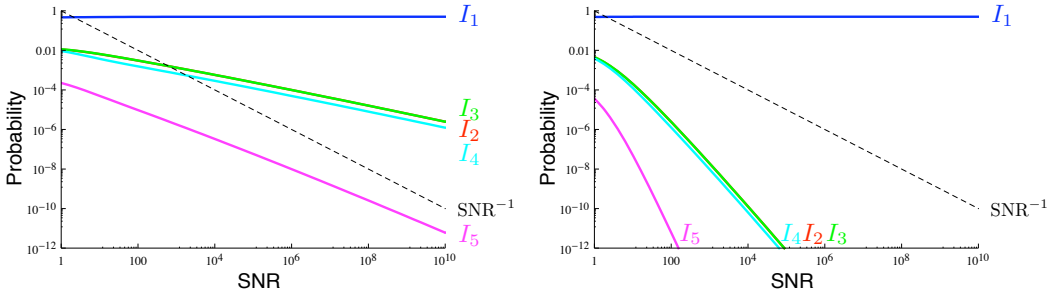

(a) $\Lambda = 20 + \log(1 + \text{SNR})$, $q = \frac{1}{2}$, $L = 10$ (b) $\Lambda = 20 + 5 \cdot \log(1 + \text{SNR})$, $q = \frac{1}{2}$, $L = 10$

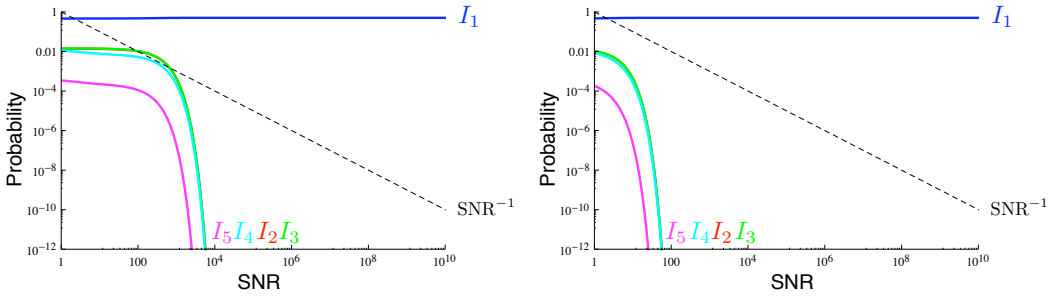

(c) $\Lambda = 20 + .01 \cdot \text{SNR}$, $q = \frac{1}{2}$, $L = 10$ (d) $\Lambda = 20 + \text{SNR}$, $q = \frac{1}{2}$, $L = 10$

Figure 3.10: Likelihood of idle states for different dynamic thresholds

Much of the same can behavior can be observed in the idle states of Figure 3.3.1. For a slow dynamic threshold (with sufficiently large K_2) errors can decay arbitrarily fast. For a fast dynamic threshold, those errors decay exponentially fast.

For slow dynamic thresholding, the probabilities of each OAF state are

$$P_{B_1|\Lambda=K_1+K_2\cdot\log(1+\mathrm{SNR})} \doteq \mathrm{SNR}^{0} \tag{3.46}$$

$$P_{B_2|\Lambda=K_1+K_2\cdot\log(1+\mathrm{SNR})} \doteq \mathrm{SNR}^{-1} \tag{3.47}$$

$$P_{B_3|\Lambda=K_1+K_2\cdot\log(1+\mathrm{SNR})} \doteq \mathrm{SNR}^{-K} \tag{3.48}$$

$$P_{B_4|\Lambda=K_1+K_2\cdot\log(1+\mathrm{SNR})} \doteq \mathrm{SNR}^{-K} \tag{3.49}$$

$$P_{B_5|\Lambda=K_1+K_2\cdot\log(1+\mathrm{SNR})} \doteq \mathrm{SNR}^{-K} \tag{3.50}$$

$$P_{I_1|\Lambda=K_1+K_2\cdot\log(1+\mathrm{SNR})} \doteq \mathrm{SNR}^{0} \tag{3.51}$$

$$P_{I_2|\Lambda=K_1+K_2\cdot\log(1+\mathrm{SNR})} \doteq \mathrm{SNR}^{-K} \tag{3.52}$$

$$P_{I_3|\Lambda=K_1+K_2\cdot\log(1+\mathrm{SNR})} \doteq \mathrm{SNR}^{-K} \tag{3.53}$$

$$P_{I_4|\Lambda=K_1+K_2\cdot\log(1+\mathrm{SNR})} \doteq \mathrm{SNR}^{-K} \tag{3.54}$$

$$P_{I_5|\Lambda=K_1+K_2\cdot\log(1+\mathrm{SNR})} \doteq \mathrm{SNR}^{-K}, \tag{3.55}$$

where the Ks are arbitrary, but not necessarily identical, positive-valued constants. The salient point here is that all error states (i.e. neutral and worst case states) decay with at least an exponential order of one.

For fast dynamic thresholding, the probabilities of each OAF state are

$$P_{B_1|\Lambda=K_1+K_2\cdot\mathrm{SNR}} \doteq \mathrm{SNR}^{0} \tag{3.56}$$

$$P_{B_2|\Lambda=K_1+K_2\cdot\mathrm{SNR}} \doteq \mathrm{SNR}^{0} \tag{3.57}$$

$$P_{B_3|\Lambda=K_1+K_2\cdot\mathrm{SNR}} \doteq \mathrm{SNR}^{-\infty} \tag{3.58}$$

$$P_{B_4|\Lambda=K_1+K_2\cdot\mathrm{SNR}} \doteq \mathrm{SNR}^{-\infty} \tag{3.59}$$

$$P_{B_5|\Lambda=K_1+K_2\cdot\mathrm{SNR}} \doteq \mathrm{SNR}^{-\infty} \tag{3.60}$$

$$P_{I_1|\Lambda=K_1+K_2\cdot\mathrm{SNR}} \doteq \mathrm{SNR}^{0} \tag{3.61}$$

$$P_{I_2|\Lambda=K_1+K_2\cdot\mathrm{SNR}} \doteq \mathrm{SNR}^{-\infty} \tag{3.62}$$

$$P_{I_3|\Lambda=K_1+K_2\cdot\mathrm{SNR}} \doteq \mathrm{SNR}^{-\infty} \tag{3.63}$$

$$P_{I_4|\Lambda=K_1+K_2\cdot\mathrm{SNR}} \doteq \mathrm{SNR}^{-\infty} \tag{3.64}$$

$$P_{I_5|\Lambda=K_1+K_2\cdot\mathrm{SNR}} \doteq \mathrm{SNR}^{-\infty}. \tag{3.65}$$

The salient point here is that some error states do not decay with SNR.

3.3.2 Effect on NAF States

In this section, we discuss the effect of the different dynamic energy threshold strategies on the state probabilities of the NAF protocol.

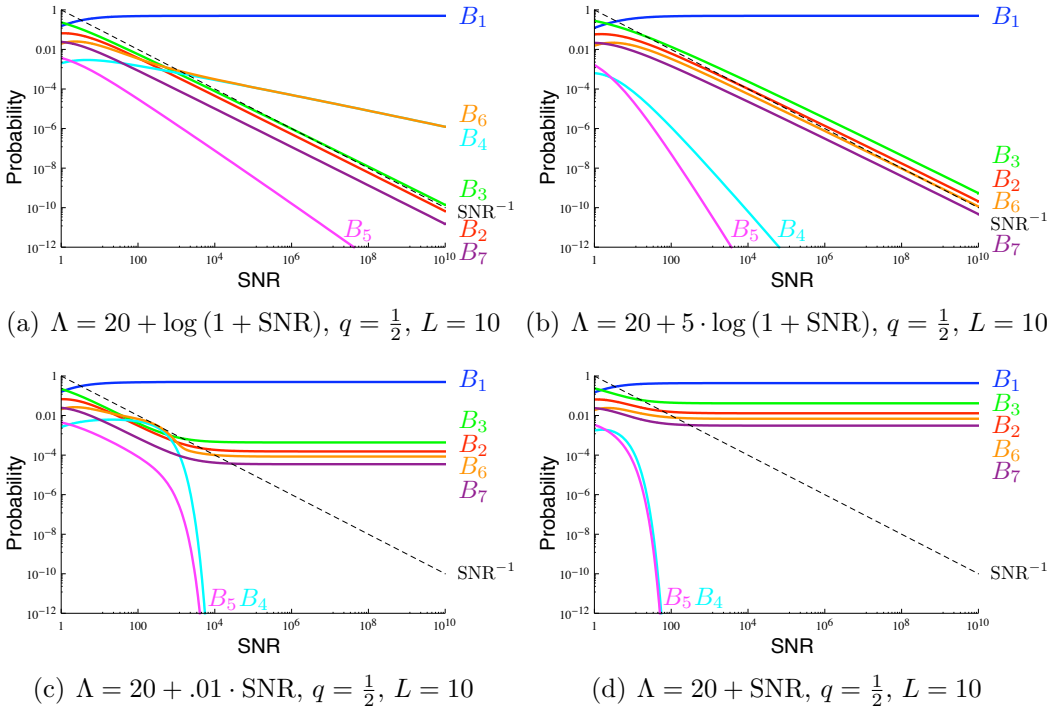

(a) $\Lambda = 20 + \log(1 + \mathrm{SNR})$, $q = \frac{1}{2}$, $L = 10$ (b) $\Lambda = 20 + 5 \cdot \log(1 + \mathrm{SNR})$, $q = \frac{1}{2}$, $L = 10$

(c) $\Lambda = 20 + .01 \cdot \mathrm{SNR}$, $q = \frac{1}{2}$, $L = 10$ (d) $\Lambda = 20 + \mathrm{SNR}$, $q = \frac{1}{2}$, $L = 10$

Figure 3.11: Likelihood of busy states for different dynamic thresholds

In Figure 3.3.2, we can see the effects of the different dynamic thresholding strategies on the NAF state likelihoods. Figures 3.11(a) and 3.11(b) show the effect of the slow dynamic threshold. With sufficiently large K_2 in equation 3.44, the probabilities of worst case states B_4 and B_5 decay arbitrarily fast with SNR. However, the other two worst case states, B_6 and B_7, decay no faster than an exponential order of one. The only state that does not decay with SNR is, as expected, the best case B_1.

In Figures 3.11(c) and 3.11(d), we can see the effects of the fast dynamic threshold. Like in the OAF protocol, the fast dynamic threshold makes some states decay exponentially fast with SNR (B_4 and B_5). However, this comes at the cost of the decay rate of the other error states. Every other state in the system does not decay

with SNR.

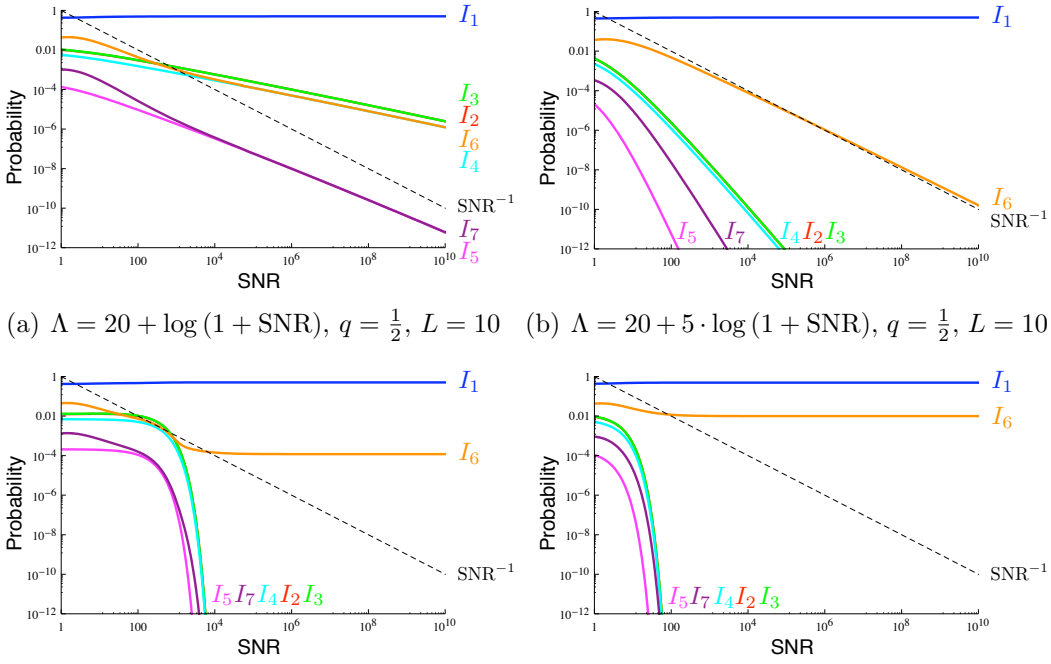

(a) $\Lambda = 20 + \log(1 + \mathrm{SNR})$, $q = \frac{1}{2}$, $L = 10$ (b) $\Lambda = 20 + 5 \cdot \log(1 + \mathrm{SNR})$, $q = \frac{1}{2}$, $L = 10$

(c) $\Lambda = 20 + .01 \cdot \mathrm{SNR}$, $q = \frac{1}{2}$, $L = 10$ (d) $\Lambda = 20 + \mathrm{SNR}$, $q = \frac{1}{2}$, $L = 10$

Figure 3.12: Likelihood of idle states for different dynamic thresholds

We see similar behavior in the idle states of the NAF protocol. In the case of the slow dynamic threshold, all error states decay with at least an exponential order of one. In the case of the fast dynamic threshold, some error states decay exponentially fast while another error state does not decay at all.

To summarize, the probabilities of each NAF state under the slow dynamic thresholding scheme decay with SNR according to

$$P_{B_1|\Lambda=K_1+K_2\cdot\log(1+\mathrm{SNR})} \doteq \mathrm{SNR}^{0} \tag{3.66}$$

$$P_{B_2|\Lambda=K_1+K_2\cdot\log(1+\mathrm{SNR})} \doteq \mathrm{SNR}^{-1} \tag{3.67}$$

$$P_{B_3|\Lambda=K_1+K_2\cdot\log(1+\mathrm{SNR})} \doteq \mathrm{SNR}^{-1} \tag{3.68}$$

$$P_{B_4|\Lambda=K_1+K_2\cdot\log(1+\mathrm{SNR})} \doteq \mathrm{SNR}^{-K} \tag{3.69}$$

$$P_{B_5|\Lambda=K_1+K_2\cdot\log(1+\mathrm{SNR})} \doteq \mathrm{SNR}^{-K} \tag{3.70}$$

$$P_{B_6|\Lambda=K_1+K_2\cdot\log(1+\mathrm{SNR})} \doteq \mathrm{SNR}^{-1} \tag{3.71}$$

$$P_{B_7|\Lambda=K_1+K_2\cdot\log(1+\mathrm{SNR})} \doteq \mathrm{SNR}^{-1} \tag{3.72}$$

$$P_{I_1|\Lambda=K_1+K_2\cdot\log(1+\mathrm{SNR})} \doteq \mathrm{SNR}^{0} \tag{3.73}$$

$$P_{I_2|\Lambda=K_1+K_2\cdot\log(1+\mathrm{SNR})} \doteq \mathrm{SNR}^{-K} \tag{3.74}$$

$$P_{I_3|\Lambda=K_1+K_2\cdot\log(1+\mathrm{SNR})} \doteq \mathrm{SNR}^{-K} \tag{3.75}$$

$$P_{I_4|\Lambda=K_1+K_2\cdot\log(1+\mathrm{SNR})} \doteq \mathrm{SNR}^{-K} \tag{3.76}$$

$$P_{I_5|\Lambda=K_1+K_2\cdot\log(1+\mathrm{SNR})} \doteq \mathrm{SNR}^{-K} \tag{3.77}$$

$$P_{I_6|\Lambda=K_1+K_2\cdot\log(1+\mathrm{SNR})} \doteq \mathrm{SNR}^{-1} \tag{3.78}$$

$$P_{I_7|\Lambda=K_1+K_2\cdot\log(1+\mathrm{SNR})} \doteq \mathrm{SNR}^{-K}. \tag{3.79}$$

The salient point here is that all error states (i.e. neutral and worst case states) decay with at least an exponential order of one.

The probabilities of each NAF state under the fast dynamic thresholding scheme decay with SNR according to

$$P_{B_1|\Lambda=K_1+K_2\cdot\mathrm{SNR}} \doteq \mathrm{SNR}^{0} \tag{3.80}$$

$$P_{B_2|\Lambda=K_1+K_2\cdot\mathrm{SNR}} \doteq \mathrm{SNR}^{0} \tag{3.81}$$

$$P_{B_3|\Lambda=K_1+K_2\cdot\mathrm{SNR}} \doteq \mathrm{SNR}^{0} \tag{3.82}$$

$$P_{B_4|\Lambda=K_1+K_2\cdot\mathrm{SNR}} \doteq \mathrm{SNR}^{-\infty} \tag{3.83}$$

$$P_{B_5|\Lambda=K_1+K_2\cdot\mathrm{SNR}} \doteq \mathrm{SNR}^{-\infty} \tag{3.84}$$

$$P_{B_6|\Lambda=K_1+K_2\cdot\mathrm{SNR}} \doteq \mathrm{SNR}^{0} \tag{3.85}$$

$$P_{B_7|\Lambda=K_1+K_2\cdot\mathrm{SNR}} \doteq \mathrm{SNR}^{0} \tag{3.86}$$

$$P_{I_1|\Lambda=K_1+K_2\cdot\mathrm{SNR}} \doteq \mathrm{SNR}^{0} \tag{3.87}$$

$$P_{I_2|\Lambda=K_1+K_2\cdot\mathrm{SNR}} \doteq \mathrm{SNR}^{-\infty} \tag{3.88}$$

$$P_{I_3|\Lambda=K_1+K_2\cdot\mathrm{SNR}} \doteq \mathrm{SNR}^{-\infty} \tag{3.89}$$

$$P_{I_4|\Lambda=K_1+K_2\cdot\mathrm{SNR}} \doteq \mathrm{SNR}^{-\infty} \tag{3.90}$$

$$P_{I_5|\Lambda=K_1+K_2\cdot\mathrm{SNR}} \doteq \mathrm{SNR}^{-\infty} \tag{3.91}$$

$$P_{I_6|\Lambda=K_1+K_2\cdot\mathrm{SNR}} \doteq \mathrm{SNR}^{0} \tag{3.92}$$

$$P_{I_7|\Lambda=K_1+K_2\cdot\mathrm{SNR}} \doteq \mathrm{SNR}^{-\infty}. \tag{3.93}$$

Under the fast dynamic thresholding scheme, several error states do not decay at all.

3.4 Summary

With this analysis in place, we know how likely the various states in the system are to occur as functions of SNR. We summarize these exponential orders of decay for the OAF and NAF protocols in the following tables:

	Static $\Lambda=K$	**Slow Dynamic** $\Lambda=K_1+K_2\cdot\log(1+\text{SNR})$	**Fast Dynamic** $\Lambda=K_1+K_2\cdot\text{SNR}$
Best	0	0	0
Neutral	-1	-1	0
Worst	0	$-K$	$-\infty$

Table 3.1: Summary of state likelihoods for OAF

	Static $\Lambda=K$	**Slow Dynamic** $\Lambda=K_1+K_2\cdot\log(1+\text{SNR})$	**Fast Dynamic** $\Lambda=K_1+K_2\cdot\text{SNR}$
Best	0	0	0
Neutral	-1	-1	0
Worst 1	0	$-K$	$-\infty$
Worst 2	0	-1	0

Table 3.2: Summary of state likelihoods for NAF

Under the static and fast dynamic threshold schemes, there exist error states that do not decrease in likelihood with SNR. However, with the slow dynamic threshold scheme, all error states decrease in likelihood. Intuitively, this slow dynamic threshold scheme should yield higher performance in the random access cooperative system as compared to the other two schemes. To quantify this comparison, we analyze the outage performance of the OAF and NAF random access systems in the following chapters. Specifically, we analyze the performance of the systems *given* any one of the network states. By combining this along with the state likelihoods presented thus far, we can finally discuss the performance of the random access cooperative systems as a whole.

Chapter 4

Orthogonal Amplify-and-Forward Analysis

The previous chapters culminated in answering the question of how often all the network states occur in the system. This chapter first answers the question of how much those states help or hurt. To accomplish this, we perform analysis to determine the conditional outage performance of the cooperative system *given* a particular network state.

Outage probability is a convenient error metric for delay-constrained systems. In these systems, no Shannon capacity exists in the sense that no rate can guarantee reliable communications [24]. Because of this, outage probability represents a fundamental lower bound on frame error probability.

The analysis in this chapter is coherent, which assumes receiving nodes have perfect knowledge of channel effects. This is a common assumption in the literature and serves as a best case bound on the performance of a system where errors in channel estimation can occur. Second, this chapter combines these results with the state likelihoods of Chapter 3 to discuss the total performance of the OAF protocol in a random-access environment.

4.1 Conditional Performance

Recalling the classifications in Section 2.1 for the OAF protocol, there are three cases of interest in this network: best, neutral, and worst. In the following sections, we analyze the performance of the system given these cases.

4.1.1 Best Case

The first case we consider is the best, where the relay successfully detects the source's packet and forwards its received waveform in the following slot.

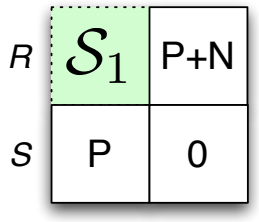

Figure 4.1: Best case state: B_1

Only state B_1 in the system exhibits this behavior. In this state, the system is equivalent to the scheduled-access system presented by Laneman [8]. As such, the outage analysis given this state is exactly the same. For completion, we reproduce this analysis here.

For a codeword of length L (i.e. frame length), the destination node receives

$$y_d[n] = h_{s,d}x_s[n] + z_d[n] \tag{4.1}$$

during the first slot, where $h_{s,d}$ is the fading between the source and destination, $x_s[n]$ is the source's codeword, $z_d[n]$ is noise at the destination, and $n \in \left[0, 1, 2, \ldots, \frac{L}{2}\right]$. In this Amplify-and-Forward protocol, the relay transmits a scaled version of what it

receives during the second slot of the frame. Formally,

$$x_r\left[n+\frac{L}{2}\right]=\beta y_r\left[n\right]=\beta\left(h_{s,r}x_s\left[n\right]+z_r\left[n\right]\right), \tag{4.2}$$

for the same $n \in \left[0,1,2,\ldots,\frac{L}{2}\right]$. Additional parameters include $h_{s,r}$ (the fading between the source and relay), z_r (the noise at the relay), and β (an amplitude scaling factor at the relay).

In the second slot, the destination receives a noisy version of the relay's transmission. Thus,

$$\begin{aligned} y_d\left[n+\frac{L}{2}\right] &= h_{r,d}x_r\left[n+\frac{L}{2}\right]+z_d\left[n+\frac{L}{2}\right] && (4.3)\\ y_d\left[n+\frac{L}{2}\right] &= h_{r,d}\beta h_{s,r}x_s\left[n\right]+h_{r,d}\beta z_r\left[n\right]+z_d\left[n+\frac{L}{2}\right], && (4.4)\end{aligned}$$

where $h_{r,d}$ is the fading between relay and destination and $n \in \left[0,1,2,\ldots,\frac{L}{2}\right]$.

We assume an average power constraint that is the same for both the source and the relay. This symmetry assumption only serves to ease the notation in the analysis that follows. It is by no means a fundamental assumption and can easily be relaxed to consider a more general case. Specifically, average power of the signals in a frame are assumed to be

$$\mathrm{E}\left[z_r^\dagger z_r\right]=\mathrm{E}\left[z_d^\dagger z_d\right]=1 \tag{4.5}$$

$$\mathrm{E}\left[x_s^\dagger x_s\right]=\mathrm{E}\left[x_r^\dagger x_r\right]=\mathrm{SNR}, \tag{4.6}$$

and hence this requires the relay amplitude scaling factor to be

$$\beta = \sqrt{\frac{\text{SNR}}{|h_{s,r}|^2\text{SNR} + 1}}. \tag{4.7}$$

To analyze this system, we can perform a simple manipulation to transform it into a virtual multi-antenna system. Instead of the destination receiving during two time slots, we can model this system as a destination that simultaneously receives over two spatially separated antennas. The model for this $[2 \times 1]$ multi-antenna system can be represented as

$$\begin{gathered}\mathbf{y_d}[n] = \mathbf{A}x_s[n] + \mathbf{B}\mathbf{z}[n] \\ \begin{bmatrix} y_d[n] \\ y_d[n + \frac{L}{2}] \end{bmatrix} = \begin{bmatrix} h_{s,d} \\ h_{r,d}\beta h_{s,r} \end{bmatrix} x_s[n] + \begin{bmatrix} 0 & 1 & 0 \\ h_{r,d}\beta & 0 & 1 \end{bmatrix} \begin{bmatrix} z_r[n] \\ z_d[n] \\ z_d[n + \frac{L}{2}] \end{bmatrix}.\end{gathered} \tag{4.8}$$

With this model in place, we can derive the maximum mutual information between scalar x_s and vector $\mathbf{y_d}$ in order to determine the maximum instantaneous rate supported by the channel for given channel gains. For brevity, this derivation is presented in Appendix A.1. From Equation (A.1), we can express this maximum mutual information for unit bandwidth as

$$\text{I}_{\text{Best}}(x_s; \mathbf{y_d}) \leq \frac{1}{2}\log\left(1 + \frac{\text{SNR}|h_{r,d}\beta h_{s,r}|^2}{|h_{r,d}\beta|^2 + 1} + \text{SNR}|h_{s,d}|^2\right), \tag{4.9}$$

where an additional factor of $\frac{1}{2}$ has been included to capture the effect of taking two slots for a single transmission. After substituting the relay scale factor of Equation (4.7) and performing algebraic simplifications, we express the maximum mutual

information as

$$\mathrm{I}_{\mathrm{Best}}(x_s; \mathbf{y_d}) \leq \frac{1}{2} \log \left(1 + \mathrm{SNR}|h_{s,d}|^2 + f\left(\mathrm{SNR}|h_{s,r}|^2, \mathrm{SNR}|h_{r,d}|^2\right)\right), \tag{4.10}$$

where $f(x,y) = \frac{xy}{x+y+1}$. For Rayleigh fading (i.e. $|h_{i,j}|^2 \sim$ exponential random variable with parameter $\lambda_{i,j}$), there is some probability of the maximum mutual information falling below some transmit rate R (*nats per second*). This event, known as an outage event, represents a fundamental loss of support from the wireless channel and effectively forms a lower bound on probability of error. Formally, the outage event can be defined as

$$\max_{x_s} \mathrm{I}_{\mathrm{Best}}(x_s; \mathbf{y_d}) < R. \tag{4.11}$$

Rewriting Equation (4.10), the outage event can be represented by

$$\mathrm{SNR}|h_{s,d}|^2 + f\left(\mathrm{SNR}|h_{s,r}|^2, \mathrm{SNR}|h_{r,d}|^2\right) < e^{2R} - 1. \tag{4.12}$$

Explicitly calculating the probability of the outage event in Equation (4.12) is intractable, but we can invoke the main theorem proven in a different work from Laneman to obtain a high SNR approximation [25]. This theorem says that, for any independent random variables U_s, V_s with the properties

$$\lim_{s\to\infty} sP[U_s < t] = g(t) \tag{4.13}$$

$$\lim_{s\to\infty} s^d P[V_s < t] = h(t), \tag{4.14}$$

where $g(t)$ and $h(t)$ are monotone increasing and integrable, and $g'(t)$ is integrable,

then

$$\lim_{s\to\infty} s^{d+1} P\left[U_s + V_s < t\right] = \int_0^t h\left(t-x\right) g'\left(x\right) dx. \tag{4.15}$$

We now revisit the outage event in Equation (4.12) with the substitutions $s = \mathrm{SNR}$, $U_s = \mathrm{SNR}|h_{s,d}|^2$, $V_s = f\left(\mathrm{SNR}|h_{s,r}|^2, \mathrm{SNR}|h_{r,d}|^2\right)$, $d = 1$, and $t = e^{2R} - 1$. Thus, the outage event can simply be written as

$$U_s + V_s < t, \tag{4.16}$$

and Equation (4.15) can be used to determine the probability of outage

$$P_{O|\mathrm{Best}} \approx \frac{1}{s^2} \lim_{s\to\infty} s^2 P\left[U_s + V_s < t\right] = \frac{1}{s^2} \int_0^t h\left(t-x\right) g'\left(x\right) dx. \tag{4.17}$$

To determine the functions $g\left(t\right)$ and $h\left(t\right)$ necessary to find this quantity, we invoke Fact C.0.1 and Claim C.0.2 respectively from Appendix C. Specifically, with the additional substitution $W = |h_{s,d}|^2$, Fact C.0.1 satisfies the first condition in Equation (4.13) with

$$\lim_{s\to\infty} sP\left[U_s < t\right] = \lambda_{s,d} t = g\left(t\right). \tag{4.18}$$

With the additional substitutions $U = |h_{s,r}|^2$ and $V = |h_{r,d}|^2$, Claim C.0.2 satisfies the second condition in Equation (4.14) with

$$\lim_{s\to\infty} sP\left[V_s < t\right] = \left(\lambda_{s,r} + \lambda_{r,d}\right) t = h\left(t\right). \tag{4.19}$$

Finally we can combine Equations (4.17), (4.18), and (4.19) to determine the high SNR approximate outage probability

$$
\begin{aligned}
P_{O|\text{Best}} &\approx \frac{1}{s^2}\int_0^t \left(\lambda_{s,r}+\lambda_{r,d}\right)(t-x)\,\lambda_{s,d}dx && (4.20)\\
&= \frac{1}{s^2}\left(\lambda_{s,r}+\lambda_{r,d}\right)\lambda_{s,d}t^2 && (4.21)\\
&= \frac{1}{\text{SNR}^2}\left(\lambda_{s,r}+\lambda_{r,d}\right)\lambda_{s,d}\left(e^{2R}-1\right)^2 && (4.22)\\
&= \left(\sqrt{\frac{2}{\left(\lambda_{s,r}+\lambda_{r,d}\right)\lambda_{s,d}}}\cdot\frac{\text{SNR}}{e^{2R}-1}\right)^{-2}, && (4.23)
\end{aligned}
$$

which exactly matches the results from Laneman [8], [25]. The probability of an outage event decays with exponential order two,[1] or

$$P_{O|\text{Best}} \doteq \text{SNR}^{-2}. \tag{4.24}$$

We can verify the high SNR behavior of the outage probability via Monte Carlo simulation.

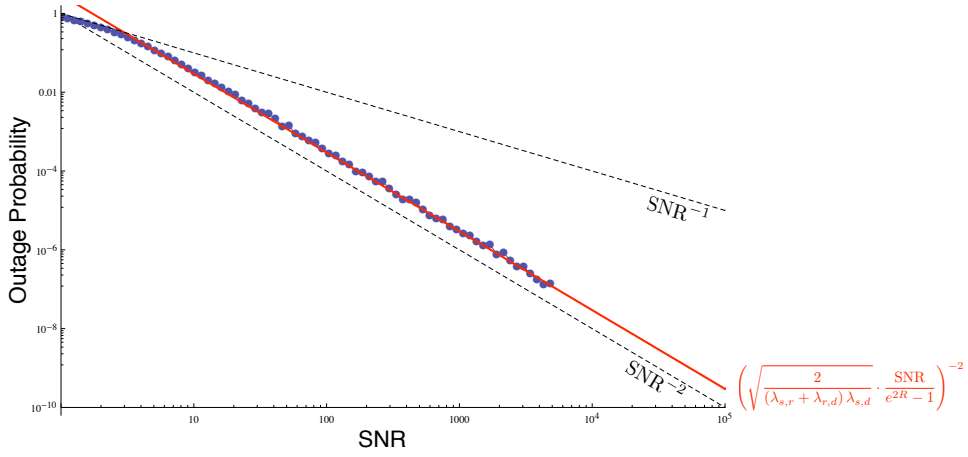

Figure 4.2: Best case outage probability Monte Carlo simulation ($R=\frac{1}{2}$ and $\lambda_{s,d}=\lambda_{s,r}=\lambda_{r,d}=1$)

Figure 4.2 shows a tight match between the analytical expression and the Monte Carlo simulation data points for high SNR. The above analysis of the best case states

[1] This is equivalently described as a diversity order two system.

that, when the relay correctly detects a source transmission, the performance gains in the system are exactly those that we would expect from previous work analyzing a fully scheduled system.

4.1.2 Neutral Case

The second case we consider is the neutral one, where the relay neither helps nor hurts the source's transmission because it never transmits.

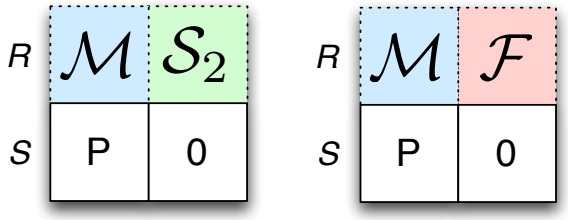

(a) B_2 (b) B_3

Figure 4.3: Neutral case states

States B_2 and B_3 exhibit this behavior. In both of these states, the relay is sensing the medium during both slots, thereby never transmitting. We analyze the outage probability of this case via a similar methodology to the analysis of the best case in Section 4.1.1. Specifically, we assume all of the same parameters as before and merely change the expressions to account for the lack of relay transmission during the second slot. In the first slot, the destination receives

$$y_d[n] = h_{s,d}x_s[n] + z_d[n]. \tag{4.25}$$

However, during the second slot, the destination receives only the thermal noise at the destination, or

$$y_d\left[n + \frac{L}{2}\right] = z_d\left[n + \frac{L}{2}\right]. \tag{4.26}$$

Transforming this into a 1×2 multi-antenna system results in the matrix formulation of

$$\mathbf{y_d}[n] = \mathbf{A}x_s[n] + \mathbf{Bz}[n]$$
$$\begin{bmatrix} y_d[n] \\ y_d[n+\frac{L}{2}] \end{bmatrix} = \begin{bmatrix} h_{s,d} \\ 0 \end{bmatrix} x_s[n] + \begin{bmatrix} 0 & 1 & 0 \\ 0 & 0 & 1 \end{bmatrix} \begin{bmatrix} z_r[n] \\ z_d[n] \\ z_d[n+\frac{L}{2}] \end{bmatrix}. \tag{4.27}$$

Like before, we can derive the maximum mutual information between scalar x_s and vector $\mathbf{y_d}$ in order to determine the maximum instantaneous rate supported by the channel for given channel gains. For brevity, this derivation is presented in Appendix A.2. From Equation (A.2), we can express this maximum mutual information as

$$\mathrm{I}_{\mathrm{Neutral}}(x_s; \mathbf{y_d}) \leq \frac{1}{2} \log\left(1 + \mathrm{SNR}|h_{s,d}|^2\right), \tag{4.28}$$

which is exactly the capacity expression of a point-to-point SISO link under quasi-static fading, except for the factor of $\frac{1}{2}$ to account for the two time slots it takes to send a single message. Intuitively, this is very satisfying; when the relay is effectively "off," the system is simply a point-to-point single-antenna link. Because of the simplicity of this expression, the outage probability can be directly computed without need for a high SNR approximation. Formally, the outage event can be defined as

$$\max_{x_s} \mathrm{I}_{\mathrm{Neutral}}(x_s; \mathbf{y_d}) < R. \tag{4.29}$$

Solving for the random channel power $|h_{s,d}|^2$ yields

$$|h_{s,d}|^2 < \frac{e^{2R} - 1}{\mathrm{SNR}}, \tag{4.30}$$

where $|h_{s,d}|^2$ is an exponential random variable with parameter $\lambda_{s,d}$. The probability of this event occurring is simply the CDF of the exponential random variable evaluated

at this point. Formally,

$$P_{O|\text{Neutral}} = 1 - e^{\lambda_{s,d}\frac{e^{2R}-1}{\text{SNR}}} \tag{4.31}$$

$$P_{O|\text{Neutral}} \doteq \text{SNR}^{-1}. \tag{4.32}$$

For the neutral case, the system has lost the diversity order improvement associated with the relay. We can verify this SNR dependence with a Monte Carlo simulation.

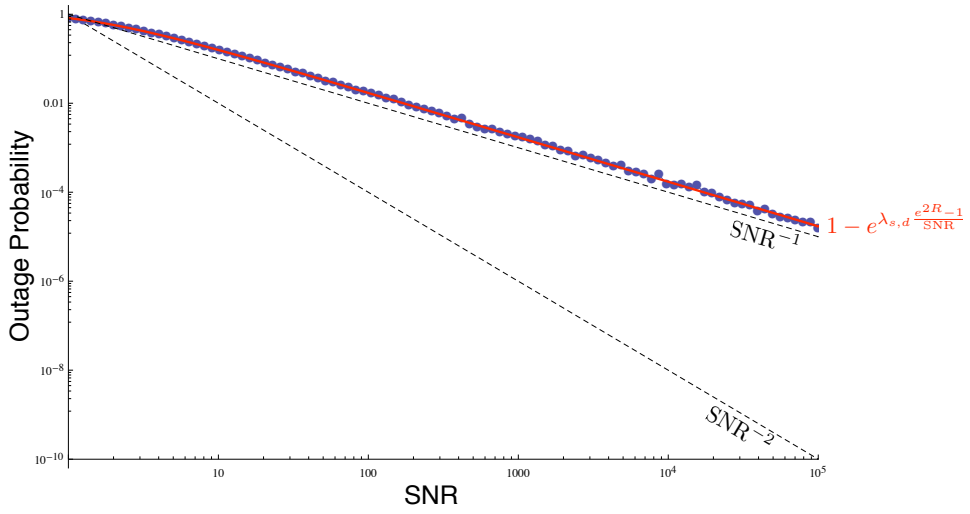

Figure 4.4: Neutral case outage probability Monte Carlo simulation ($R = \frac{1}{2}$ and $\lambda_{s,d} = 1$)

Figure 4.4 shows a tight match between the analytical expression and the Monte Carlo simulation data points.

4.1.3 Worst Case

The final case we consider is the worst, where the relay actively impedes the source's communication by transmitting noise during the first slot of the frame.

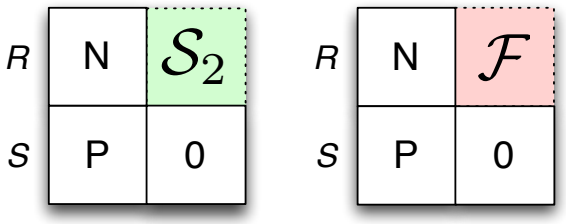

(a) B_4 (b) B_5

Figure 4.5: Worst case states

States B_4 and B_5 exhibit this behavior. To calculate the outage probability of the system given this state, we assume all of the same parameters as before and merely change the expressions to account for the relay's noise transmission during the first slot. In the first slot, the destination receives

$$y_d[n] = h_{s,d}x_s[n] + z_d[n] + h_{r,d}\beta z_r\left[n - \frac{L}{2}\right], \tag{4.33}$$

where $z_r\left[n - \frac{L}{2}\right]$ is the noise at the relay during the second slot of the previous frame. During the second slot, the destination receives only the thermal noise at the destination, or

$$y_d\left[n + \frac{L}{2}\right] = z_d\left[n + \frac{L}{2}\right]. \tag{4.34}$$

Transforming this into a 1×2 multi-antenna system results in the matrix formu-

lation of

$$\mathbf{y_d}[n] = \mathbf{A}x_s[n] + \mathbf{Bz}[n]$$

$$\begin{bmatrix} y_d[n] \\ y_d[n+\frac{L}{2}] \end{bmatrix} = \begin{bmatrix} h_{s,d} \\ 0 \end{bmatrix} x_s[n] + \begin{bmatrix} h_{r,d}\beta & 1 & 0 \\ 0 & 0 & 1 \end{bmatrix} \begin{bmatrix} z_r[n-\frac{L}{2}] \\ z_d[n] \\ z_d[n+\frac{L}{2}] \end{bmatrix}. \tag{4.35}$$

Like before, we can derive the maximum mutual information between scalar x_s and vector $\mathbf{y_d}$ in order to determine the maximum instantaneous rate supported by the channel for given channel gains. For brevity, this derivation is presented in Appendix A.3. From Equation (A.3), we can express this maximum mutual information as

$$\mathrm{I}_{\mathrm{Worst}}(x_s; \mathbf{y_d}) \leq \frac{1}{2}\log\left(1 + \frac{\mathrm{SNR}|h_{s,d}|^2}{|h_{r,d}\beta|^2 + 1}\right). \tag{4.36}$$

This equation says that the relay only serves to *reduce* the effective SNR in the system by the scaling factor β and the instantaneous channel gain $h_{r,d}$. As will become clear later in the chapter, we only need to consider analytically convenient, loose bounds on this mutual information. Noting that Equation (4.36) is a decreasing function of β, we can loosely upper bound the maximum mutual information by assigning $\beta = 0$. To loosely lower bound the maximum mutual information, we can assume that the capacity of the link in the worst case is zero. More formally,

$$0 \leq \max_{x_s} \mathrm{I}_{\mathrm{Worst}}(x_s; \mathbf{y_d}) = \frac{1}{2}\log\left(1 + \frac{\mathrm{SNR}|h_{s,d}|^2}{|h_{r,d}\beta|^2 + 1}\right) \leq \frac{1}{2}\log\left(1 + \mathrm{SNR}|h_{s,d}|^2\right). \tag{4.37}$$

Notice that the upper bound on the maximum mutual information expression in Equation (4.37) is identical to that in the neutral case of Section 4.1.2. In that Equation (4.31), we determined outage probability of that maximum mutual information.

Thus, we can write the bounds on the outage probability of the worst case as

$$1 \geq P_{O|\text{Worst}} \geq 1 - e^{\lambda_{s,d} \frac{e^{2R}-1}{\text{SNR}}}. \tag{4.38}$$

Using the exponential order shorthand yields

$$\text{SNR}^0 \dot{\geq} P_{O|\text{Worst}} \dot{\geq} \text{SNR}^{-1}. \tag{4.39}$$

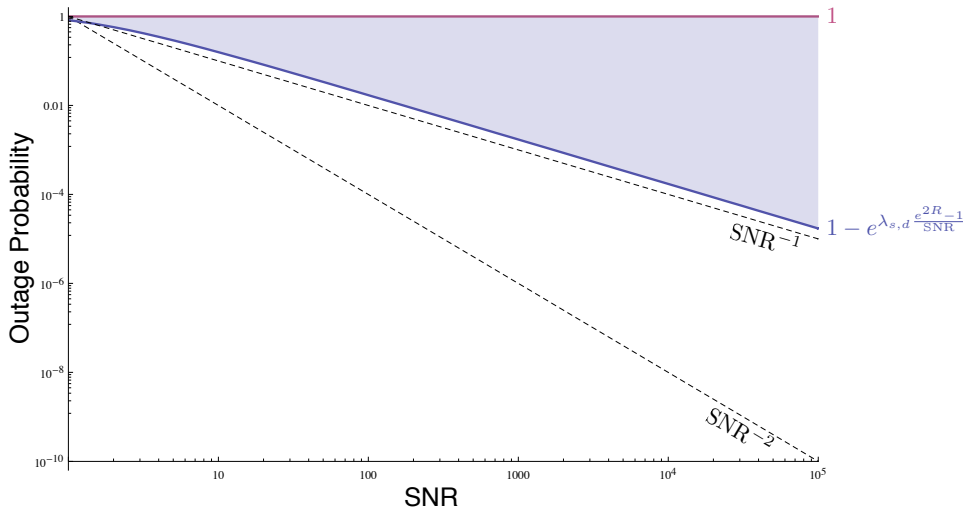

Figure 4.6: Worst case outage probability bounds

Figure 4.6 shows these bounds on the outage probability of the worst case. At best, the worst case behaves like the neutral case. At worst, we assume the worst case is permanently in outage.

4.2 Total Performance

Finally, all of the groundwork has been laid in order to discuss the overall performance of the OAF protocol in a random-access environment. There are two critical pieces here: the likelihood of states and the performance given each of those states. We use the law of total probability to combine these two pieces. Formally,

$$P_O = \frac{1}{q}\left(P_{B_1} \cdot P_{O|\text{Best}} + (P_{B_2} + P_{B_3}) \cdot P_{O|\text{Neutral}} + (P_{B_4} + P_{B_5}) \cdot P_{O|\text{Worst}}\right), \quad (4.40)$$

where the $1/q$ term scales the state likelihoods so that $P_{B_1}+P_{B_2}+P_{B_3}+P_{B_4}+P_{B_5} = 1$. In the following sections, we will revisit the different energy detection thresholding strategies in order to discuss this overall system performance.

4.2.1 Static Relay Detection

Equations (3.20) - (3.24) express the exponential orders of the state probabilities for a static relay threshold (i.e. $\Lambda = K$). To summarize, the best case and worst cases do not decay in likelihood with SNR, but the neutral cases decay with exponential order one. Substituting these likelihoods into Equation 4.40 yields

$$P_{O|\Lambda=K} \propto \left(\text{SNR}^0 \cdot P_{O|\text{Best}} + \text{SNR}^{-1} \cdot P_{O|\text{Neutral}} + \text{SNR}^0 \cdot P_{O|\text{Worst}}\right). \quad (4.41)$$

Equations (4.24), (4.32), and the optimistic loose bound in (4.39) express the exponential orders of the outage probabilities given the different cases. Substituting these probabilities into the total outage probability expression yields

$$\begin{aligned} P_{O|\Lambda=K} &\dot{\geq} \left(\mathrm{SNR}^{0} \cdot \mathrm{SNR}^{-2} + \mathrm{SNR}^{-1} \cdot \mathrm{SNR}^{-1} + \mathrm{SNR}^{0} \cdot \mathrm{SNR}^{-1}\right) \\ &\doteq \left(\mathrm{SNR}^{-2} + \mathrm{SNR}^{-2} + \mathrm{SNR}^{-1}\right) \\ P_{O|\Lambda=K} &\dot{\geq} \mathrm{SNR}^{-1}. \end{aligned} \tag{4.42}$$

Equations (4.24), (4.32), and the pessimistic loose bound in (4.39) express the exponential orders of the outage probabilities given the different cases. Substituting these probabilities into the total outage probability expression yields

$$\begin{aligned} P_{O|\Lambda=K} &\dot{\leq} \left(\mathrm{SNR}^{0} \cdot \mathrm{SNR}^{-2} + \mathrm{SNR}^{-1} \cdot \mathrm{SNR}^{-1} + \mathrm{SNR}^{0} \cdot \mathrm{SNR}^{0}\right) \\ &\doteq \left(\mathrm{SNR}^{-2} + \mathrm{SNR}^{-2} + \mathrm{SNR}^{0}\right) \\ P_{O|\Lambda=K} &\dot{\leq} \mathrm{SNR}^{0}. \end{aligned} \tag{4.43}$$

Combining the bounds yields

$$\mathrm{SNR}^{-1} \dot{\leq} P_{O|\Lambda=K} \dot{\leq} \mathrm{SNR}^{0}. \tag{4.44}$$

Even with an optimistic loose bound on outage probability of the worst case, the best possible diversity order is one. In other words, with a static energy detection threshold at the relay, full diversity is impossible. We can verify this behavior via Monte-Carlo simulation.

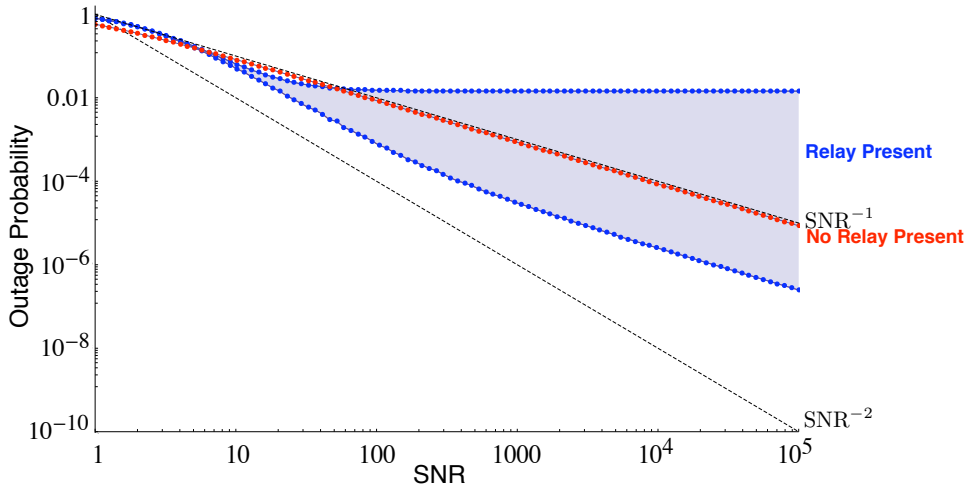

Figure 4.7: Outage Probability with $\Lambda = 20$

Figure 4.7 shows that the performance with presence of the altruistic relay in the network performs asymptotically no better than having no relay in all. In fact, it is possible that the performance could be asymptotically worse than not cooperating. We now turn to dynamic relay thresholds to determine if this problem can be avoided.

4.2.2 Dynamic Relay Detection

Recall from Chapter 3 that we can analyze the performance of the system under two forms of dynamic thresholding strategies. In the case that the threshold changes logarithmically with SNR, we call the strategy a slow dynamic threshold. In the case that the threshold changes proportionally with SNR, we call the strategy a fast dynamic threshold. In the following sections, we analyze the effects of both of these strategies on overall system performance.

4.2.2.1 Slow Dynamic Threshold

Equations (3.46) - (3.50) express the exponential orders of the state probabilities for a slow dynamic relay threshold (i.e. $\Lambda = K_1 + K_2 \cdot \log(1 + \text{SNR})$). Substituting these

probabilities into the total outage probability expression yields

$$P_{O|\Lambda=K_1+K_2\cdot\log(1+\mathrm{SNR})} \propto \left(\mathrm{SNR}^0 \cdot P_{O|\mathrm{Best}} + \mathrm{SNR}^{-1} \cdot P_{O|\mathrm{Neutral}} + \mathrm{SNR}^{-K} \cdot P_{O|\mathrm{Worst}}\right). \tag{4.45}$$

Equations (4.24) and (4.32) express the exponential orders of the outage probabilities given the different cases. Additionally, we will first use the optmistic bound on the outage probability of the worst case from Equation (4.39). Substituting these probabilities into the total outage probability expression yields a lower bound on outage probability of

$$\begin{aligned} P_{O|\Lambda=K_1+K_2\cdot\log(1+\mathrm{SNR})} &\dot{\geq} \left(\mathrm{SNR}^0 \cdot \mathrm{SNR}^{-2} + \mathrm{SNR}^{-1} \cdot \mathrm{SNR}^{-1} + \mathrm{SNR}^{-K} \cdot \mathrm{SNR}^{-1}\right) \\ &\doteq \left(\mathrm{SNR}^{-2} + \mathrm{SNR}^{-2} + \mathrm{SNR}^{-K}\right) \\ P_{O|\Lambda=K_1+K_2\cdot\log(1+\mathrm{SNR})} &\dot{\geq} \mathrm{SNR}^{-2}. \end{aligned} \tag{4.46}$$

Next, we will use the highly pessimistic bound on the outage probability of the worst case from Equation (4.39). This bound assumes the network goes into outage whenever the worst case events occur. Substituting these probabilities into the total outage probability expression yields

$$\begin{aligned} P_{O|\Lambda=K_1+K_2\cdot\log(1+\mathrm{SNR})} &\dot{\leq} \left(\mathrm{SNR}^0 \cdot \mathrm{SNR}^{-2} + \mathrm{SNR}^{-1} \cdot \mathrm{SNR}^{-1} + \mathrm{SNR}^{-K} \cdot \mathrm{SNR}^{0}\right) \\ &\doteq \left(\mathrm{SNR}^{-2} + \mathrm{SNR}^{-2} + \mathrm{SNR}^{-K}\right) \\ P_{O|\Lambda=K_1+K_2\cdot\log(1+\mathrm{SNR})} &\dot{\leq} \mathrm{SNR}^{-2}. \end{aligned} \tag{4.47}$$

Combining these two bounds yields

$$P_{O|\Lambda=K_1+K_2\cdot\log(1+\mathrm{SNR})} \doteq \mathrm{SNR}^{-2}. \tag{4.48}$$

As such, the diversity order is two, which is the full spatial diversity that can be achieved. We can verify this behavior via Monte-Carlo simulation.

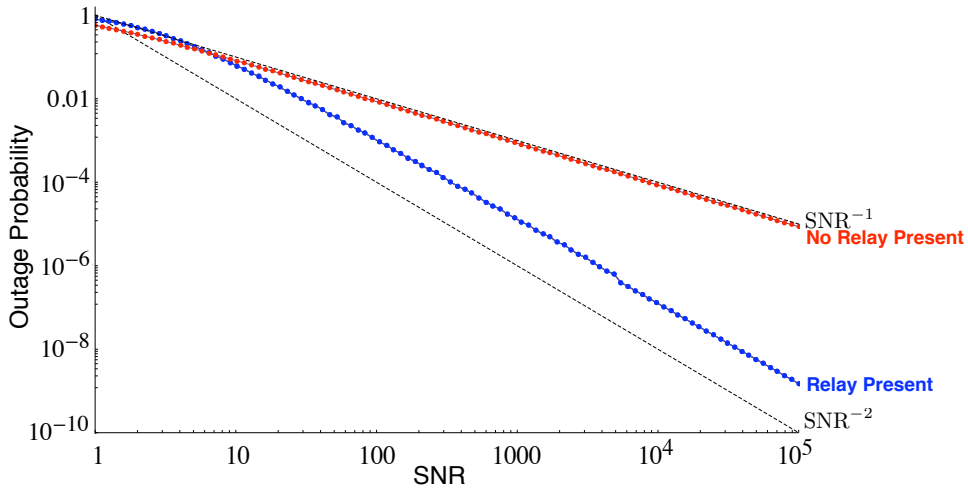

Figure 4.8: Outage Probability with $\Lambda = 20 + \log(1 + \mathrm{SNR})$

Figure 4.8 shows that that the slow dynamic thresholding strategy achieves full spatial diversity.

4.2.2.2 Fast Dynamic Threshold

Equations (3.56) - (3.60) express the exponential orders of the state probabilities for a fast dynamic relay threshold (i.e. $\Lambda = K_1 + K_2 \cdot \mathrm{SNR}$). Substituting these probabilities into the total outage probability expression yields

$$P_{O|\Lambda=K_1+K_2\cdot\mathrm{SNR}} \propto \left(\mathrm{SNR}^0 \cdot P_{O|\mathrm{Best}} + \mathrm{SNR}^0 \cdot P_{O|\mathrm{Neutral}} + \mathrm{SNR}^{-\infty} \cdot P_{O|\mathrm{Worst}}\right). \tag{4.49}$$

Equations (4.24), (4.32), and the bounds of 4.39 express the exponential orders of

the outage probabilities given the different cases. First, we establish a lower bound on total outage probability by substituting these probabilities with the optimistic bound of the worst case into the expression, yielding

$$\begin{aligned} P_{O|\Lambda=K_1+K_2\cdot\mathrm{SNR}} &\dot{\geq} \left(\mathrm{SNR}^0\cdot\mathrm{SNR}^{-2}+\mathrm{SNR}^0\cdot\mathrm{SNR}^{-1}+\mathrm{SNR}^{-\infty}\cdot\mathrm{SNR}^{-1}\right) \\ &\doteq \left(\mathrm{SNR}^{-2}+\mathrm{SNR}^{-1}+\mathrm{SNR}^{-\infty}\right) \\ P_{O|\Lambda=K_1+K_2\cdot\mathrm{SNR}} &\dot{\geq} \mathrm{SNR}^{-1}. \end{aligned} \tag{4.50}$$

Similarly, we establish an upper bound on total outage probability by making use of the pessimistic bound in Equation (4.39). This substitution yields

$$\begin{aligned} P_{O|\Lambda=K_1+K_2\cdot\mathrm{SNR}} &\dot{\leq} \left(\mathrm{SNR}^0\cdot\mathrm{SNR}^{-2}+\mathrm{SNR}^0\cdot\mathrm{SNR}^{-1}+\mathrm{SNR}^{-\infty}\cdot\mathrm{SNR}^{0}\right) \\ &\doteq \left(\mathrm{SNR}^{-2}+\mathrm{SNR}^{-1}+\mathrm{SNR}^{-\infty}\right) \\ P_{O|\Lambda=K_1+K_2\cdot\mathrm{SNR}} &\dot{\leq} \mathrm{SNR}^{-1}. \end{aligned} \tag{4.51}$$

Combining the two bounds yields

$$P_{O|\Lambda=K_1+K_2\cdot\mathrm{SNR}} \doteq \mathrm{SNR}^{-1}. \tag{4.52}$$

Because the likelihood of the worst case states decays so fast, the outage probability of those states do not dominate the overall behavior of the system. However, because the fast dynamic threshold makes the neutral case not decay with SNR, it becomes the dominating term, yielding a diversity order of one. We can verify this behavior via Monte-Carlo simulation.

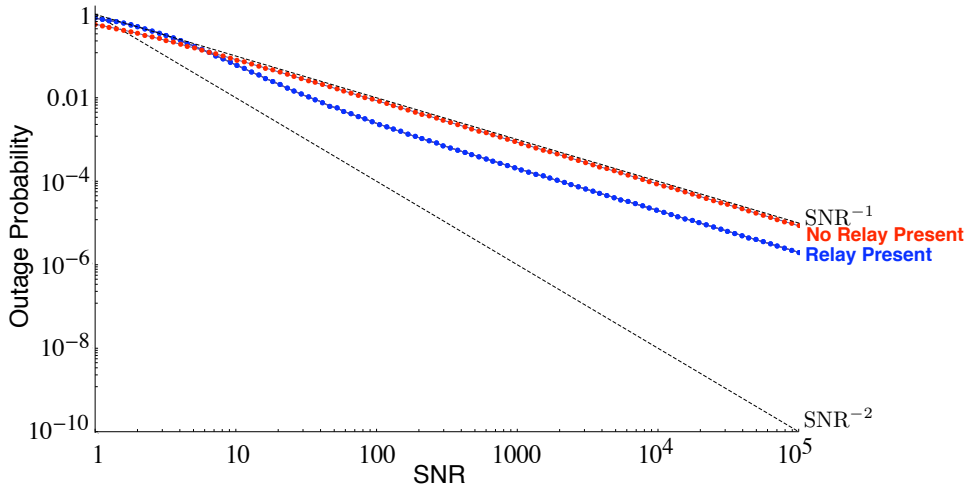

Figure 4.9: Outage Probability with $\Lambda = 20 + \mathrm{SNR}$

Figure 4.9 shows that, asymptotically, the presence of the altruistic relay does not aid the source's ability to communicate when the relay's energy detection uses a fast dynamic threshold.

4.3 Summary

The first main result of this thesis regards the diversity order of the OAF protocol in a random-access environment. We have shown that, in the case of a slow dynamic energy detection threshold that moves with the logarithm of average SNR, full diversity can be achieved. Asymptotically, the random-access cooperative network performs no worse than the scheduled cooperative network presented by Laneman [8].

However, we have also shown that in both the static threshold and the fast dynamic threshold cases, the network has a diversity-order loss relative to a scheduled network. For the static threshold, the dominating error term arises from a constant probability of states where the relay actively transmits noise during a frame. For the fast dynamic threshold, the dominating error term arises from a constant probability of states where the relay misses the detection of the source's packet. In the next chapter, we perform similar analysis to describe the effects on the NAF protocol.

Chapter 5

Non-Orthogonal Amplify-and-Forward Analysis

In this chapter we analyze the outage performance of the NAF protocol under the various states presented in Chapter 2. We then combine these results with the state likelihoods of Chapter 3 to discuss the total performance of the NAF protocol in a random-access environment.

5.1 Conditional Performance

Recalling the classifications in Section 2.2 for the NAF protocol, there are four cases of interest in this network: best, neutral, and two forms of the worst. In the following sections, we analyze the performance of the system given these cases.

5.1.1 Best Case

The first case we consider is the best, where the relay successfully detects the source's packet and forwards its received waveform in the following slot.

Only state B_1 in the system exhibits this behavior. For a codeword of length L (i.e. frame length), the destination node receives

$$y_d[n] = h_{s,d}x_s[n] + z_d[n] \tag{5.1}$$

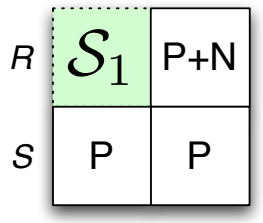

Figure 5.1: Best case state: B_1

during the first slot, where $h_{s,d}$ is the fading between the source and destination, $x_s[n]$ is the source's codeword, $z_d[n]$ is noise at the destination, and $n \in \left[0, 1, 2, \ldots, \frac{L}{2}\right]$. In this Amplify-and-Forward protocol, the relay transmits a scaled version of what it receives during the second slot of the frame. Formally,

$$x_r\left[n + \frac{L}{2}\right] = \beta y_r[n] = \beta\left(h_{s,r}x_s[n] + z_r[n]\right), \tag{5.2}$$

for the same $n \in \left[0, 1, 2, \ldots, \frac{L}{2}\right]$. Additional parameters include $h_{s,r}$ (the fading between the source and relay), z_r (the noise at the relay), and β (an amplitude scaling factor at the relay). In the second slot, the destination receives a noisy version of the relay's transmission. Additionally, we consider a specific form of the NAF protocol where the source repeats its waveform in the second slot as well. Thus,

$$y_d\left[n + \frac{L}{2}\right] = h_{s,d}x_s[n] + h_{r,d}x_r\left[n + \frac{L}{2}\right] + z_d\left[n + \frac{L}{2}\right] \tag{5.3}$$

$$y_d\left[n + \frac{L}{2}\right] = h_{s,d}x_s[n] + h_{r,d}\beta h_{s,r}x_s[n] + h_{r,d}\beta z_r[n] + z_d\left[n + \frac{L}{2}\right], \tag{5.4}$$

where $h_{r,d}$ is the fading between relay and destination and $n \in \left[0, 1, 2, \ldots, \frac{L}{2}\right]$.

We assume the same average power constraints as those presented in Chapter 4. Like before, we analyze this system by performing a simple manipulation to transform it into a virtual multi-antenna system. Instead of the destination receiving over two time slots, we can model this system as a destination that receives over two spatially

separated antennas. Thus, the model for this $[2 \times 1]$ multi-antenna system can be represented as

$$\mathbf{y_d}[n] = \mathbf{A}x_s[n] + \mathbf{Bz}[n]$$

$$\begin{bmatrix} y_d[n] \\ y_d[n+\frac{L}{2}] \end{bmatrix} = \begin{bmatrix} h_{s,d} \\ h_{s,d} + h_{r,d}\beta h_{s,r} \end{bmatrix} x_s[n] + \begin{bmatrix} 0 & 1 & 0 \\ h_{r,d}\beta & 0 & 1 \end{bmatrix} \begin{bmatrix} z_r[n] \\ z_d[n] \\ z_d[n+\frac{L}{2}] \end{bmatrix}. \tag{5.5}$$

With this model in place, we can derive the maximum mutual information between scalar x_s and vector $\mathbf{y_d}$ in order to determine the maximum instantaneous rate supported by the channel for given channel gains. For brevity, this derivation is presented in Appendix B.1. From Equation (B.1), we can express this maximum mutual information as

$$\mathrm{I}_{\mathrm{Best}}(x_s; \mathbf{y_d}) \leq \frac{1}{2} \log \left(1 + \frac{\mathrm{SNR}|h_{s,d} + h_{r,d}\beta h_{s,r}|^2}{|h_{r,d}\beta|^2 + 1} + \mathrm{SNR}|h_{s,d}|^2 \right), \tag{5.6}$$

where the factor of $\frac{1}{2}$ has been added to account for the two time slots necessary to transmit a single message to the source.

We define an outage event to be

$$\max_{x_s} \mathrm{I}_{\mathrm{Best}}(x_s; \mathbf{y_d}) < R. \tag{5.7}$$

We can observe the high SNR behavior of this outage probability via Monte Carlo simulation.

From Figure 5.2, we observe that the probability of an outage event decays with exponential order two, or

$$P_{O|\mathrm{Best}} \doteq \mathrm{SNR}^{-2}. \tag{5.8}$$

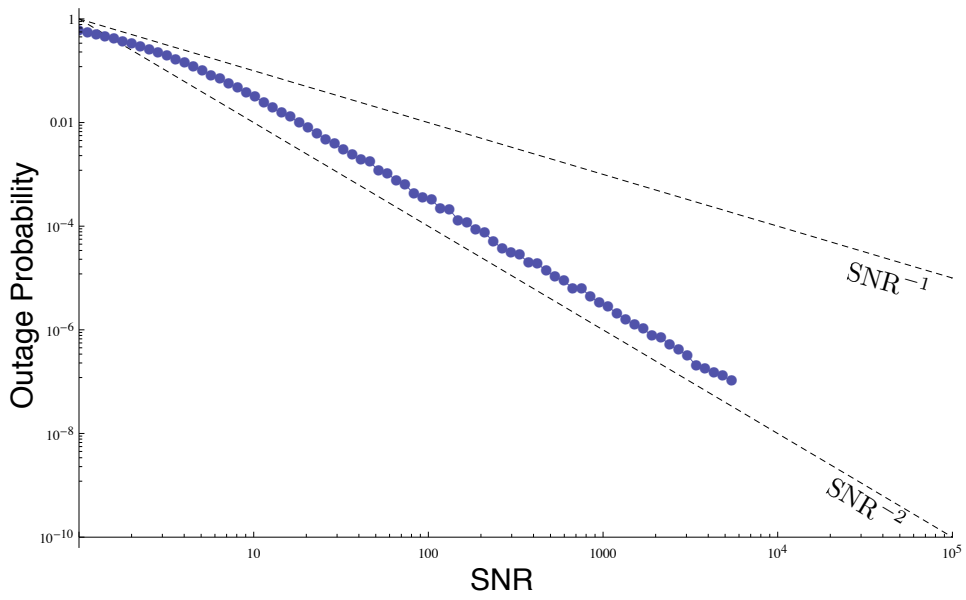

Figure 5.2: Best case outage probability Monte Carlo simulation ($R = \frac{1}{2}$ and $\lambda_{s,d} = \lambda_{s,r} = \lambda_{r,d} = 1$)

When the relay is successfully detects a source transmission, full diversity is achieved.

5.1.2 Neutral Case

The second case we consider is the neutral one, where the relay neither helps nor hurts the source's transmission because it never transmits.

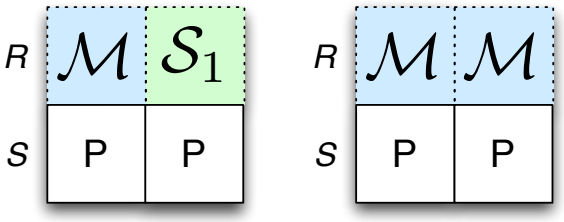

(a) B_2 (b) B_3

Figure 5.3: Neutral case states

States B_2 and B_3 exhibit this behavior. In both of these states, the relay is sensing the medium during both slots, thereby never transmitting. We assume all of the same

parameters as before and merely change the expressions to account for the lack of relay transmission during the second slot. In the first slot, the destination receives

$$y_d[n] = h_{s,d}x_s[n] + z_d[n]. \tag{5.9}$$

Because the relay is silent in the next slot, the destination receives only the source's retransmission, or

$$y_d\left[n + \frac{L}{2}\right] = h_{s,d}x_s[n] + z_d\left[n + \frac{L}{2}\right]. \tag{5.10}$$

Transforming this into a 1×2 multi-antenna system results in the matrix formulation of

$$\begin{gathered}\mathbf{y_d}[n] = \mathbf{A}x_s[n] + \mathbf{Bz}[n] \\ \begin{bmatrix} y_d[n] \\ y_d[n+\frac{L}{2}] \end{bmatrix} = \begin{bmatrix} h_{s,d} \\ h_{s,d} \end{bmatrix} x_s[n] + \begin{bmatrix} 0 & 1 & 0 \\ 0 & 0 & 1 \end{bmatrix} \begin{bmatrix} z_r[n] \\ z_d[n] \\ z_d[n+\frac{L}{2}] \end{bmatrix}.\end{gathered} \tag{5.11}$$

Like before, we can derive the maximum mutual information between scalar x_s and vector $\mathbf{y_d}$ in order to determine the maximum instantaneous rate supported by the channel for given channel gains. For brevity, this derivation is presented in Appendix B.2. From Equation (B.2), we can express this maximum mutual information as

$$\mathrm{I}_{\mathrm{Neutral}}(x_s; \mathbf{y_d}) \leq \frac{1}{2}\log\left(1 + 2 \cdot \mathrm{SNR}|h_{s,d}|^2\right), \tag{5.12}$$

which is exactly the capacity expression of a point-to-point SISO link under quasi-static fading with an SNR improvement due to the additional power from the source. Formally, the outage event can be defined as

$$\max_{x_s} \mathrm{I}_{\mathrm{Neutral}}(x_s; \mathbf{y_d}) < R. \tag{5.13}$$

Solving for the random channel power $|h_{s,d}|^2$ yields

$$|h_{s,d}|^2 < \frac{e^{2R}-1}{2 \cdot \text{SNR}}, \tag{5.14}$$

where $|h_{s,d}|^2$ is an exponential random variable with parameter $\lambda_{s,d}$. The probability of this event occurring is simply the CDF of the exponential random variable evaluated at this point. Formally,

$$P_{O|\text{Neutral}} = 1 - e^{\lambda_{s,d}\frac{e^{2R}-1}{2\cdot\text{SNR}}} \tag{5.15}$$

$$P_{O|\text{Neutral}} \doteq \text{SNR}^{-1}. \tag{5.16}$$

In other words, for the neutral case, the system has lost the diversity order improvement associated with the relay. Despite having an analytical expression for the outage probability of this case, we can verify the high-SNR behavior with a Monte Carlo simulation.

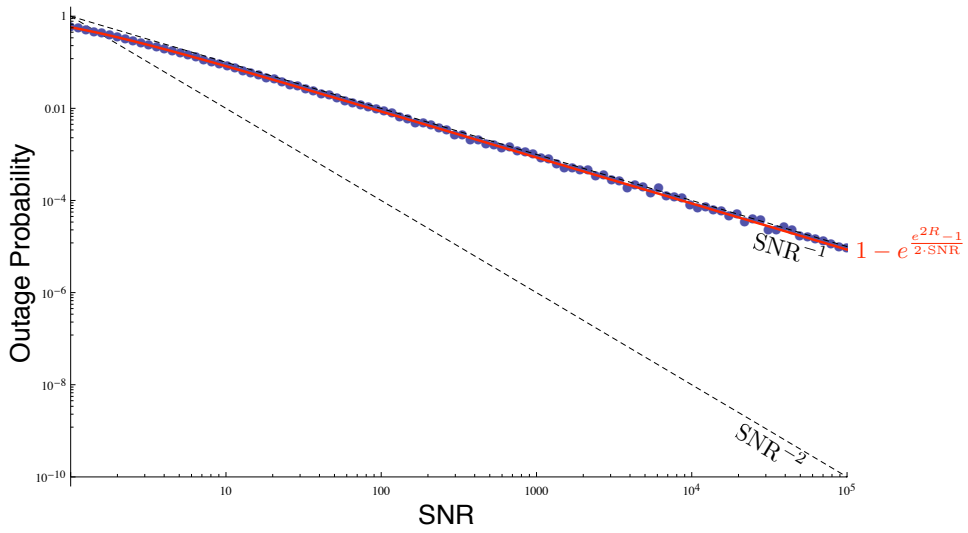

Figure 5.4: Neutral case outage probability Monte Carlo simulation

Figure 5.4 shows a tight match between the analytical expression and the Monte Carlo simulation data points.

5.1.3 Worst Case 1

The next case we consider is the one of the worst, where the relay actively impedes the source's communication by transmitting noise during the first slot of the frame.

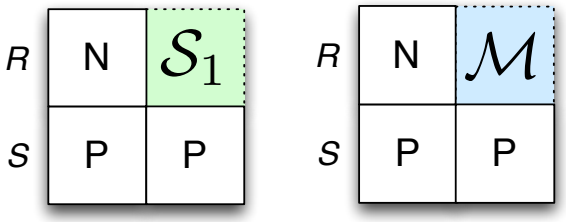

(a) B_4 (b) B_5

Figure 5.5: First worst case states

States B_4 and B_5 exhibit this behavior. To calculate the outage probability of the system given this state, we assume all of the same parameters as before and merely change the expressions to account for the relay's noise transmission during the first slot. In the first slot, the destination receives

$$y_d[n] = h_{s,d}x_s[n] + z_d[n] + h_{r,d}\beta z_r\left[n - \frac{L}{2}\right], \tag{5.17}$$

where $z_r\left[n - \frac{L}{2}\right]$ is the noise at the relay during the second slot of the previous frame. During the second slot, the destination receives only the source's retransmission, or

$$y_d\left[n + \frac{L}{2}\right] = h_{s,d}x_s[n] + z_d\left[n + \frac{L}{2}\right]. \tag{5.18}$$

Transforming this into a 1×2 multi-antenna system results in the matrix formu-

lation of

$$\mathbf{y_d}[n] = \mathbf{A}x_s[n] + \mathbf{Bz}[n]$$

$$\begin{bmatrix} y_d[n] \\ y_d[n+\frac{L}{2}] \end{bmatrix} = \begin{bmatrix} h_{s,d} \\ h_{s,d} \end{bmatrix} x_s[n] + \begin{bmatrix} h_{r,d}\beta & 1 & 0 \\ 0 & 0 & 1 \end{bmatrix} \begin{bmatrix} z_r[n] \\ z_d[n] \\ z_d[n+\frac{L}{2}] \end{bmatrix}. \tag{5.19}$$

Like before, we can derive the maximum mutual information between scalar x_s and vector $\mathbf{y_d}$ in order to determine the maximum instantaneous rate supported by the channel for given channel gains. For brevity, this derivation is presented in Appendix B.3. From Equation (B.3), we can express this maximum mutual information as

$$\mathrm{I}_{\text{Worst 1}}(x_s; \mathbf{y_d}) \leq \frac{1}{2} \log \left(1 + \mathrm{SNR}|h_{s,d}|^2 + \frac{\mathrm{SNR}|h_{s,d}|^2}{|h_{r,d}\beta|^2 + 1} \right). \tag{5.20}$$

Comparing the worst case mutual information expression for the NAF protocol to that for that OAF protocol [Equations (5.20) and (4.36)], we can see a fundamental difference between the OAF and NAF protocols. The noise transmission from the relay only affects the first slot of the frame. In the NAF protocol, this means that the source's retransmission during the second slot cannot be corrupted. In the OAF protocol, this "safe time" is wasted since the source is idle during that slot. We now provide upper and lower bounds to Equation (5.20) and show that the diversity order of those bounds are identical. For the lower bound on maximum mutual information, we recognize that the last term in the logarithm is a a non-negative quantity, and thus, can be removed. For the upper bound, we notice that the expression is a non-increasing function of β, and thus, is maximized for $\beta = 0$. Hence, we can write these bounds as

$$\log\left(1 + \mathrm{SNR}|h_{s,d}|^2\right) \leq \max_{x_s} \mathrm{I}_{\text{Worst 1}}(x_s; \mathbf{y_d}) \leq \log\left(1 + 2 \cdot \mathrm{SNR}|h_{s,d}|^2\right). \tag{5.21}$$

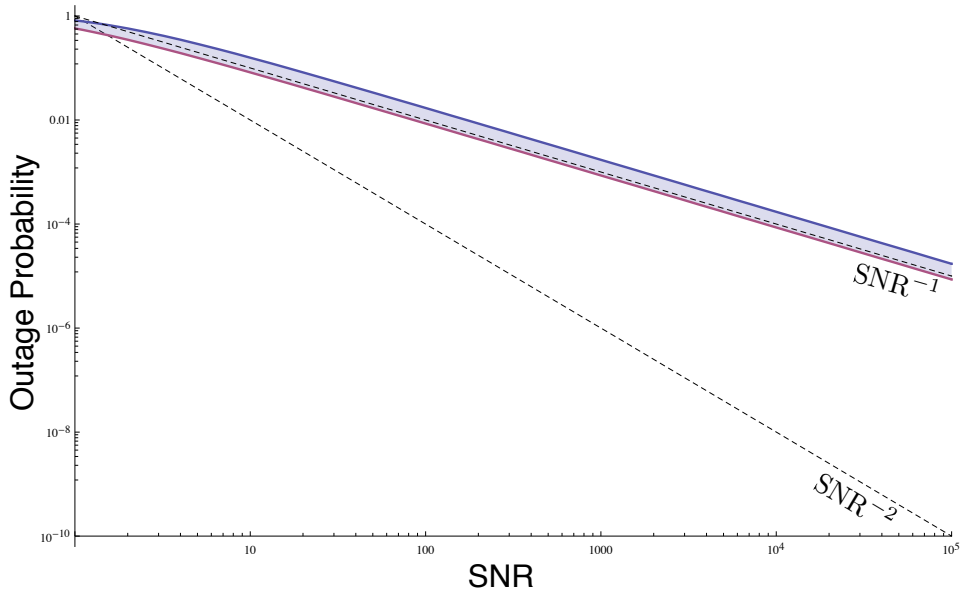

Figure 5.6: Worst case outage probability bounds

Figure 5.6 shows the upper and lower bounds on outage probability. Notice that the upper bound of Equation (5.21) is the maximum mutual information of a direct SISO link with an SNR gain. This is exactly the maximum mutual information of the neutral case of the NAF protocol. In Section 5.1.2, we showed that the outage probability of this system decays with exponential order one. The lower bound of the expression is the maximum mutual information of a direct SISO link without an SNR gain. This is exactly the maximum mutual information of the neutral case of the OAF protocol. In Section 4.1.2, we showed that the outage probability of this system also decays with exponential order one. Thus,

$$\mathrm{SNR}^{-1} \dot{\geq} P_{O|\text{Worst 1}} \dot{\geq} \mathrm{SNR}^{-1}. \tag{5.22}$$

The bounds are asymptotically tight, and thus,

$$P_{O|\text{Worst 1}} \doteq \mathrm{SNR}^{-1}. \tag{5.23}$$

Unlike the worst case of the OAF protocol, the first worst case of the NAF protocol

is guaranteed to not asymptotically degrade performance beyond diversity order one.

5.1.4 Worst Case 2

The final case we consider is the other worst, where the relay actively impedes the source's communication by transmitting interference during the first slot of the frame from a late detection in the previous frame.

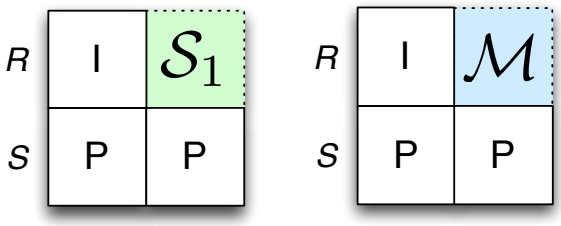

(a) B_6 (b) B_7

Figure 5.7: Second Worst case states

States B_6 and B_7 exhibit this behavior. To calculate the outage probability of the system given this state, we assume all of the same parameters as before and merely change the expressions to account for the relay's interference transmission during the first slot. In the first slot, the destination receives

$$y_d[n] = h_{s,d}x_s[n] + z_d[n] + h_{r,d}\beta\hat{x_s}\left[n - \frac{L}{2}\right], \tag{5.24}$$

where $\hat{x_s}[n-\frac{L}{2}]$ is the previous slot's, and thus interfering, source's waveform. During the second slot, the destination receives only the thermal noise at the destination, or

$$y_d\left[n + \frac{L}{2}\right] = z_d\left[n + \frac{L}{2}\right]. \tag{5.25}$$

Transforming this into a 1×2 multi-antenna system results in the matrix formu-

lation of

$$\mathbf{y_d}[n] = \mathbf{A}x_s[n] + \mathbf{Bz}[n]$$

$$\begin{bmatrix} y_d[n] \\ y_d[n+\frac{L}{2}] \end{bmatrix} = \begin{bmatrix} h_{s,d} \\ h_{s,d} \end{bmatrix} x_s[n] + \begin{bmatrix} h_{r,d}\beta & 1 & 0 \\ 0 & 0 & 1 \end{bmatrix} \begin{bmatrix} \hat{x_s}[n-\frac{L}{2}] \\ z_d[n] \\ z_d[n+\frac{L}{2}] \end{bmatrix}. \tag{5.26}$$

We can derive the maximum mutual information between scalar x_s and vector $\mathbf{y_d}$ in order to determine the maximum instantaneous rate supported by the channel for given channel gains. For brevity, this derivation is presented in Appendix B.4. From Equation (B.4), we can express this maximum mutual information as

$$\mathrm{I}_{\text{Worst Case 2}}(x_s; \mathbf{y_d}) \leq \frac{1}{2}\log\left(1 + \mathrm{SNR}|h_{s,d}|^2 + \frac{\mathrm{SNR}|h_{s,d}|^2}{\mathrm{SNR}|h_{r,d}\beta|^2 + 1}\right). \tag{5.27}$$

Despite the slightly different form as compared to the first worst case in Equation (5.20), the same bounds still apply. Formally,

$$\log\left(1 + \mathrm{SNR}|h_{s,d}|^2\right) \leq \max_{x_s} \mathrm{I}_{\text{Worst 2}}(x_s; \mathbf{y_d}) \leq \log\left(1 + 2 \cdot \mathrm{SNR}|h_{s,d}|^2\right). \tag{5.28}$$

In Section 5.1.3, we established that both of these bounds yield outage probabilities that decay with exponential order one. Thus,

$$P_{O|\text{Worst 2}} \doteq \mathrm{SNR}^{-1}. \tag{5.29}$$

5.2 Total Performance

Like the analysis in Chapter 4, there are two critical pieces of information: the likelihood of states and the performance given each of those states. We use the law of total probability to combine these two pieces to discuss the total outage probability of the NAF protocol in a random access environment. Formally,

$$P_O = \frac{1}{q}\Big(P_{B_1}\cdot P_{O|\text{Best}} + (P_{B_2}+P_{B_3})\cdot P_{O|\text{Neutral}} + (P_{B_4}+P_{B_5})\cdot P_{O|\text{Worst 1}} + (P_{B_6}+P_{B_7})\cdot P_{O|\text{Worst 2}}\Big), \tag{5.30}$$

where the $1/q$ term scales the state likelihoods so that $\sum_i P_{B_i} = 1$. In the following sections, we will revisit the different energy detection thresholding strategies in order to discuss this overall system performance.

5.2.1 Static Relay Detection

Equations (3.30) - (3.36) express the exponential orders of the state probabilities for static relay threshold (i.e. $\Lambda = K$). Recall that the best case and worst cases do not decay in likelihood with SNR, but the neutral cases decay with exponential order one. Substituting these likelihoods into Equation (5.30) yields

$$P_{O|\Lambda=K} = \frac{1}{q}\Big(\text{SNR}^0\cdot P_{O|\text{Best}} + \text{SNR}^{-1}\cdot P_{O|\text{Neutral}} + \text{SNR}^0\cdot P_{O|\text{Worst 1}} + \text{SNR}^0\cdot P_{O|\text{Worst 2}}\Big). \tag{5.31}$$

Equations (5.8), (5.16), (5.23), and (5.29) express the exponential orders of the outage probabilities given the different cases. Substituting these probabilities into

the total outage probability expression yields

$$\begin{aligned} P_{O|\Lambda=K} &\doteq \left(\mathrm{SNR}^{0}\cdot\mathrm{SNR}^{-2}+\mathrm{SNR}^{-1}\cdot\mathrm{SNR}^{-1}+\mathrm{SNR}^{0}\cdot\mathrm{SNR}^{-1}+\mathrm{SNR}^{0}\cdot\mathrm{SNR}^{-1}\right) \\ &\doteq \left(\mathrm{SNR}^{-2}+\mathrm{SNR}^{-2}+\mathrm{SNR}^{-1}+\mathrm{SNR}^{-1}\right) \\ P_{O|\Lambda=K} &\doteq \mathrm{SNR}^{-1}. \end{aligned} \tag{5.32}$$

With a static energy detection threshold at the relay, full diversity is impossible. We can verify this behavior via Monte-Carlo simulation.

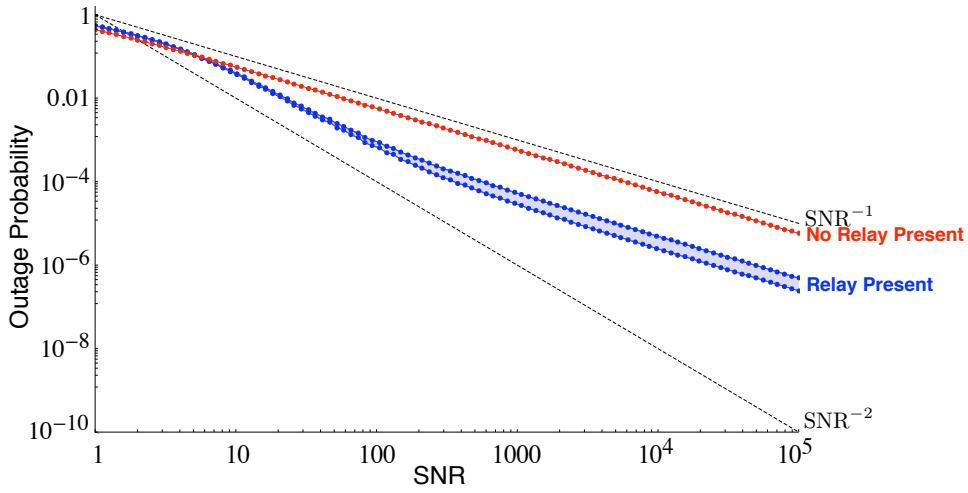

Figure 5.8: Outage Probability with $\Lambda = 20$

Figure 5.8 shows that the performance with presence of the altruistic relay in the network performs asymptotically no better than having no relay in all. However, it certainly performs no worse, which is not necessarily the case for the OAF protocol. We now turn to dynamic relay thresholds to determine if this problem can be avoided.

5.2.2 Dynamic Relay Detection

Recall from Chapter 3 that we can analyze the performance of the system under two forms of dynamic thresholding strategies. In the case that the threshold changes

logarithmically with SNR, we call the strategy a slow dynamic threshold. In the case that the threshold changes proportionally with SNR, we call the strategy a fast dynamic threshold. In the following sections, we analyze the effects of both of these strategies on overall system performance.

5.2.2.1 Slow Dynamic Threshold

Equations (3.66) - (3.72) express the exponential orders of the state probabilities for the slow dynamic relay threshold (i.e. $\Lambda = K_1 + K_2 \cdot \log(1 + \text{SNR})$). Substituting these likelihoods into Equation (5.30) yields

$$P_{O|\Lambda=K_1+K_2\cdot\log(1+\text{SNR})} = \frac{1}{q}\Big(\text{SNR}^0 \cdot P_{O|\text{Best}} + \text{SNR}^{-1} \cdot P_{O|\text{Neutral}} + \text{SNR}^{-K} \cdot P_{O|\text{Worst 1}} + \text{SNR}^{-K} \cdot P_{O|\text{Worst 2}}\Big). \quad (5.33)$$

Equations (5.8), (5.16), (5.23), and (5.29) express the exponential orders of the outage probabilities given the different cases. Substituting these probabilities into the total outage probability expression yields

$$P_{O|\Lambda=K_1+K_2\cdot\log(1+\text{SNR})} \doteq \Big(\text{SNR}^0 \cdot \text{SNR}^{-2} + \text{SNR}^{-1} \cdot \text{SNR}^{-1} + \text{SNR}^{-K} \cdot \text{SNR}^{-1} + \text{SNR}^{-K} \cdot \text{SNR}^{-1}\Big), \quad (5.34)$$

which becomes

$$\begin{aligned} P_{O|\Lambda=K_1+K_2\cdot\log(1+\text{SNR})} &\doteq \big(\text{SNR}^{-2} + \text{SNR}^{-2} + \text{SNR}^{-K} + \text{SNR}^{-K}\big) \\ P_{O|\Lambda=K_1+K_2\cdot\log(1+\text{SNR})} &\doteq \text{SNR}^{-2}. \end{aligned} \quad (5.35)$$

The diversity order is two, which is the full spatial diversity that can be achieved. We can verify this behavior via Monte-Carlo simulation.

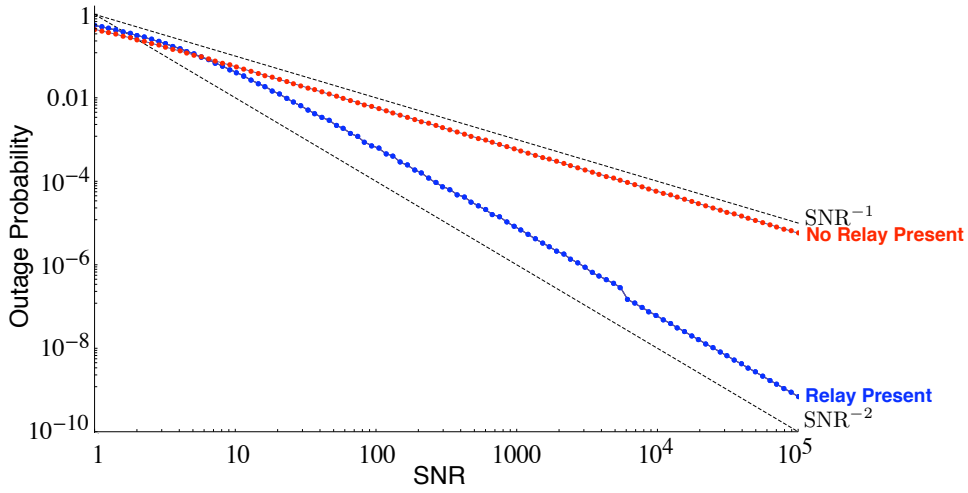

Figure 5.9: Outage Probability with $\Lambda = 20 + \log(1 + \text{SNR})$

Figure 5.9 shows that the slow dynamic thresholding strategy achieves full spatial diversity.

5.2.2.2 Fast Dynamic Threshold

Equations (3.80) - (3.86) express the exponential orders of the state probabilities for fast dynamic relay threshold (i.e. $\Lambda = K_1 + K_2 \cdot \text{SNR}$). Substituting these likelihoods into Equation (5.30) yields

$$P_{O|\Lambda=K_1+K_2\cdot\text{SNR}} = \frac{1}{q}\Big(\text{SNR}^0 \cdot P_{O|\text{Best}} + \text{SNR}^0 \cdot P_{O|\text{Neutral}} + \text{SNR}^{-\infty} \cdot P_{O|\text{Worst 1}} + \text{SNR}^{-\infty} \cdot P_{O|\text{Worst 2}}\Big). \quad (5.36)$$

Equations (5.8), (5.16), (5.23), and (5.29) express the exponential orders of the outage probabilities given the different cases. Substituting these probabilities into the total outage probability expression yields

$$P_{O|\Lambda=K_1+K_2\cdot\mathrm{SNR}} \doteq \Big(\mathrm{SNR}^{0}\cdot\mathrm{SNR}^{-2}+\mathrm{SNR}^{0}\cdot\mathrm{SNR}^{-1} + \mathrm{SNR}^{-\infty}\cdot\mathrm{SNR}^{-1}+\mathrm{SNR}^{-\infty}\cdot\mathrm{SNR}^{-1}\Big), \tag{5.37}$$

which becomes

$$\begin{aligned} P_{O|\Lambda=K_1+K_2\cdot\mathrm{SNR}} &\doteq \left(\mathrm{SNR}^{-2}+\mathrm{SNR}^{-1}+\mathrm{SNR}^{-\infty}+\mathrm{SNR}^{-\infty}\right) \\ P_{O|\Lambda=K_1+K_2\cdot\mathrm{SNR}} &\doteq \mathrm{SNR}^{-1}. \end{aligned} \tag{5.38}$$

Because the fast dynamic threshold makes the neutral case not decay with SNR, it becomes the dominating term. This yields a diversity order of one. We can verify this behavior via Monte-Carlo simulation.

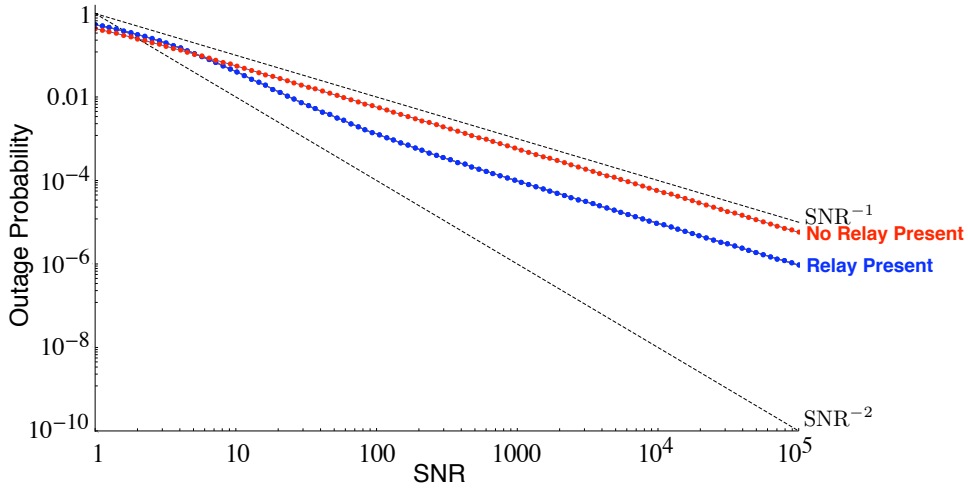

Figure 5.10: Outage Probability with $\Lambda = 20 + \mathrm{SNR}$

Figure 5.10 shows that, asymptotically, the presence of the altruistic relay does not aid the source's ability to communicate when the relay's energy detection uses a fast dynamic threshold.

5.3 Summary

The second main result of this thesis regards the diversity order of the NAF protocol in a random-access environment. Like in the OAF protocol, in the case of a slow dynamic energy detection threshold that moves with the logarithm of average SNR, full diversity can be achieved. In other words, asymptotically, the random-access cooperative network performs no worse than a scheduled cooperative network.

We have also shown that in both the static threshold case and the fast dynamic threshold case, the random-access network results in a diversity-order loss relative to the scheduled network. For the static threshold, the dominating error term arises from a constant probability of states where the relay actively transmits noise during a frame. Unlike the OAF protocol, the NAF protocol, at the very least, still performs asymptotically no worse than having no relay present.

For the fast dynamic threshold, the dominating error term arises from a constant probability of states where the relay misses the detection of the source's packet.

Chapter 6

Conclusions

In this thesis, we have shown that the asymptotic gains in outage performance offered by amplify-and-forward cooperation can be maintained in a random-access environment, provided the relay's packet detection system meets certain criteria. When energy detection is employed as that packet detection system, the threshold on energy must dynamically shift with average SNR. In particular, a system with a thresholding scheme that shifts with the logarithm of SNR is able to achieve full diversity.

If this dynamic threshold moves too quickly with SNR (e.g. proportionally with SNR), missed detections dominate the performance of the system and result in a diversity-order loss. Likewise, if the threshold fails to move with SNR (i.e. a static threshold), false alarms dominate the performance of the system and result in a diversity-order loss.

In a sense, this is distressing. The entire motivation behind amplify-and-forward cooperation is that the relay would be very easy and inexpensive to design, build, and deploy. These results reveal that the relay needs to know *a priori* the average SNR of the yet-unknown packet in order to adequately help that packet's source communicate. While the assumption of this knowledge may be reasonable in the three-node network studied in this thesis, we acknowledge that such an assumption

may be unrealistic in multi-user networks where different source nodes have different average SNRs with respect to the relay. As such, despite the loss of diversity-order, static energy thresholds are very desirable.

Does a diversity-order loss that comes with using static energy thresholds mean that that there is no point to deploying cooperative networks? To discuss the answer of this question, we observe a final Monte Carlo simulation that shows the effects of different static thresholds on the performance of the NAF protocol.

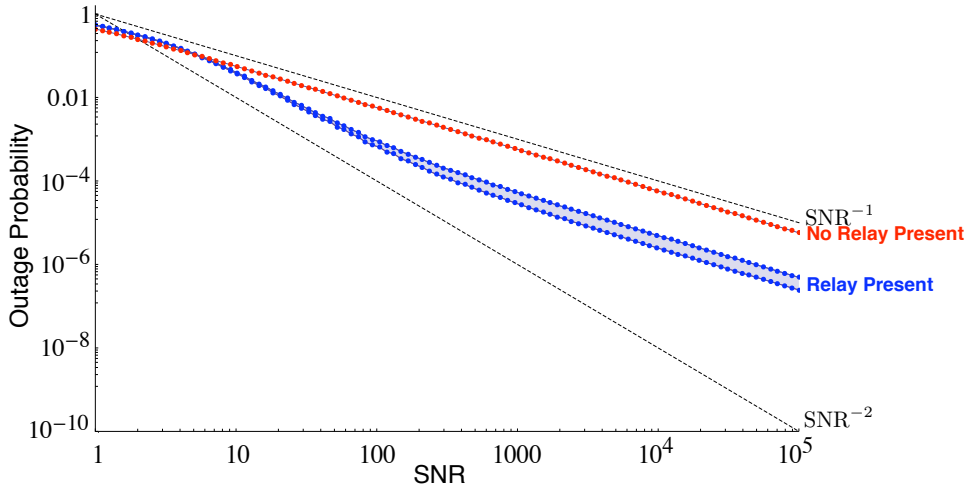

(a) $\Lambda = 20$

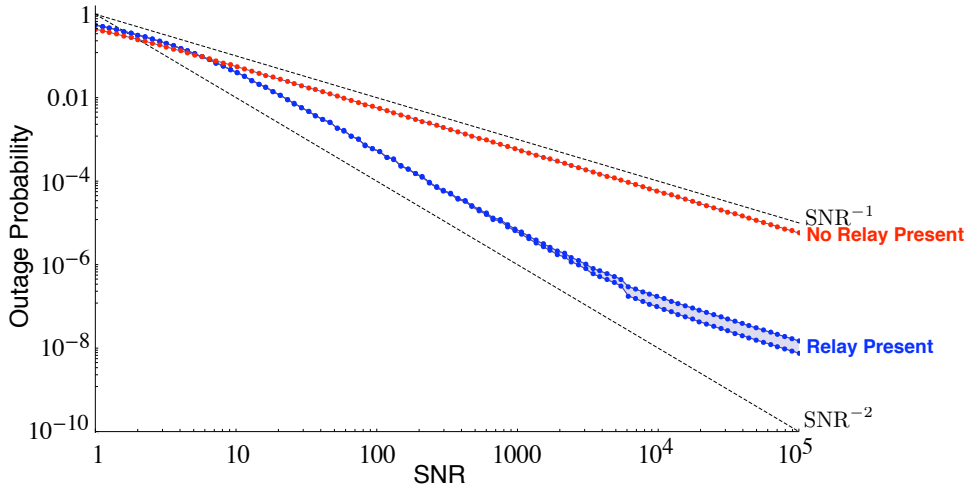

(b) $\Lambda = 35$

Figure 6.1: Outage probability of NAF with different static energy thresholds

The diversity order is, indeed, only one in both figures. However, notice that

by increasing the static threshold we can somewhat "delay the inevitable" and push back the diversity-order one behavior to arbitrary SNR values. In fact, notice that for smaller SNR values, the outage probability appears to decay as if it achieved full-diversity.

In any actual implementation, SNR is finite and the values that it can take on depend on the radio being used. Thus, a network designer can still employ a static energy threshold at the relay if a large enough threshold is chosen. It must be high enough so that the dominating error terms only begin to reveal themselves past the SNR values that the system would reasonably operate in. Effectively, this would make the system perform as if it were achieving full-diversity in the SNR regime of interest.

Thus, even with the asymptotic loss in performance associated with a static energy detection threshold at the relay, significant gains in reliability can still be realized.

6.1 Extensions and Future Work

In addition to the main results regarding the diversity order of random-access cooperative networks, this thesis presents another contribution that is more procedural in nature. Specifically, we have dealt with the notion of false alarms, where nodes believe a transmission to be present when, in fact, there is none. We have shown how this type of error significantly affects the state of a network even when only a small number of nodes are employed. Future work could apply a similar style of analysis to larger networks, which are more attractive from the standpoint of eventual implementations and deployment. Additionally, while we focused on analyzing amplify-and-forward protocols, a similar style of analysis can be applied to pure decode-and-forward and hybrid schemes.

Appendix A

Mutual Information Calculations for OAF

A.1 Best Case

In this section, we compute the maximum mutual information of the OAF protocol under the best case assumption. The analysis of the best case is equivalent to that from Laneman [8], which in turn is borrowed heavily from Telatar [1]. We begin with the system model from Equation (4.8):

$$\mathbf{y_d}[n] = \mathbf{A}x_s[n] + \mathbf{B}\mathbf{z}[n]$$

$$\begin{bmatrix} y_d[n] \\ y_d[n+\frac{L}{2}] \end{bmatrix} = \begin{bmatrix} h_{s,d} \\ h_{r,d}\beta h_{s,r} \end{bmatrix} x_s[n] + \begin{bmatrix} 0 & 1 & 0 \\ h_{r,d}\beta & 0 & 1 \end{bmatrix} \begin{bmatrix} z_r[n] \\ z_d[n] \\ z_d[n+\frac{L}{2}] \end{bmatrix},$$

for $n \in \left[0, 1, 2, \ldots, \frac{L}{2}\right]$. The mutual information of this system satisfies

$$\mathrm{I}_{\mathrm{Best}}(x_s; \mathbf{y_d}) \leq \log\det\left(\mathbf{I} + \left(\mathrm{SNR}\cdot\mathbf{A}\mathbf{A}^\dagger\right)\left(\mathbf{B}\mathrm{E}\left[\mathbf{z}\mathbf{z}^\dagger\right]\mathbf{B}^\dagger\right)^{-1}\right),$$

with equality for x_s being a zero-mean, circularly symmetric, complex Gaussian. For the best case analysis, the pertinent components of this expression are

$$\mathbf{A}\mathbf{A}^{\dagger} = \begin{bmatrix} |h_{s,d}|^2 & h_{s,d}^{\dagger}\left(h_{r,d}\beta h_{s,r}\right) \\ \left(h_{r,d}\beta h_{s,r}\right)^{\dagger} h_{s,d} & |h_{r,d}\beta h_{s,r}|^2 \end{bmatrix}$$

$$\mathbf{B}\mathrm{E}\left[\mathbf{z}\mathbf{z}^{\dagger}\right]\mathbf{B}^{\dagger} = \begin{bmatrix} 1 & 0 \\ 0 & |h_{r,d}\beta|^2 + 1 \end{bmatrix}.$$

After substitutions and algebraic manipulations, we compute the determinant as

$$\begin{aligned} &\det\left(\mathbf{I} + \left(\mathrm{SNR}\cdot\mathbf{A}\mathbf{A}^{\dagger}\right)\left(\mathbf{B}\mathrm{E}\left[\mathbf{z}\mathbf{z}^{\dagger}\right]\mathbf{B}^{\dagger}\right)^{-1}\right) \\ &\quad = \det\left(\begin{bmatrix} 1 & 0 \\ 0 & 1 \end{bmatrix} + \begin{bmatrix} \mathrm{SNR}|h_{s,d}|^2 & \mathrm{SNR}h_{s,d}^{\dagger}\left(h_{r,d}\beta h_{s,r}\right) \\ \mathrm{SNR}\left(h_{r,d}\beta h_{s,r}\right)^{\dagger} h_{s,d} & \mathrm{SNR}|h_{r,d}\beta h_{s,r}|^2 \end{bmatrix}\begin{bmatrix} 1 & 0 \\ 0 & \frac{1}{|h_{r,d}\beta|^2+1} \end{bmatrix}\right) \\ &\quad = 1 + \frac{\mathrm{SNR}|h_{r,d}\beta h_{s,r}|^2}{|h_{r,d}\beta|^2+1} + \mathrm{SNR}|h_{s,d}|^2. \end{aligned}$$

Thus, we can express the maximum mutual information for the best case as

$$\mathrm{I}_{\mathrm{Best}}(x_s;\mathbf{y_d}) \leq \log\left(1 + \frac{\mathrm{SNR}|h_{r,d}\beta h_{s,r}|^2}{|h_{r,d}\beta|^2+1} + \mathrm{SNR}|h_{s,d}|^2\right). \tag{A.1}$$

A.2 Neutral Case

In this section, we compute the maximum mutual information of the OAF protocol under neutral case assumptions. We begin with the system model from Equation (4.27):

$$\mathbf{y_d}[n] = \mathbf{A}x_s[n] + \mathbf{B}\mathbf{z}[n]$$

$$\begin{bmatrix} y_d[n] \\ y_d[n+\frac{L}{2}] \end{bmatrix} = \begin{bmatrix} h_{s,d} \\ 0 \end{bmatrix} x_s[n] + \begin{bmatrix} 0 & 1 & 0 \\ 0 & 0 & 1 \end{bmatrix} \begin{bmatrix} z_r[n] \\ z_d[n] \\ z_d[n+\frac{L}{2}] \end{bmatrix},$$

for $n \in \left[0, 1, 2, \ldots, \frac{L}{2}\right]$. The mutual information of this system satisfies

$$\mathrm{I}_{\mathrm{Neutral}}(x_s; \mathbf{y_d}) \leq \log\det\left(\mathbf{I} + \left(\mathrm{SNR}\cdot\mathbf{A}\mathbf{A}^\dagger\right)\left(\mathbf{B}\mathrm{E}\left[\mathbf{z}\mathbf{z}^\dagger\right]\mathbf{B}^\dagger\right)^{-1}\right),$$

with equality for x_s being a zero-mean, circularly symmetric, complex Gaussian. For the neutral case analysis, the pertinent components of this expression are

$$\mathbf{A}\mathbf{A}^\dagger = \begin{bmatrix} |h_{s,d}|^2 & 0 \\ 0 & 0 \end{bmatrix}$$

$$\mathbf{B}\mathrm{E}\left[\mathbf{z}\mathbf{z}^\dagger\right]\mathbf{B}^\dagger = \begin{bmatrix} 1 & 0 \\ 0 & 1 \end{bmatrix}.$$

After substitutions and algebraic manipulations, we compute the determinant as

$$\begin{aligned}
&\det\left(\mathbf{I}+\left(\mathrm{SNR}\cdot\mathbf{A}\mathbf{A}^{\dagger}\right)\left(\mathbf{B}\mathrm{E}\left[\mathbf{z}\mathbf{z}^{\dagger}\right]\mathbf{B}^{\dagger}\right)^{-1}\right)\\
&\qquad=\det\left(\begin{bmatrix}1&0\\0&1\end{bmatrix}+\begin{bmatrix}\mathrm{SNR}|h_{s,d}|^2&0\\0&0\end{bmatrix}\begin{bmatrix}1&0\\0&1\end{bmatrix}\right)\\
&\qquad=1+\mathrm{SNR}|h_{s,d}|^2.
\end{aligned}$$

Thus, we can express the maximum mutual information for the neutral case as

$$\mathrm{I}_{\mathrm{Neutral}}(x_s;\mathbf{y_d})\leq\log\left(1+\mathrm{SNR}|h_{s,d}|^2\right). \tag{A.2}$$

A.3 Worst Case

In this section, we compute the maximum mutual information for the OAF protocol under worst case assumptions. We begin with the system model from Equation (4.35):

$$\mathbf{y_d}[n] = \mathbf{A}x_s[n] + \mathbf{Bz}[n]$$

$$\begin{bmatrix} y_d[n] \\ y_d[n+\frac{L}{2}] \end{bmatrix} = \begin{bmatrix} h_{s,d} \\ 0 \end{bmatrix} x_s[n] + \begin{bmatrix} h_{r,d}\beta & 1 & 0 \\ 0 & 0 & 1 \end{bmatrix} \begin{bmatrix} z_r[n-\frac{L}{2}] \\ z_d[n] \\ z_d[n+\frac{L}{2}] \end{bmatrix}.$$

for $n \in \left[0, 1, 2, \ldots, \frac{L}{2}\right]$. The mutual information of this system satisfies

$$\mathrm{I}_{\mathrm{Worst}}(x_s; \mathbf{y_d}) \leq \log\det\left(\mathbf{I} + \left(\mathrm{SNR}\cdot\mathbf{A}\mathbf{A}^\dagger\right)\left(\mathbf{B}\mathrm{E}\left[\mathbf{z}\mathbf{z}^\dagger\right]\mathbf{B}^\dagger\right)^{-1}\right),$$

with equality for x_s being a zero-mean, circularly symmetric, complex Gaussian. For the worst case analysis, the pertinent components of this expression are

$$\mathbf{A}\mathbf{A}^\dagger = \begin{bmatrix} |h_{s,d}|^2 & 0 \\ 0 & 0 \end{bmatrix}$$

$$\mathbf{B}\mathrm{E}\left[\mathbf{z}\mathbf{z}^\dagger\right]\mathbf{B}^\dagger = \begin{bmatrix} |h_{r,d}\beta|^2 + 1 & 0 \\ 0 & 1 \end{bmatrix}.$$

After substitutions and algebraic manipulations, we compute the determinant as

$$\begin{aligned}
&\det\left(\mathbf{I}+\left(\mathrm{SNR}\cdot\mathbf{A}\mathbf{A}^{\dagger}\right)\left(\mathbf{B}\mathrm{E}\left[\mathbf{z}\mathbf{z}^{\dagger}\right]\mathbf{B}^{\dagger}\right)^{-1}\right)\\
&\qquad=\det\left(\begin{bmatrix}1 & 0\\ 0 & 1\end{bmatrix}+\begin{bmatrix}\mathrm{SNR}|h_{s,d}|^2 & 0\\ 0 & 0\end{bmatrix}\begin{bmatrix}\frac{1}{|h_{r,d}\beta|^2+1} & 0\\ 0 & 1\end{bmatrix}\right)\\
&\qquad=1+\frac{\mathrm{SNR}|h_{s,d}|^2}{|h_{r,d}\beta|^2+1}.
\end{aligned}$$

Thus, we can express the maximum mutual information for the worst case as

$$\mathrm{I}_{\mathrm{Worst}}(x_s;\mathbf{y_d})\leq\log\left(1+\frac{\mathrm{SNR}|h_{s,d}|^2}{|h_{r,d}\beta|^2+1}\right). \tag{A.3}$$

Appendix B

Mutual Information Calculations for NAF

B.1 Best Case

In this section, we compute the maximum mutual information of the NAF protocol under the best case assumption. We begin with the system model from Equation (5.5):

$$\mathbf{y_d}[n] = \mathbf{A}x_s[n] + \mathbf{Bz}[n]$$

$$\begin{bmatrix} y_d[n] \\ y_d[n+\frac{L}{2}] \end{bmatrix} = \begin{bmatrix} h_{s,d} \\ h_{s,d} + h_{r,d}\beta h_{s,r} \end{bmatrix} x_s[n] + \begin{bmatrix} 0 & 1 & 0 \\ h_{r,d}\beta & 0 & 1 \end{bmatrix} \begin{bmatrix} z_r[n] \\ z_d[n] \\ z_d[n+\frac{L}{2}] \end{bmatrix},$$

for $n \in \left[0, 1, 2, \ldots, \frac{L}{2}\right]$. The mutual information of this system satisfies

$$\mathrm{I}_{\mathrm{Best}}(x_s; \mathbf{y_d}) \leq \log\det\left(\mathbf{I} + \left(\mathrm{SNR} \cdot \mathbf{A}\mathbf{A}^\dagger\right)\left(\mathbf{B}\mathrm{E}\left[\mathbf{z}\mathbf{z}^\dagger\right]\mathbf{B}^\dagger\right)^{-1}\right),$$

with equality for x_s being a zero-mean, circularly symmetric, complex Gaussian. For the best case analysis, the pertinent components of this expression are

$$\mathbf{A}\mathbf{A}^{\dagger} = \begin{bmatrix} |h_{s,d}|^2 & h_{s,d}^{\dagger}\left(h_{s,d} + h_{r,d}\beta h_{s,r}\right) \\ \left(h_{s,d} + h_{r,d}\beta h_{s,r}\right)^{\dagger} h_{s,d} & |h_{s,d} + h_{r,d}\beta h_{s,r}|^2 \end{bmatrix}$$

$$\mathbf{B}\mathrm{E}\left[\mathbf{z}\mathbf{z}^{\dagger}\right]\mathbf{B}^{\dagger} = \begin{bmatrix} 1 & 0 \\ 0 & |h_{r,d}\beta|^2 + 1 \end{bmatrix}.$$

After substitutions and algebraic manipulations, we compute the determinant as

$$\begin{aligned} &\det\left(\mathbf{I} + \left(\mathrm{SNR}\cdot\mathbf{A}\mathbf{A}^{\dagger}\right)\left(\mathbf{B}\mathrm{E}\left[\mathbf{z}\mathbf{z}^{\dagger}\right]\mathbf{B}^{\dagger}\right)^{-1}\right) \\ =&\det\left(\begin{bmatrix} 1 & 0 \\ 0 & 1 \end{bmatrix} + \begin{bmatrix} \mathrm{SNR}|h_{s,d}|^2 & \mathrm{SNR}h_{s,d}^{\dagger}\left(h_{s,d} + h_{r,d}\beta h_{s,r}\right) \\ \mathrm{SNR}\left(h_{s,d} + h_{r,d}\beta h_{s,r}\right)^{\dagger} h_{s,d} & \mathrm{SNR}|h_{s,d} + h_{r,d}\beta h_{s,r}|^2 \end{bmatrix}\begin{bmatrix} 1 & 0 \\ 0 & \frac{1}{|h_{r,d}\beta|^2+1} \end{bmatrix}\right) \\ =&1 + \frac{\mathrm{SNR}|h_{s,d} + h_{r,d}\beta h_{s,r}|^2}{|h_{r,d}\beta|^2 + 1} + \mathrm{SNR}|h_{s,d}|^2. \end{aligned}$$

Thus, we can express the maximum mutual information for the best case as

$$\mathrm{I}_{\mathrm{Best}}(x_s; \mathbf{y_d}) \leq \log\left(1 + \frac{\mathrm{SNR}|h_{s,d} + h_{r,d}\beta h_{s,r}|^2}{|h_{r,d}\beta|^2 + 1} + \mathrm{SNR}|h_{s,d}|^2\right). \tag{B.1}$$

B.2 Neutral Case

In this section, we compute the maximum mutual information of the NAF protocol under neutral case assumptions. We begin with the system model from Equation (5.11):

$$\mathbf{y_d}[n] = \mathbf{A}x_s[n] + \mathbf{B}\mathbf{z}[n]$$

$$\begin{bmatrix} y_d[n] \\ y_d[n+\frac{L}{2}] \end{bmatrix} = \begin{bmatrix} h_{s,d} \\ h_{s,d} \end{bmatrix} x_s[n] + \begin{bmatrix} 0 & 1 & 0 \\ 0 & 0 & 1 \end{bmatrix} \begin{bmatrix} z_r[n] \\ z_d[n] \\ z_d[n+\frac{L}{2}] \end{bmatrix},$$

for $n \in \left[0, 1, 2, \ldots, \frac{L}{2}\right]$. The mutual information of this system satisfies

$$\mathrm{I}_{\mathrm{Neutral}}(x_s; \mathbf{y_d}) \leq \log\det\left(\mathbf{I} + \left(\mathrm{SNR}\cdot\mathbf{A}\mathbf{A}^\dagger\right)\left(\mathbf{B}\mathrm{E}\left[\mathbf{z}\mathbf{z}^\dagger\right]\mathbf{B}^\dagger\right)^{-1}\right)$$

with equality for x_s being a zero-mean, circularly symmetric, complex Gaussian. For the neutral case analysis, the pertinent components of this expression are

$$\mathbf{A}\mathbf{A}^\dagger = \begin{bmatrix} |h_{s,d}|^2 & |h_{s,d}|^2 \\ |h_{s,d}|^2 & |h_{s,d}|^2 \end{bmatrix}$$

$$\mathbf{B}\mathrm{E}\left[\mathbf{z}\mathbf{z}^\dagger\right]\mathbf{B}^\dagger = \begin{bmatrix} 1 & 0 \\ 0 & 1 \end{bmatrix}.$$

After substitutions and algebraic manipulations, we compute the determinant as

$$\begin{aligned}
&\det\left(\mathbf{I}+\left(\mathrm{SNR}\cdot\mathbf{A}\mathbf{A}^{\dagger}\right)\left(\mathbf{B}\mathrm{E}\left[\mathbf{z}\mathbf{z}^{\dagger}\right]\mathbf{B}^{\dagger}\right)^{-1}\right)\\
&\qquad=\det\left(\begin{bmatrix}1&0\\0&1\end{bmatrix}+\begin{bmatrix}\mathrm{SNR}|h_{s,d}|^2&\mathrm{SNR}|h_{s,d}|^2\\\mathrm{SNR}|h_{s,d}|^2&\mathrm{SNR}|h_{s,d}|^2\end{bmatrix}\begin{bmatrix}1&0\\0&1\end{bmatrix}\right)\\
&\qquad=1+2\cdot\mathrm{SNR}|h_{s,d}|^2.
\end{aligned}$$

Thus, we can express the maximum mutual information for the neutral case as

$$\mathrm{I}_{\mathrm{Neutral}}(x_s;\mathbf{y_d})\leq\log\left(1+2\cdot\mathrm{SNR}|h_{s,d}|^2\right). \tag{B.2}$$

B.3 Worst Case 1

In this section, we compute the maximum mutual information for the NAF protocol under the first worst case assumption (noise-driven error at relay). We begin with the system model from Equation (5.19):

$$\mathbf{y_d}[n] = \mathbf{A}x_s[n] + \mathbf{B}\mathbf{z}[n]$$

$$\begin{bmatrix} y_d[n] \\ y_d[n+\frac{L}{2}] \end{bmatrix} = \begin{bmatrix} h_{s,d} \\ h_{s,d} \end{bmatrix} x_s[n] + \begin{bmatrix} h_{r,d}\beta & 1 & 0 \\ 0 & 0 & 1 \end{bmatrix} \begin{bmatrix} z_r[n] \\ z_d[n] \\ z_d[n+\frac{L}{2}] \end{bmatrix},$$

for $n \in \left[0, 1, 2, \ldots, \frac{L}{2}\right]$. The mutual information of this system satisfies

$$\mathrm{I}_{\text{Worst Case 1}}(x_s; \mathbf{y_d}) \leq \log\det\left(\mathbf{I} + \left(\mathrm{SNR}\cdot\mathbf{A}\mathbf{A}^\dagger\right)\left(\mathbf{B}\mathrm{E}\left[\mathbf{z}\mathbf{z}^\dagger\right]\mathbf{B}^\dagger\right)^{-1}\right),$$

with equality for x_s being a zero-mean, circularly symmetric, complex Gaussian. For the first worst case analysis, the pertinent components of this expression are

$$\mathbf{A}\mathbf{A}^\dagger = \begin{bmatrix} |h_{s,d}|^2 & |h_{s,d}|^2 \\ |h_{s,d}|^2 & |h_{s,d}|^2 \end{bmatrix}$$

$$\mathbf{B}\mathrm{E}\left[\mathbf{z}\mathbf{z}^\dagger\right]\mathbf{B}^\dagger = \begin{bmatrix} |h_{r,d}\beta|^2 + 1 & 0 \\ 0 & 1 \end{bmatrix}.$$

After substitutions and algebraic manipulations, we compute the determinant as

$$\begin{aligned}
&\det\left(\mathbf{I}+\left(\mathrm{SNR}\cdot\mathbf{A}\mathbf{A}^{\dagger}\right)\left(\mathbf{B}\mathrm{E}\left[\mathbf{z}\mathbf{z}^{\dagger}\right]\mathbf{B}^{\dagger}\right)^{-1}\right)\\
&\qquad=\det\left(\begin{bmatrix}1 & 0\\ 0 & 1\end{bmatrix}+\begin{bmatrix}\mathrm{SNR}|h_{s,d}|^2 & \mathrm{SNR}|h_{s,d}|^2\\ \mathrm{SNR}|h_{s,d}|^2 & \mathrm{SNR}|h_{s,d}|^2\end{bmatrix}\begin{bmatrix}\frac{1}{|h_{r,d}\beta|^2+1} & 0\\ 0 & 1\end{bmatrix}\right)\\
&\qquad=1+\mathrm{SNR}|h_{s,d}|^2+\frac{\mathrm{SNR}|h_{s,d}|^2}{|h_{r,d}\beta|^2+1}.
\end{aligned}$$

Thus, we can express the maximum mutual information for the first worst case as

$$\mathrm{I}_{\text{Worst Case 1}}(x_s;\mathbf{y_d})\leq\log\left(1+\mathrm{SNR}|h_{s,d}|^2+\frac{\mathrm{SNR}|h_{s,d}|^2}{|h_{r,d}\beta|^2+1}\right). \tag{B.3}$$

B.4 Worst Case 2

In this section, we compute the maximum mutual information for the NAF protocol under the second worst case assumption (interference-driven error at relay). We begin with the system model from Equation (5.26):

$$\mathbf{y_d}[n] = \mathbf{A}x_s[n] + \mathbf{B}\mathbf{z}[n]$$

$$\begin{bmatrix} y_d[n] \\ y_d[n+\frac{L}{2}] \end{bmatrix} = \begin{bmatrix} h_{s,d} \\ h_{s,d} \end{bmatrix} x_s[n] + \begin{bmatrix} h_{r,d}\beta & 1 & 0 \\ 0 & 0 & 1 \end{bmatrix} \begin{bmatrix} \hat{x_s}[n] \\ z_d[n] \\ z_d[n+\frac{L}{2}] \end{bmatrix},$$

for $n \in \left[0, 1, 2, \ldots, \frac{L}{2}\right]$. The mutual information of this system satisfies

$$\mathrm{I}_{\text{Worst Case 2}}(x_s; \mathbf{y_d}) \leq \log\det\left(\mathbf{I} + \left(\mathrm{SNR}\cdot\mathbf{A}\mathbf{A}^\dagger\right)\left(\mathbf{B}\mathrm{E}\left[\mathbf{z}\mathbf{z}^\dagger\right]\mathbf{B}^\dagger\right)^{-1}\right),$$

with equality for x_s being a zero-mean, circularly symmetric, complex Gaussian. For the second worst case analysis, the pertinent components of this expression are

$$\mathbf{A}\mathbf{A}^\dagger = \begin{bmatrix} |h_{s,d}|^2 & |h_{s,d}|^2 \\ |h_{s,d}|^2 & |h_{s,d}|^2 \end{bmatrix}$$

$$\mathbf{B}\mathrm{E}\left[\mathbf{z}\mathbf{z}^\dagger\right]\mathbf{B}^\dagger = \begin{bmatrix} \mathrm{SNR}|h_{r,d}\beta|^2 + 1 & 0 \\ 0 & 1 \end{bmatrix}.$$

After substitutions and algebraic manipulations, we compute the determinant as

$$\begin{aligned}
&\det\left(\mathbf{I}+\left(\mathrm{SNR}\cdot\mathbf{A}\mathbf{A}^{\dagger}\right)\left(\mathbf{B}\mathrm{E}\left[\mathbf{z}\mathbf{z}^{\dagger}\right]\mathbf{B}^{\dagger}\right)^{-1}\right)\\
&\qquad=\det\left(\begin{bmatrix}1 & 0\\ 0 & 1\end{bmatrix}+\begin{bmatrix}\mathrm{SNR}|h_{s,d}|^2 & \mathrm{SNR}|h_{s,d}|^2\\ \mathrm{SNR}|h_{s,d}|^2 & \mathrm{SNR}|h_{s,d}|^2\end{bmatrix}\begin{bmatrix}\frac{1}{\mathrm{SNR}|h_{r,d}\beta|^2+1} & 0\\ 0 & 1\end{bmatrix}\right)\\
&\qquad=1+\mathrm{SNR}|h_{s,d}|^2+\frac{\mathrm{SNR}|h_{s,d}|^2}{\mathrm{SNR}|h_{r,d}\beta|^2+1}.
\end{aligned}$$

Thus, we can express the maximum mutual information for the second worst case as

$$\mathrm{I}_{\text{Worst Case 2}}(x_s;\mathbf{y_d})\leq\log\left(1+\mathrm{SNR}|h_{s,d}|^2+\frac{\mathrm{SNR}|h_{s,d}|^2}{\mathrm{SNR}|h_{r,d}\beta|^2+1}\right). \tag{B.4}$$

Appendix C

Asymptotic CDF Approximations

In this appendix, we collect two important results regarding the asymptotic behavior of functions of exponential distributions. These results are required for the outage probability calculations in Chapters 4 and 5.

Fact C.0.1. *Let W be an exponential random variable with decay parameter λ_W. The following is satisfied:*

$$\lim_{s\to\infty} sP\left[sW < t\right] = \lambda_W t. \tag{C.1}$$

Claim C.0.2. *Let U, V be exponential random variables with decay parameters λ_U, λ_V. The following is satisfied:*

$$\lim_{s\to\infty} sP\left[f\left(sU, sV\right) < t\right] = \left(\lambda_U + \lambda_V\right) t, \tag{C.2}$$

where $f\left(x, y\right) = \frac{xy}{x+y+1}$

Proof of Claim C.0.2. The proof of this claim follows the same structure as the proof in Laneman's original work [8]. The proof presented here contains modifications in notation as well as simplifying steps. The structure of the proof is to show that a lower bound on the limit equals an upper bound on the limit. Thus, we can conclude

that the limit exists and equals the bounds.

The first step of the proof is to find a lower bound on the limit. We first begin with algebraic manipulations of the probability expression within the limit:

$$\begin{aligned} P\left[f\left(sU, sV\right) < t\right] &= P\left[\frac{sUsV}{sU + sV + 1} < t\right] \\ &= P\left[\frac{sU + sV + 1}{sUsV} \geq \frac{1}{t}\right] \\ &= P\left[\frac{1}{sV} + \frac{1}{sU} + \frac{1}{sVsU} \geq \frac{1}{t}\right]. \end{aligned} \tag{C.3}$$

Since $\frac{1}{sVsU} \geq 0$, we can lower bound this probability by

$$\begin{aligned} P\left[f\left(sU, sV\right) < t\right] &\geq P\left[\frac{1}{sV} + \frac{1}{sU} \geq \frac{1}{t}\right] \\ &\geq P\left[\max\left(\frac{1}{sV}, \frac{1}{sU}\right) \geq \frac{1}{t}\right] \\ &= 1 - P\left[\min\left(sV, sU\right) \geq t\right]. \end{aligned} \tag{C.4}$$

The probability in the above expression is equivalent to the probability of both sV and sU being greater than or equal to t. Formally,

$$\begin{aligned} P\left[f\left(sU, sV\right) < t\right] &\geq 1 - e^{-\lambda_V \frac{t}{s}} \cdot e^{-\lambda_U \frac{t}{s}} \\ &= 1 - e^{-(\lambda_V + \lambda_U)\frac{t}{s}}, \end{aligned} \tag{C.5}$$

which we recognize to be of a form similar to a CDF of an exponential distribution. Consider an exponential random variable W with decay parameter $\lambda_W = \lambda_V + \lambda_U$. We can rewrite Equation (C.5) as

$$\begin{aligned} P\left[f\left(sU, sV\right) < t\right] &\geq 1 - e^{-\lambda_W \frac{t}{s}} \\ &= P\left[sW < t\right]. \end{aligned} \tag{C.6}$$

Replacing the limits back into the expression and using Fact C.0.1 yields

$$\begin{aligned} \lim_{s\to\infty} sP\left[f\left(sU, sV\right) < t\right] &\geq \lim_{s\to\infty} sP\left[sW < t\right] \\ &= \lambda_W t \\ \lim_{s\to\infty} sP\left[f\left(sU, sV\right) < t\right] &\geq \left(\lambda_V + \lambda_U\right) t. \end{aligned} \tag{C.7}$$

With Equation (C.7), we have completed the lower bound on the limit. To upper bound the limit, we return to Equation (C.3), which is repeated here:

$$\begin{aligned} P\left[f\left(sU, sV\right) < t\right] &= P\left[\frac{1}{sV} + \frac{1}{sU} + \frac{1}{sVsU} \geq \frac{1}{t}\right] \\ &= P\left[\frac{1}{sV} \geq \frac{\frac{1}{t} - \frac{1}{sU}}{1 + \frac{1}{sU}}\right] \\ &= \int_0^\infty P\left[\frac{1}{sV} \geq \frac{\frac{1}{t} - \frac{1}{su}}{1 + \frac{1}{su}}\right] p_U\left(u\right) du. \end{aligned} \tag{C.8}$$

Let $l > 1$ be a fixed constant. We can then split the above integral into two parts, yielding

$$\begin{aligned} P\left[f\left(sU, sV\right) < t\right] = &\int_0^{\frac{lt}{s}} P\left[\frac{1}{sV} \geq \frac{\frac{1}{t} - \frac{1}{su}}{1 + \frac{1}{su}}\right] p_U\left(u\right) du \\ &+ \int_{\frac{lt}{s}}^\infty P\left[\frac{1}{sV} \geq \frac{\frac{1}{t} - \frac{1}{su}}{1 + \frac{1}{su}}\right] p_U\left(u\right) du. \end{aligned} \tag{C.9}$$

We can upper bound the first term in the above expression by making the probability equal one. Formally,

$$P\left[f\left(sU, sV\right) < t\right] = \int_0^{\frac{lt}{s}} p_U\left(u\right) du + \int_{\frac{lt}{s}}^{\infty} P\left[\frac{1}{sV} \geq \frac{\frac{1}{t} - \frac{1}{su}}{1 + \frac{1}{su}}\right] p_U\left(u\right) du. \tag{C.10}$$

The first integral is, by definition, the CDF of U evaluated at $\frac{lt}{s}$, or

$$P\left[f\left(sU, sV\right) < t\right] = P\left[U \leq \frac{lt}{s}\right] + \int_{\frac{lt}{s}}^{\infty} P\left[\frac{1}{sV} \geq \frac{\frac{1}{t} - \frac{1}{su}}{1 + \frac{1}{su}}\right] p_U\left(u\right) du. \tag{C.11}$$

We can further bound this expression by recognizing that

$$P\left[U \leq \frac{lt}{s}\right] = \frac{sP\left[U \leq \frac{lt}{s}\right]}{s} \tag{C.12}$$

$$\leq \frac{\lambda_U lt}{s}. \tag{C.13}$$

Thus, Equation (C.11) can be further upper-bounded by

$$P\left[f\left(sU, sV\right) < t\right] \leq \frac{\lambda_U lt}{s} + \int_{\frac{lt}{s}}^{\infty} P\left[\frac{1}{sV} \geq \frac{\frac{1}{t} - \frac{1}{su}}{1 + \frac{1}{su}}\right] p_U\left(u\right) du. \tag{C.14}$$

We now shift our attention to placing an upper bound on the second term of Equation (C.14). Let $k > l$ be another fixed constant. We can split the integral into two more parts, yielding

$$\int_{\frac{lt}{s}}^{\infty} P\left[\frac{1}{sV} \geq \frac{\frac{1}{t}-\frac{1}{su}}{1+\frac{1}{su}}\right] p_U(u)\,du = \int_{\frac{lt}{s}}^{\frac{kt}{s}} P\left[\frac{1}{sV} \geq \frac{\frac{1}{t}-\frac{1}{su}}{1+\frac{1}{su}}\right] p_U(u)\,du + \int_{\frac{kt}{s}}^{\infty} P\left[\frac{1}{sV} \geq \frac{\frac{1}{t}-\frac{1}{su}}{1+\frac{1}{su}}\right] p_U(u)\,du. \quad \text{(C.15)}$$

Note that the integrands above are non-increasing functions of u. This means that we can upper bound the second term of Equation (C.15) by removing the integral and substituting $u = \frac{kt}{s}$, yielding

$$\int_{\frac{lt}{s}}^{\infty} P\left[\frac{1}{sV} \geq \frac{\frac{1}{t}-\frac{1}{su}}{1+\frac{1}{su}}\right] p_U(u)\,du \leq \int_{\frac{lt}{s}}^{\frac{kt}{s}} P\left[\frac{1}{sV} \geq \frac{\frac{1}{t}-\frac{1}{su}}{1+\frac{1}{su}}\right] p_U(u)\,du + P\left[\frac{1}{sV} \geq \frac{\frac{1}{t}-\frac{1}{kt}}{1+\frac{1}{kt}}\right]. \quad \text{(C.16)}$$

This new term can be further upper-bounded by recognizing that

$$P\left[\frac{1}{sV} \geq \frac{\frac{1}{t}-\frac{1}{kt}}{1+\frac{1}{kt}}\right] = \frac{sP\left[sV < \frac{1+\frac{1}{kt}}{\frac{1}{t}-\frac{1}{kt}}\right]}{s} \quad \text{(C.17)}$$

$$\leq \frac{\lambda_V\left(\frac{1+\frac{1}{kt}}{\frac{1}{t}-\frac{1}{kt}}\right)}{s}. \quad \text{(C.18)}$$

Thus, Equation (C.16) can be rewritten as

$$\int_{\frac{lt}{s}}^{\infty} P\left[\frac{1}{sV} \geq \frac{\frac{1}{t}-\frac{1}{su}}{1+\frac{1}{su}}\right] p_U(u)\,du \leq \int_{\frac{lt}{s}}^{\frac{kt}{s}} P\left[\frac{1}{sV} \geq \frac{\frac{1}{t}-\frac{1}{su}}{1+\frac{1}{su}}\right] p_U(u)\,du + \frac{\lambda_V\left(\frac{1+\frac{1}{kt}}{\frac{1}{t}-\frac{1}{kt}}\right)}{s}. \quad \text{(C.19)}$$

Additionally, noting a property of the exponential distribution that $p_U(u) < \lambda_U$,

we can additionally upper bound and simplify the expression to be

$$\int_{\frac{lt}{s}}^{\infty} P\left[\frac{1}{sV} \geq \frac{\frac{1}{t}-\frac{1}{su}}{1+\frac{1}{su}}\right] p_U(u)\,du \leq \lambda_U \int_{\frac{lt}{s}}^{\frac{kt}{s}} P\left[\frac{1}{sV} \geq \frac{\frac{1}{t}-\frac{1}{su}}{1+\frac{1}{su}}\right] du + \frac{\lambda_V\left(\frac{1+\frac{1}{kt}}{\frac{1}{t}-\frac{1}{kt}}\right)}{s}. \tag{C.20}$$

An analogous bound to Equation (C.20) is

$$P\left[\frac{1}{sV} \geq \frac{\frac{1}{t}-\frac{1}{su}}{1+\frac{1}{su}}\right] = \frac{sP\left[sV < \frac{1+\frac{1}{su}}{\frac{1}{t}-\frac{1}{stu}}\right]}{s} \tag{C.21}$$

$$\leq \frac{\lambda_V\left(\frac{1+\frac{1}{su}}{\frac{1}{t}-\frac{1}{su}}\right)}{s}. \tag{C.22}$$

Substituting Equation (C.22) into Equation (C.20) for the remaining integrand yields

$$\int_{\frac{lt}{s}}^{\infty} P\left[\frac{1}{sV} \geq \frac{\frac{1}{t}-\frac{1}{su}}{1+\frac{1}{su}}\right] p_U(u)\,du \leq \lambda_U \int_{\frac{lt}{s}}^{\frac{kt}{s}} \frac{\lambda_V\left(\frac{1+\frac{1}{su}}{\frac{1}{t}-\frac{1}{su}}\right)}{s} du + \frac{\lambda_V\left(\frac{1+\frac{1}{kt}}{\frac{1}{t}-\frac{1}{kt}}\right)}{s}. \tag{C.23}$$

The remaining definite integral can be explicitly computed. After simplifications, this yields

$$\lambda_U \int_{\frac{lt}{s}}^{\frac{kt}{s}} \frac{\lambda_V\left(\frac{1+\frac{1}{su}}{\frac{1}{t}-\frac{1}{su}}\right)}{s} du = \frac{1}{s} \cdot \frac{\lambda_U \lambda_V\left[(k-l)t + (t+1)\log\left((k-1)t\right) - (t+1)\log\left((l-1)t\right)\right]}{s}. \tag{C.24}$$

To simplify the the remaining steps of the proof, we define a function as

$$F(s) \stackrel{\text{def}}{=} \frac{\lambda_U \lambda_V \left[(k-l)t + (t+1)\log\left((k-1)t\right) - (t+1)\log\left((l-1)t\right)\right]}{s}. \quad \text{(C.25)}$$

Finally, we can combine Equations (C.14), (C.19), yielding

$$P\left[f\left(sU, sV\right) < t\right] \leq \frac{\lambda_U l t}{s} + \frac{\lambda_V \left(\frac{1+\frac{1}{kt}}{\frac{1}{t}-\frac{1}{kt}}\right)}{s} + \frac{F(s)}{s}. \quad \text{(C.26)}$$

Noting that $F(s) \to 0$ as $s \to \infty$, we can reintroduce the limit back into the expression to yield

$$\lim_{s\to\infty} P\left[f\left(sU, sV\right) < t\right] \leq \lambda_U l t + \lambda_V \left(\frac{1+\frac{1}{kt}}{\frac{1}{t}-\frac{1}{kt}}\right). \quad \text{(C.27)}$$

Because l and k are arbitrary constants, l can be chosen arbitrarily close to one and k can be chosen to be arbitrarily large. Thus,

$$\lim_{s\to\infty} sP\left[f\left(sU, sV\right) < t\right] \leq \left(\lambda_U + \lambda_V\right) t, \quad \text{(C.28)}$$

which completes the upper bound of the limit. Combining Equations (C.7) and (C.28) yields

$$\left(\lambda_U + \lambda_V\right) t \leq \lim_{s\to\infty} sP\left[f\left(sU, sV\right) < t\right] \leq \left(\lambda_U + \lambda_V\right) t. \quad \text{(C.29)}$$

and thus,

$$\lim_{s\to\infty} sP\left[f\left(sU, sV\right) < t\right] = \left(\lambda_U + \lambda_V\right) t, \quad \text{(C.30)}$$

which completes the proof. □

Bibliography

[1] İ. E. Telatar. "On the capacity of multi-antenna gaussian channels". Technical report, Bell Labs, Lucent Technologies, 1995. 1, A.1

[2] E.C. van der Meulen. "Three-terminal communication channels". *Adv. Appl. Prob*, 3(1):120–154, 1971. 1.1

[3] E.C. Van der Meulen. *"Transmission of Information in a T-terminal Discrete Memoryless Channel"*. PhD thesis, University of California at Berkeley., 1969. 1.1

[4] T. Cover and A.E. Gamal. "Capacity theorems for the relay channel". *IEEE Transactions on Information Theory*, 25(5):572–584, Sep 1979. 1.1

[5] A. Sendonaris, E. Erkip, and B. Aazhang. "User cooperation diversity. Part I: System description". *IEEE Transactions on Communications*, 51(11):1927–1938, Nov. 2003. 1.1

[6] A. Sendonaris, E. Erkip, and B. Aazhang. "User cooperation diversity. Part II: Implementation aspects and performance analysis". *IEEE Transactions on Communications*, 51(11):1939–1948, Nov. 2003.

[7] A. Sendonaris, E. Erkip, and B. Aazhang. "Increasing uplink capacity via user cooperation diversity". *Proceedings of the IEEE International Symposium on Information Theory*, 1998. 1.1

[8] J.N. Laneman, D.N.C. Tse, and G.W. Wornell. "Cooperative diversity in wireless networks: Efficient protocols and outage behavior". *IEEE Transactions on Information Theory*, 50(12):3062–3080, Dec. 2004. 1.1, 3, 4.1.1, 4.1.1, 4.3, A.1, C.0.2

[9] J.N. Laneman and G.W. Wornell. "Distributed space-time-coded protocols for exploiting cooperative diversity in wireless networks". *IEEE Transactions on Information Theory*, 49(10):2415–2425, Oct. 2003. 1.1

[10] K. Raj Kumar and Giuseppe Caire. "Coding and decoding for the dynamic decode and forward relay protocol". *IEEE Transactions on Information Theory*, submitted 2008. 1.1

[11] K. Azarian, H. El Gamal, and P. Schniter. "On the achievable diversity-multiplexing tradeoff in half-duplex cooperative channels". *IEEE Transactions on Information Theory*, 51(12):4152–4172, Dec. 2005. 1.1, 3.1.4

[12] R.U. Nabar, F.W. Kneubuhler, and H. Bolcskei. "Performance limits of amplify-and-forward based fading relay channels". *Proceedings of the IEEE International Conference on Acoustics, Speech, and Signal Processing*, 4:iv–565–iv–568 vol.4, 17-21 May 2004.

[13] R.U. Nabar, H. Bolcskei, and F.W. Kneubuhler. "Fading relay channels: performance limits and space-time signal design". *IEEE Journal on Selected Areas in Communications*, 22(6):1099–1109, Aug. 2004. 1.1

[14] A. Stefanov and E. Erkip. "Cooperative coding for wireless networks". *IEEE Transactions on Communications*, 52(9):1470–1476, Sept. 2004. 1.1

[15] M. Janani, A. Hedayat, T.E. Hunter, and A. Nosratinia. "Coded cooperation in wireless communications: space-time transmission and iterative decoding". *IEEE Transactions on Signal Processing*, 52(2):362–371, Feb. 2004.

[16] T.E. Hunter and A. Nosratinia. "Cooperation diversity through coding". *Proceedings of the IEEE International Symposium on Information Theory*, pages 220–, 2002.

[17] T.E. Hunter and A. Nosratinia. "Diversity through coded cooperation". *IEEE Transactions on Wireless Communications*, 5(2):283–289, Feb. 2006. 1.1

[18] R. Lin and A.P. Petropulu. "A new wireless network medium access protocol based on cooperation". *IEEE Transactions on Signal Processing*, 53(12):4675–4684, Dec. 2005. 1.1

[19] Rui Lin and A.R. Petropulu. "Cooperative transmission for random access wireless networks". *Proceedings of the Thirty-Eighth Asilomar Conference on Signals, Systems and Computers*, 2:1922–1926 Vol.2, 7-10 Nov. 2004. 1.1

[20] Wei Shuangqing. "Diversity-Multiplexing Tradeoff of Asynchronous Cooperative Diversity in Wireless Networks". *IEEE Transactions on Information Theory*, submitted 2007. 1.1

[21] H. Urkowitz. "Energy detection of unknown deterministic signals". *Proceedings of the IEEE*, 55(4):523–531, April 1967. 3

[22] F.F. Digham, M.-S. Alouini, and M.K. Simon. "On the energy detection of unknown signals over fading channels". *IEEE International Conference on Communications, 2003. ICC '03*, 5:3575–3579 vol.5, 11-15 May 2003. 3

[23] F. F. Digham, M.S. Alouini, and M. K. Simon. "On the energy detection of

unknown signals over fading channels". *IEEE Transactions on Communications*, 55(1):21–24, Jan. 2007. 3

[24] L.H. Ozarow, S. Shamai, and A.D. Wyner. "Information theoretic considerations for cellular mobile radio". *IEEE Transactions on Vehicular Technology*, 43(2):359–378, May 1994. 4

[25] J.N. Laneman. "Limiting analysis of outage probabilities for diversity schemes in fading channels". *Global Telecommunications Conference, 2003. GLOBECOM '03. IEEE*, 3:1242–1246 vol.3, 1-5 Dec. 2003. 4.1.1, 4.1.1